TAMPEREEN TEKNILLINEN YLIOPISTO
TAMPERE UNIVERSITY OF TECHNOLOGY

Erkki Härö

Simulation Tool Development for Quench Modelling

Re-Thinking Heat Diffusion in High Temperature Superconductors

Julkaisu 1394 • Publication 1394

Tampere 2016

Tampereen teknillinen yliopisto. Julkaisu 1394
Tampere University of Technology. Publication 1394

Erkki Härö

Simulation Tool Development for Quench Modelling

Re-Thinking Heat Diffusion in High Temperature Superconductors

Thesis for the degree of Doctor of Science in Technology to be presented with due permission for public examination and criticism in Tietotalo Building, Auditorium TB109, at Tampere University of Technology, on the 1st of July 2016, at 12 noon.

Tampereen teknillinen yliopisto - Tampere University of Technology
Tampere 2016

ISBN 978-952-15-3768-4 (printed)
ISBN 978-952-15-3772-1 (PDF)
ISSN 1459-2045

Abstract

Loss of the superconducting state, namely quench, is a dangerous event for superconducting magnets. This is especially the case for possible future accelerator magnets including high temperature superconductors (HTS) . These magnets are characterized with high magnetic fields and high current densities, and in case of a quench the current is transferred to the copper matrix, which easily leads to a damaged magnet. To predict the time scale and temperature evolution in case of a possible quench, numerical simulations are crucial. Understanding the quench in HTS magnets, by means of numerical simulations, is required to develop adequate quench detection and protection systems.

In this thesis, we first describe the background of the research by presenting the quench event in detail. Then we move on to the numerical modelling of quench, which requires a multiphysical approach where at least magnetostatic and heat diffusion problems have to be solved. To solve such problems, we have developed an in-house software QueST (finite element method based Quench Simulation Tool) with an object-oriented mindset for convenient future development. Then we proceed to study the quench characteristics of HTS magnets, utilizing QueST, while comparing to their low temperature superconductor (LTS) counterparts. We show that the quench evolution is different in HTS magnets, where the quench frontier does not propagate with the temperature front due to the large temperature margin. In addition, due to the large temperature margin of HTS magnets, we propose that the traditional analytical approaches, utilized with LTS magnets, are questionable e.g. for computing hot spot temperatures or minimum quench energies (MQE), and thus, numerical approaches are required. Finally, we scrutinize quench for an HTS research magnet showing that the hot spot temperature increases rapidly and a fast quench detection system is required to protect the magnet. We present an alternative method to ignite the quench in simulations, removing the temperature peak, which is present when utilizing a short heat pulse trigger.

Preface

My journey at the Tampere University of Technology (TUT) started in August 2007. Electrical engineering was a clear choice for me since high school, however, the choice of particular branch, whether it is electronics or power engineering or something in between, was more than cloudy at that point. Just after few weeks of studying, the exceptional teaching skills of Risto Mikkonen and Aki Korpela caught my eye (and I was not the only one).[1] Mandatory courses kept going and next year it was time for Lauri Kettunen and Saku Suuriniemi to surprise me with the same extremely high level of teaching at the courses of Electromagnetic fields and waves. Because of the high quality of teaching, I decided to take as many courses as possible from the research group of Electromagnetics[2](EM).

After two years of studying in TUT, I decided to apply for the summer job at the EM offered by Risto, and to my surprise, I was accepted. I was amazed by the unique atmosphere at the EM, which was extremely hard-working and ambitious but at the same time so relaxed and friendly. During two summers and teaching duties at the semesters I had the privilege to get to know to Antti Stenvall, whose guiding was essential for a young and clueless student trying to get into superconductor modelling. At the third year in EM, while writing my M.Sc. thesis, we were in the summer school of superconductivity in Turku with my future colleague, Valtteri Lahtinen, when Antti received information that his application was accepted for two doctoral students[3]. This was the beginning of a journey for almost 5 years in the EM which is now coming to an end. In summary, I have had the privilege to enjoy the teaching and working atmosphere of the EM for almost ten years, and thus, I think some thanks are

[1] That year Circuit Analysis I course was lectured at the same time by both of these gentlemen, and it was difficult to choose whose lecture to participate.

[2] At that time Institute of Electromagnetics

[3] This thesis was supported by Stability Analysis of Superconducting Hybrid Magnets (Academy of Finland, #250652) and by EuCARD-2, which is co-funded by the partners and the European Commission under Capacities 7th Framework Programme, Grant Agreement 312453.

more than necessary.

First of all I want to thank Antti for believing in me and taking me into this extremely interesting project. Furthermore, I want to thank you for being a great teacher and mentor who always had time to listen, while also being a great friend all these years in the office as well as in our travels. Thanks to Risto for accepting me as a summer research assistant in the first place. Without that opportunity, I most likely would not be writing these words right now. Thank you Lauri for keeping such a unique atmosphere at the EM all these years. Thanks to Aki for keeping the coffee room filled with coffee as well as serious and not-so-serious conversations. It was a big hit for the students of TUT and especially to our coffee room that you had to leave EM. Thank you Valtteri for being a great room mate in the office as well as in the travels and helping with whatever things I might had in mind. Thank you Matti Pellikka for helping with all the coding related problems especially at the beginning of this thesis. Thanks to Mika Lyly and Joonas Järvelä for providing guidance whenever needed during the years at the EM. Many thanks go to Lasse Söderlund, Maija-Liisa Paasonen and Terhi Salminen for taking care of admistrative tasks so I could focus on the research.

The list would be too long if I was to thank all the people who worked at the EM, but should you know, you all deserve to be thanked for. All the events, whether it was sports related or not, were fun and in good spirit. This kind of working community is something that should not be taken for granted!

I also had the opportunity to work in CERN for 4 months in 2014. I would like to thank Luca Bottura and Lucio Rossi who made this short visit possible. I would also like to thank Glyn Kirby and Jeroen van Nugteren who provided assistance in all matters related to work and personal things while in CERN. Glyn and Jeroen are to be thanked for their contribution to the research commited for this thesis. In addition, thanks also belong to the participants of the EuCARD and EuCARD-2 project all over the Europe.

I also thank the pre-examiners of this thesis, Tomas Holubek (Karlsruhe Institute of Technology, GER) and Fernando Toral Fernandez (CIEMAT, SPA) who spent time to evaluate and provide useful comments to improve the quality of this thesis. I also want to thank Tomas Holubek and Petriina Paturi (University of Turku, FIN) for taking the time to act as opponents for the public defense.

In the end, I would like to thank my parents, family and friends for their unconditional support throughout the years. Last, but most importantly, thank you Reea. You have supported me, not only during the thesis work, but also many years before that and hopefully also in years to come! You mean a world a to me!

In Sipoo, April 30, 2016

Erkki Härö

List of publications and author's contribution

Publication 1

E. Härö, A. Stenvall, T. Lecrevisse, J. Fleiter, J.-M. Rey, M. Sorbi, M. Devaux, C. Trophime, P. Fazilleau, G. Volpini, P. Tixador, F. Hornung, and C. Pes 2013
IEEE Trans. Appl. Supercond. **23** 4600104
"Quench Considerations and Protection Scheme of a High Field HTS Dipole Insert Coil"
doi:10.1109/TASC.2012.2228890

Publication 2

A. Stenvall, E. Härö, P. Fazilleau, M. Devaux, M. Durante, T. Lecrevisse, J.-M. Rey, J. Fleiter, M. Sorbi, G. Volpini, and P. Tixador 2013
CERN Yellow Report 2013-006, Proc. Workshop on Accelerator Magnet, Superconductor, Design and Optimization
"Protection of the 6 T YBCO Insert in the 13 T Nb_3Sn Fresca II Dipole"
doi:10.5170/CERN-2013-006

Publication 3

E. Härö and A. Stenvall 2014
IEEE Trans. Appl. Supercond. **24** 4900705
"Reducing Modelling Domain to Speed-Up Simulations of HTS Coils"
doi:10.1109/TASC.2013.2288773

Publication 4

E. Härö, J. Järvelä, and A. Stenvall 2015
J. Supercond. Nov. Magn. **28** 1705.
"Variation of Quench Propagation Velocities in YBCO Cables"
doi:10.1007/s10948-015-2976-y

Publication 5

E. Härö, A. Stenvall, J. van Nugteren, and G. Kirby 2015
IEEE Trans. Appl. Supercond. **25** 4901107.
"Hot Spot Temperature in an HTS Coil: Simulations with MIITs and Finite Element Method"
doi:10.1109/TASC.2015.2396945

Publication 6

E. Härö, A. Stenvall, J. van Nugteren, and G. Kirby 2015
IEEE Trans. Appl. Supercond. **25** 4701505.
"Modelling of Minimum Energy Required to Quench an HTS Magnet with a Strip Heater"
doi:10.1109/TASC.2015.2493125

Author's contribution

The author has written all the text in publications with the exception of **Publication 2**, which was written by A. Stenvall. In addition, in all publications, the discussions with A. Stenvall were crucial in all stages of the writing process.

All the simulations and programming work was done by the author, with few exceptions. The idea for quench protection circuit in **Publication 1** was first presented by J. Järvelä, and later simulated by A. Stenvall. In **Publication 2**, the simulations related to the current decay were concluded by A. Stenvall, while all the other simulations were done by the author. In addition, J. van Nugteren and G. Kirby provided invaluable information regarding operation parameters and magnet design details for **Publication 5** and **Publication 6**.

Detailed author's contribution for each publication

Publication 1: The author programmed magnetostatic and heat diffusion equation solvers on top of a C++-based open source code. This software was used in all the later publications as well with some modifications. The author wrote the text and performed the quench simulations for the studied magnet. In addition, the author implemented the critical current data provided by T. Lecrevisse [73] to the software. Furthermore, the author presented the computational model of the quench simulation software in detail in the publication.

Publication 2: The author implemented the studied magnet design for the quench simulation software and scrutinized the quench simulations. Especially, the temperature distribution, current sharing temperature and hot spot temperature simulations were performed by the author. The author also contributed to the writing process of the publication.

Publication 3: The author included the power law approximation for the superconductor resistivity to the quench simulation software. In addition, cable and insulation layers were included in the magnet design by the author. All the simulations as well as the writing process was concluded by the author.

Publication 4: The author implemented the possibility for normal zone propagation velocity simulation to the developed quench simulation software. He did the post-processing computations for the normal zone propagation velocity in Matlab. The author wrote the publication.

Publication 5: The author created a Matlab code to compute the adiabatic temperature increase and compared the results to the finite element method based analysis. He also implemented a critical current fit for the FEM software according to the data provided by J. Fleiter [38]. The author wrote the publication.

Publication 6: The author simulated energy required to quench an HTS magnet using the above mentioned FEM software. He also computed minimum quench energy utilizing Wilson's analytical formula using Matlab, and compared the results in the publication. The author wrote the publication.

Contents

Lists of symbols and abbreviations

a	Time delay
A	Cross-sectional area
$\mathbf{A}$	Magnetic vector potential
B	Magnetic flux density
$\mathbf{B}$	Vector field version of magnetic flux density
B_{peak}	Magnetic flux density at maximal pinning force
B_c	Critical magnetic flux density
B_{c1}	Lower critical magnetic flux density
B_{c2}	Upper critical magnetic flux density
C_p	Heat capacity
d	Constant parameter
D	Diode
E	Electric field intensity
$\mathbf{E}$	Vector field version of electric field intensity
E_c	Electric field criterion
f	Material proportion
F	Function
h	heat transfer coefficient
H	Magnetic field intensity
$\mathbf{H}$	Vector field version of magnetic field intensity
i	index
I	Current
I_{0T}	Critical current at 0 T
I_c	Critical current
J	Current density
$\mathbf{J}$	Vector field version of current density
J_c	Critical current density
J_{c0}	Critical current density at T_0
J_m	Current density in the matrix metal
J_{op}	Operation current density

k	Time step index
L	Inductance
m	Number of materials
M	Mass matrix
n	n-value of the superconductor
N	Basis function
p	Perimeter
P	Point
P_h	Heater power
Q	Heat generation
$\mathbf{Q}$	Load vector
Q_c	Maximum heat generation
Q_h	Heater energy
$\mathbf{r}$	Vector of coordinates
R_d	Dump resistor
R_{mzi}	MPZ ellipsoid radii
R_{norm}	Normal zone resistance
s	Switch
t	Time
t_h	Active heater time
T	Temperature
T_0	Initial temperature
T_b	Helium bath temperature
T_c	Critical temperature
T_{cs}	Current sharing temperature
T_{max}	Maximum hot spot temperature
T_{op}	Operation temperature
U_a	Unit step function
v_{nzp}	Normal zone progation velocity
V	Voltage
V_{MPZ}	Volume of the MPZ ellipsoid
V_s	Voltage of the current source

α	Magnetic field angle relative to tape surface
α_s	Stekly's criterion
β	Constant parameter
β_0	Constant parameter
Γ	MIITs
Γ_q	Quench tax
Δ	Difference / Distance

Δt	Time step size
λ	Heat conductivity
μ	Permeability
∇	Formal vector of partial derivatives
ρ	Resistivity
ρ_{eff}	Effective resistivity
ρ_{Cu}	Resistivity of copper
ρ_m	Resistivity of the matrix metal
θ	Generalized Euler algorithm coefficient
Θ	Generalized Euler algorithm coefficient
ϕ	Magnetic flux

AC	Alternating current
BaLaCuO	Barium-lanthanum-copper-oxide
Bi-2212	Bismuth based high-temperature superconductor
Bi-2223	Bismuth based high-temperature superconductor
CERN	The European organization for nuclear research
$CuBe_2$	Copper-beryllium
DC	Constant current (direct current)
DOF(s)	Degree(s) of freedom
EuCARD	European coordination for accelerator research & development
EuCARD2	Enhanced European coordination for accelerator research & development
FCL	Fault current limiter
FEA	Finite element analysis
FeaTHeR	Five tesla HTS research magnet
FEM	Finite element method
G-10	Fiberglass epoxy
GUI	Graphical user interface
HE-LHC	High-energy large hadron collider
HL-LHC	High-luminosity large hadron collider
HEP	High energy physics
HTS	High-temperature superconductor
ITER	International thermonuclear experimental reactor
JSON	JavaScript object notation
LHC	Large Hadron Collider
LHe	Liquid helium
LTS	Low-temperature superconductor
MERQ	Minimum energy required to quench

MgB_2	Magnesium diboride
MIITs	Units of Mega-Current^2 x Time
MPZ	Minimum propagating zone
MQE	Minimum quench energy
MRI	Magnetic resonance imaging
NbTi	Niobium-titanium
Nb_3Sn	Niobium-tin
OPIT	Oxide-powder-in-tube manufacturing method
PDE	Partial differential equation
QueST	Finite element method based quench simulation tool
REBCO	Rare earth material based superconductor
RRR	Residual resistivity ratio
SMES	Superconducting magnetic energy storage
YBCO	Yttrium based high-temperature superconductor

Chapter 1

Introduction

Although superconductivity has been known for over 100 years, commercial applications are still rare. Superconductivity is the enabling technology in magnetic resonance imaging (MRI) devices, which represent the largest single commercial application of superconductivity [22]. Another large base of users for superconductivity can be found from the Big Science projects such as ITER [95] and the Large Hadron Collider (LHC) [12, 119]. Within these projects low temperature superconductors (LTS) have been used until now in the main working compounds, such as detector magnets or coils keeping the plasma together. However, due to the urge to reach higher magnetic fields, and thus, ability to achieve higher particle collision energies, the accelerator magnet community has been starting to push frontiers also in the field of high temperature superconductor (HTS) magnets in addition to already used HTS current lead technology [5]. One possible direction for the future high-energy upgrade for the LHC (HE-LHC) is to utilize HTS materials to reach magnetic fields densities up to 20 T in the bending magnets. The concept of a 5 T HTS insert magnet has been studied in the EuCARD [114] and EuCARD2 [122] projects.

Accelerator magnets are typically characterized by high magnetic field densities and current densities. The 5 T HTS insert magnet being developed in EuCARD2 is designed to be operated in the magnetic field density of 16 T and engineering current density of up to 600 A/mm^2. As the superconducting phenomenon guarantees lossless current carrying capabilities, no heat is generated in the cable in direct current (DC) conditions. However, if the superconducting state is lost, i.e. a quench occurs, the current transfers to the copper resulting in a dangerous situation due to massive heat generation. To protect expensive superconducting magnets, the quench event has to be understood and the

quench detection and protection systems have to be designed appropriately.

Due to the high current densities, and consequently, high magnetic fields, multiple relevant scientific questions are introduced:

- Is it possible to utilize HTS magnets in accelerator magnets?
- What kind of problems are introduced from the quench detection and protection viewpoint?
- How relevant the quench protection methods of LTS magnets are for HTS magnets?

1.1 Motivation

Quench protection is an important part of the engineering R&D work of superconducting magnets. Completely new HTS magnet design, studied in the EuCARD2 project as part of the LHC upgrade plans, is difficult and expensive to manufacture. Due to the possibility to destroy the magnet in case of a quench, the numerical modelling before the measurements plays a vital role in the design process. Safe operation of the magnet system has to be ensured before initiating the upgrade of the LHC as a severe incident in the system may cause a delay of two years in the operation, due to the almost 10 000 superconducting magnets in the LHC [119].

The quench event of LTS magnets is well known and documented [156, Ch.9]. However, the quench event of HTS magnets still requires studying, even though the existence of HTS materials was discovered almost 30 years ago. Especially, when an HTS accelerator magnet is operated at liquid helium (LHe) temperature range, measurement data is almost non-existent. In these operation conditions HTS magnets behave differently in case of a quench, compared to their LTS counterparts, due to the much higher temperature margin. Due to the different nature of the quench event between HTS and LTS magnets a valid question occurs: is it possible to utilize well-known quench modelling and protection methods of LTS magnets also for HTS magnets?

The scientific contribution of this thesis comes from the investigation of the quench characteristics of HTS materials and magnets utilizing numerical modelling. We studied the possibility of the usage of HTS magnets for accelerator magnet applications. Especially, we investigated multiple quench modelling methods, previously utilized with LTS magnets, to analyze their usefulness for HTS magnets. Main research questions that this thesis answers to are:

- Are analytical methods widely used for LTS magnets suitable for HTS magnets in particle accelerators?
- How does the quench evolution differ in LTS and HTS magnets?
- How to improve numerical modelling methods for HTS magnets?
- What kind of software entity is adequate for the needs of an engineer studying quench in superconducting accelerator magnets?

Modelling a quench event in a superconducting magnet requires a multi-physical approach. One has to solve at least magnetic field and heat conduction problems, and possibly utilize different domains for different problems. As part of my doctoral studies we decided to start an in-house software development project for quench modelling. This way we were not bound by the limitations of commercial software. Another motivation to start the software development project was continuity. In many cases the work of a doctoral student is, at least partially, wasted after the studies. Here we decided to build a foundation on a platform, where the development is easy to continue afterwards.

An unfortunate shortcoming regarding the software development project is the absence of benchmarking against measurement results. Due to the delays in measurements regarding the HTS magnet designed in the EuCARD2 project the benchmark was not possible to accomplish. However, the development of the software project will continue and the simulation results will be compared to the measurement results when the measurements can be carried out.

This thesis was conducted within the Academy of Finland project "Stability Analysis of Superconducting Hybrid Magnets" and European Commission project Enhanced Coordination for Accelerator Research & Development 2 (EuCARD-2). The former project was related to the simulation tool development and its utilization on the quench modelling of the superconducting magnets. The latter project was related more to the quench modelling of the HTS research magnet.

1.2 Structure of the Thesis

This thesis begins by introducing the superconductivity as a phenomenon in Chapter 2. A quick peek into the history and the special characteristics of superconductivity are given. Then, the utilization of superconductors in particle physics is presented, where the main focus is on the accelerator magnet technology. The present technology and upcoming upgrade plans for the LHC are

presented. In the end of the Chapter the quench event of superconductors is described and the appropriate background for numerical modelling of quench is presented.

In the following Chapter we discuss the software development for quench simulations. One result of my doctoral studies is the in-house developed quench simulation software, which is presented in detail as the software was utilized in the simulations throughout the thesis. The constituents of the software and their connections, with the addition of future development areas, are explained. In the end, one particular software engineering example is presented regarding the optimization of the software.

In Chapter 4 we study how common quench characteristics differ in HTS compared to their LTS counterparts. First, the normal zone propagation in HTS magnets is studied computationally and the difference of quench event between LTS and HTS is discussed. Then, widely used analytical approaches for LTS are compared to the numerical simulations, and their usefulness for HTS is discussed. Especially, hot spot temperatures and minimum quench energies are studied in detail. Furthermore, throughout the Chapter, viewpoints to quench measurements are expressed based on the simulations.

In the 5th Chapter quench simulation is scrutinized for an HTS research magnet design. In the beginning the studied case is presented and issues related to quench simulation, especially regarding the quench initiation and reduction of modelling domain, are discussed. Then, the quench simulation results for the magnet are presented and conclusions are drawn.

Finally, in Chapter 6, the summary of the work is presented and conclusions are drawn.

Chapter 2

Background

This chapter presents the basic framework for this thesis. As the superconductivity is the phenomenon that is underlying the studies that are presented in this thesis, first the history and basic properties of superconductivity are presented. There are different ways to classify superconductors, which is done to demonstrate different aspects of superconductivity and its usability in commercial and scientific areas. Later, stability aspects and the quench event in superconductors are introduced. In addition, the background for numerical modelling of the quench event is presented as this is the area of interest to be developed during the thesis.

2.1 Superconductivity

2.1.1 History of superconductivity

The discovery of superconductivity can be tracked back to the measurements of Heike Kamerlingh Onnes in 1911 [102]. The main interest of Onnes was cryogenics and especially the liquification of helium. Utilizing liquid helium Onnes measured resistivity of various metals also in pressurized conditions which decrease the temperature of helium boiling point. While doing these measurements the superconductivity was discovered by accident, and at first was recognized as a short circuit. After multiple measurements Onnes was convinced that there exists no voltage, while current being present, in his mercury sample and a new phenomenon called superconductivity was discovered.

The first important property of superconductivity, total loss of resistivity, was observed on other materials as well by Onnes. He discovered, that under

a certain, material dependent, critical temperature, T_c, in addition to mercury also tin, lead and indium were able to transport current without Ohmic losses. Later it was discovered, that the superconductivity can also be a property of ceramics [8] and iron-based alloys [57] in addition to metals. Second property of superconductivity, the Meissner effect, was discovered in 1933 by Meissner and Ochsenfeld [41]. Meissner effect means that the superconductor repels the exterior magnetic field completely. As opposed to the ideal perfect conductor there exists no magnetic flux density ($\mathbf{B}$) inside the conductor even in a case where the cooling to the superconducting state is performed within an external field.[1]

After its discovery by measurements, the complete theory for superconductivity was first introduced by Bardeen, Cooper and Schrieffer [6] in the 1950s. The BCS theory, named after its founders, described the superconductors at the quantum level and predicted that the maximum possible T_c is 30 K. For a long time the BCS theory was regarded as the perfect theory for superconductivity, however, almost 30 years later Bednorz and Müller discovered a ceramic superconductor in the BaLaCuO system, which had a slightly higher T_c than 30 K [8]. After the discovery by Bednorz and Müller, the maximum T_c of 30 K estimated by BCS theory was utilized as a divider between superconductors: low-temperature superconductors (LTS) with T_c of less than 30 K and and high-temperature superconductors (HTS) with T_c of more than 30 K. Furthermore, the research for materials with higher T_c sky-rocketed with the optimistic objective of discovering a superconductor that could be utilized at room temperature [91].

While being discovered over 100 years ago, the commercial applications utilizing superconductivity are still rare. The most attractive application commercially is the magnetic resonance imaging (MRI) [83] which accounted for almost 80% of all the superconductor market in 2014 [22]. The second largest account was by far, with 19% in 2014, different R&D projects and Big Science projects, which include particle accelerator magnets [59, 93, 103] for example, where the superconductivity act as an enabling technology. In both of these areas LTS technology has been the natural choice for decades due to the longer development work, which translates into the market share of 99% of the superconducting market. However, due to the urge to push forward to larger magnetic flux densities, in the range of 20 T, in Big Science projects such as in the successor of Large Hadron Collider (LHC) [12, 119] and within the ITER project [95], the share of HTS technology will rise in the coming decades.

[1] However, the magnetic flux density is repelled completely only with extremely small values of B.

Other potential large scale superconducting applications include power cables [85, 86, 142], fault current limiters (FCL) [79, 142, 159], wind turbine generators [1, 108, 142], transformers [37, 74, 76], induction heating [124] and superconducting magnetic energy storage (SMES) [17, 51, 113, 142], to name a few. The commercialization of these technologies is still work in progress partly due to the existing more reliable technology being present.

2.1.2 Critical quantities

When discovering superconductivity, Onnes noticed the total loss of resistance of a mercury sample when the operation temperature decreased below its T_c, 4.15 K. However, temperature is not the only critical quantity. The surface defined by T_c, critical magnetic flux density B_c and critical current density J_c defines if the material is in the superconducting state or not. Critical surface for a flat HTS tape is presented in figure 2.1. It is notable that the operation near T_c, for example, is impossible in practical applications due to the extremely low values of B_c and J_c. Engineers work with these quantities to design a device that exploits the quantities in a best possible way for the application. On the other hand material scientists work to improve all the critical quantities to ease the engineering work.

In addition to the magnitude of $\mathbf{B}$, $||\mathbf{B}||:=B$, the angle of $\mathbf{B}$, (α), can also have an influence on the critical surface. This is called anisotropy of the superconductor that is present especially on textured thin films and on flat tapes. For example the critical current density in bismuth-based $Bi_2Sr_2Ca_2Cu_3O_x$ (Bi-2223) and in Yttrium-based YBCO tapes is highly anisotropic [63, 67]. However, a round wire can be manufactured from $Bi_2Sr_2CaCu_2O_x$ (Bi-2212), where anisotropy is not present [72]. It is notable though, that the anisotropy always exists in crystal level [146].

If superconducting tape is manufactured from an anisotropic material, the tape is textured such that the critical current is the highest when $\mathbf{B}$ is parallel to the tape's wide surface (0°) and lowest when it is perpendicular to the tape's wide surface (90°). Figure 2.2 illustrates the orientation of $\mathbf{B}$ towards the tape surface. Anisotropy needs to be taken into account when designing a device as J_c can be less than half of the maximum J_c when $\mathbf{B}$ is perpendicular to the tape surface as presented in figure 2.1.

The resistive transition is instant, when the critical surface of figure 2.1 is breached, only for ideal superconductors. According to Bruzzone [16], Walter suggested in 1974 that the relationship between the magnitude of electric field ($||\mathbf{E}||$) and current density ($||\mathbf{J}||$), which are assumed parallel in this work,

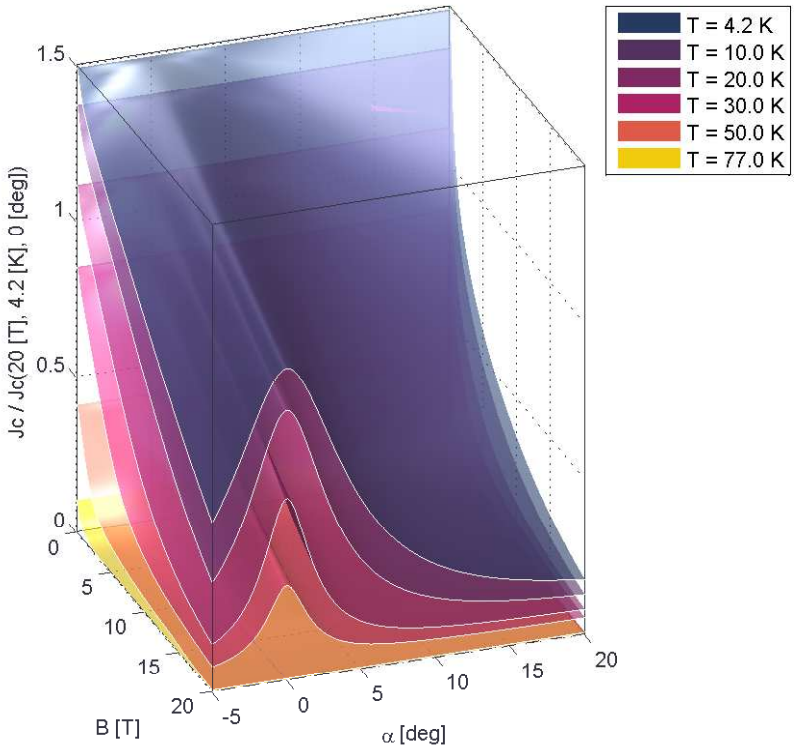

Figure 2.1: The critical surface for an HTS material where the tape anisotropy is illustrated with field angle α.

in a superconductor can be characterized utilizing a power-law [156]

$$E = E_c \left(\frac{J}{J_c} \right)^n , \tag{2.1}$$

where E is the magnitude of the electric field, E_c is the critical electric field, n is the n-value and J is the magnitude of the current density, respectively. This was based on macroscopic observations that the transition from the superconducting state to the normal state happens rapidly but not instantly. Typical values for E_c are 0.1 and 1 μV/cm [30, 46].

Superconductor index number n, also called the n-value or the exponent n, in (2.1) represents the steepness of the resistive transition [156]. For ideal superconductor the n-value is infinite, and the transition to the normal conducting state is instant. In reality the n-value is finite, which means that there

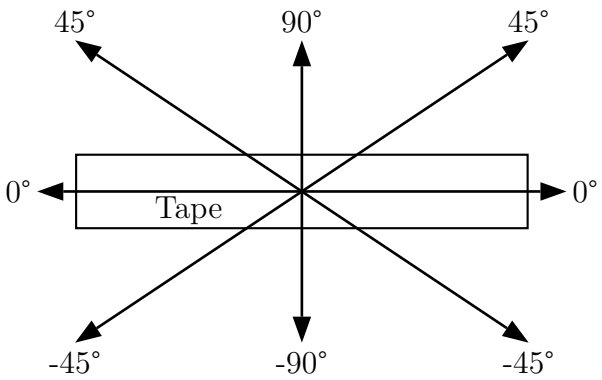

Figure 2.2: Description of the angular dependency of **B** for flat tape superconductors.

is Joule heat generation even with subcritical currents due to E and J being present simultaneously. However, this also means an opportunity to operate a short period of time with a current density that is above J_c. Figure 2.3 presents the E-J relation with different values of n and the relation of a ideal superconductor.

2.1.3 Classification of superconductors

Superconductors can be classified in multiple ways. One is to classify them according to their T_c as described earlier. Another possibility, that was utilized before the superconductors with high T_c were discovered, is to classify superconductors according to their ability to tolerate applied magnetic fields. Furthermore, different types of superconductors have different capabilities and properties. Here we present the different classifications for superconductors and describe the most common superconductors at the moment.

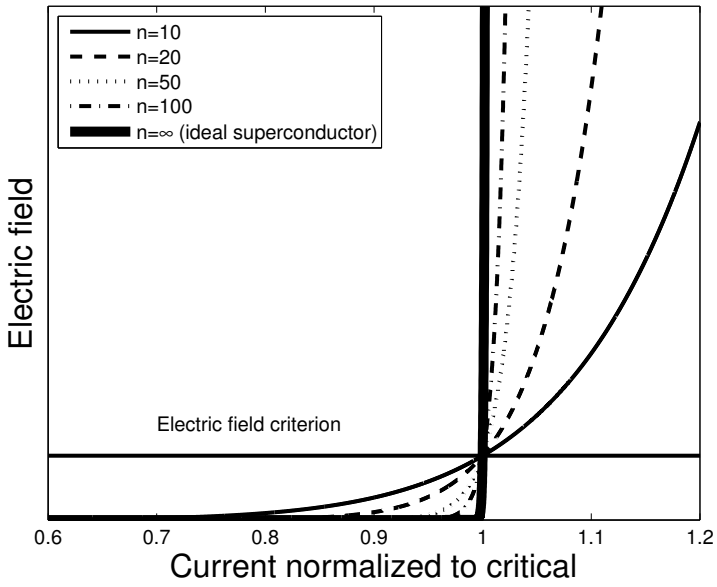

Figure 2.3: Schematic view of the resistive transition.

Type I and type II superconductors

In type I superconductors the magnetic flux density cannot enter the superconductor excluding a very small surface layer. However, after the applied magnetic flux density increases over the critical value B_c [24, p.28-30] the superconducting state is lost. For type I superconductors B_c values are in the order of 10 mT [93, p.12-13], which makes them extremely unattractive even for moderate field applications [115, p.46].

Type II superconductors, on the other hand, have two critical magnetic flux densities: the lower B_{c1} and the upper B_{c2} [24, p.29-33]. Below B_{c1} type II superconductor behaves similarly to the type I superconductor generating shielding currents on the edge of the conductor and repelling the applied magnetic flux density. After exceeding B_{c1} the magnetic flux can penetrate into the superconductor in quantized flux vortices. The superconductor keeps the ability to transport lossless current even though the flux vortices form normal conducting zones inside the superconductor. When the upper critical field B_{c2} is reached the superconductivity is lost due to the vortices penetrating entire volume of the material [93, p.13-17].

Type II superconductors are much more promising for applications due to

B_{c2} being in the range of Teslas for common superconductor materials [148]. For example, NbTi based MRI machines operate typically in magnetic field of 1.5 T or 3 T [23]. However, when a type II superconductor is exposed to the magnetic field, the Lorentz force is applied to the flux vortex when a current is flowing in the conductor, moving the vortex through the material and generating heat. This phenomenon, called flux flow resistance, means that type II superconductors can generate heat even with direct current (DC) when they are subject to the magnetic field [61]. However, the flux movement can be significantly reduced by introducing anomalitites, so-called pinning centers, in the superconducting material. Flux vortices get stuck to these pinning centers and remain in place even when the Lorentz force is applied to them. Thus, it is profitable to add impurities to the superconducting material in the manufacturing process to increase the current carrying capacity of the conductor [132, p.82]. However, when the current in the superconducting material increases, the flux vortices are detached from the pinning centers with increasing pace. Moderate increase in electric field is observed before reaching the critical current, after which the increase becomes exponential. The power-law illustrates this effect in figure 2.3. Type II superconductors with pinning center are called hard superconductors [93, p.17-23]. Hard superconductors are extremely interesting from applications point of view, as they have high enough critical quantities including B_{c2} to be utilized in applications. Superconducting materials studied in this work are hard superconductors, and thus, from now on we use notation B_c in place of B_{c2}.

LTS and HTS superconductors

Another criteria to classify superconductors is their T_c. LTS materials are generally metallic compounds and have $T_c \leq 23.3$ K [97]. Several type II LTS superconductors have B_c up to 10 T but the commercial applications are limited to mainly two materials: niobium-titanium (NbTi) and niobium-tin (Nb_3Sn) alloys [148]. NbTi is used in low field applications like field coils of MRI devices and the dipoles in the present LHC. Nb_3Sn on the other hand is used in place of NbTi if larger J is required in combination with higher B. NbTi materials can be commercially manufactured in long lengths [81] with low cost. Manufacturing a magnet using NbTi is easy because it is strong and ductile material [148] and it is possible to apply the heat treatment to the NbTi material and then wind the magnet, which is the so-called *react-and-wind* method. Nb_3Sn magnets on the other hand are more difficult to manufacture due to the brittle nature of reacted Nb_3Sn material, and thus, Nb_3Sn magnets are often built using the opposite, *wind-and-react*, method [25, 71]. The main

characteristics of NbTi and Nb_3Sn are listed in Table 2.1.

HTS materials are ceramic compounds or newer iron-based alloys [57] with T_c higher than 30 K. The most important HTS materials today are bismuth-based BSCCO (Bi-2223 and Bi-2212), YBCO and magnesiumdiboride (MgB_2). Despite their extremely high T_c the main disadvantages are difficult conductor fabrication compared to the LTS materials and relatively low field performance in high temperatures [148]. BSCCO conductors are fabricated in tape geometry utilizing the oxide-powder-in-tube (OPIT) method [129] while the coated conductor technology is utilized with YBCO [47]. Due to the low field performance of LTS magnets compared to HTS magnets, one of the most interesting application for HTS magnets is accelerator magnets where the HTS magnet can be used as an insert for an LTS outsert with the operation temperature of 4.2 K [26], which is the main topic of this thesis. HTS conductors have also been used as current leads for reducing the heat leak to applications operating below 30 K [87]. MgB_2 is an interesting material between LTS and HTS materials. It has a T_c of 39 K, thus considerably higher than LTS materials, but still below liquid nitrogen region [148]. However, as presented in Table 2.1, B_c and J_c are not yet at the required levels to challenge LTS or HTS materials but MgB_2 has the advantage of being a cheap common material with low manufacturing costs.

Table 2.1: Most common superconducting materials and their critical quantities. Anisotropy means the relative difference of J_c when the orientation of applied **B** is varied. Data for the table is taken from [148].

Material Type	Material	T_c(K)	Anisotropy	J_c(A/cm^2)	B_c(T)
LTS	NbTi	9	Negligible	$\sim 10^6$	11-12
LTS	Nb_3Sn	18	Negligible	$\sim 10^6$	25-29
HTS	MgB_2	39	1.5-5	$\sim 10^5$	15-20
HTS	Bi2223	110	50-200	$\sim 10^7$	>100
HTS	YBCO	92	5-7	$\sim 10^6$	>100

2.1.4 Particle accelerator magnets

Particle accelerators are devices that accelerate electrically charged particles to high velocity and then collide two such bundles of particles. In circular accelerators, superconducting magnets are required to produce very high mag-

netic fields with very high quality to control the trajectories of charged particles [128]. In this thesis we focus only on circular particle accelerator magnets used in High Energy Physics (HEP), and especially to the Large Hadron Collider (LHC) and the future upgrades under consideration. However, it is notable that particle accelerator magnets are used also in other areas, such as in isotope creation for medical imaging, radiotherapy for cancer treatment and basic material and chemistry research [2]. Also, other accelerator types than circular synchrotrons exist [153].

For HEP purposes particle accelerators are used as colliders. The particles are accelerated to very high velocities, so that their energies are in the GeV or TeV range. Then they are collided against each other in the so-called detector magnets[2], where the high energy density localized in the collision provides a possibility for new particles to emerge [128]. The ambitious goal is to discover the building blocks of the universe which would lead to a more comprehensive understanding how the universe was formed in the beginning.

In circular accelerators the particles are controlled utilizing magnetic fields of different shapes: dipole fields bend the particle trajectories and the quadrupole fields keep the particle bundles focused [93]. The energy density of the collision and the maximum mass of the particles to be created depends on the sum of the kinetic energy of the colliding particles. Even though the dipoles and quadrupoles already are characterized with long lengths, high fields, high current densities and high stored energies, the urge to push for discovery of new particles requires higher energies for colliding particles. In a circular particle accelerator the maximum energy of the particle is proportional to the dipole fields that is available to exert the bending force [152, p. 39]. Therefore, in order to increase the energy of the collisions the magnetic field of the dipoles have to be increased, or alternatively a particle accelerator machine with a larger diameter has to be built.

The LHC at CERN is a 27 km long synchrotron collider installed in a tunnel with a diameter of 4 m about 90 m underground [14, 15, 118]. The magnet system operates at 1.9 K by means of superfluid helium and there are 1232 main dipoles each about 15 m long producing a magnetic field of approximately 9 T at nominal operation current 11 850 A [116]. The design value for the beam energy is 7 TeV. The next upgrade for the LHC is the so-called high luminosity upgrade around 2020, where the present NbTi technology will be replaced with Nb_3Sn magnets at the interaction region just before the collisions to improve the beam focusing and hence increase the luminosity at the collisions [121, 123, 160]. Only the interaction region quadrupole magnets are replaced, since the

[2]ATLAS, for example, is a detector magnet in the LHC [58]

energy of the LHC ring will be kept at the design value, thus there is no need to replace the NbTi dipoles.

The high-energy upgrade for LHC (HE-LHC) is designed to increase the beam energy up to 16.5 TeV by increasing the magnetic field up to 20 T by 2030 [120].[3] There are still multiple possible scenarios how to execute the upgrade. One possibility is to utilize Nb_3Sn magnets which are able to withstand magnetid fields up to 15 T. The other option is to manufacture hybrid magnets where the NbTi is utilized in low field region, Nb_3Sn magnets in intermediate field region and HTS magnet in the high field region [143]. HTS magnets can withstand magnetic fields higher than 15 T, however, they are 3-5 times more expensive than LTS magnets [48, 120], thus, it is not feasible to exploit exclusively in HTS magnets. Figure 2.4 presents the critical current densities as a function of applied magnetic field for materials to be utilized in HE-LHC for the future upgrade.

Preparing for HE-LHC upgrade a program called European Coordination for Accelerator Research & Development (EuCARD) was started in 2009 [114]. The subject of work package 7 (WP7) of the EuCARD project was to develop high field magnets in the range of 13-20 T. A very high field HTS insert magnet study was part of the WP7, where possibilities to utilize an HTS insert inside an LTS outsert, namely FRESCA II [94] were studied. The continuation of EuCARD is the EuCARD-2 project, which started in 2013 [122]. The aim of WP10 in the EuCARD-2 project is to design and manufacture an HTS insert producing 5 T magnetic field in stand-alone operation. This thesis is partially conducted within the EuCARD and EuCARD-2 projects. In particular, the stability and protection analysis of the HTS insert designs in these projects is included in this thesis.

2.2 Stability and quench

In superconductor technology stability refers to maintaining the superconducting state. Thus, when the stability is lost, the superconducting material shifts into the normal conducting state. This event is called quench. A quench is usually an undesirable event, even though FCL devices exploit the quench event in their normal operation [98]. Stability sets the limits of framework for engineers to design superconducting devices. Even when the device is designed to operate in extremely stable conditions, the quench protection has to

[3] High luminosity upgrade is scheduled to be implemented, however, the high-energy upgrade is still at the conceptual design phase.

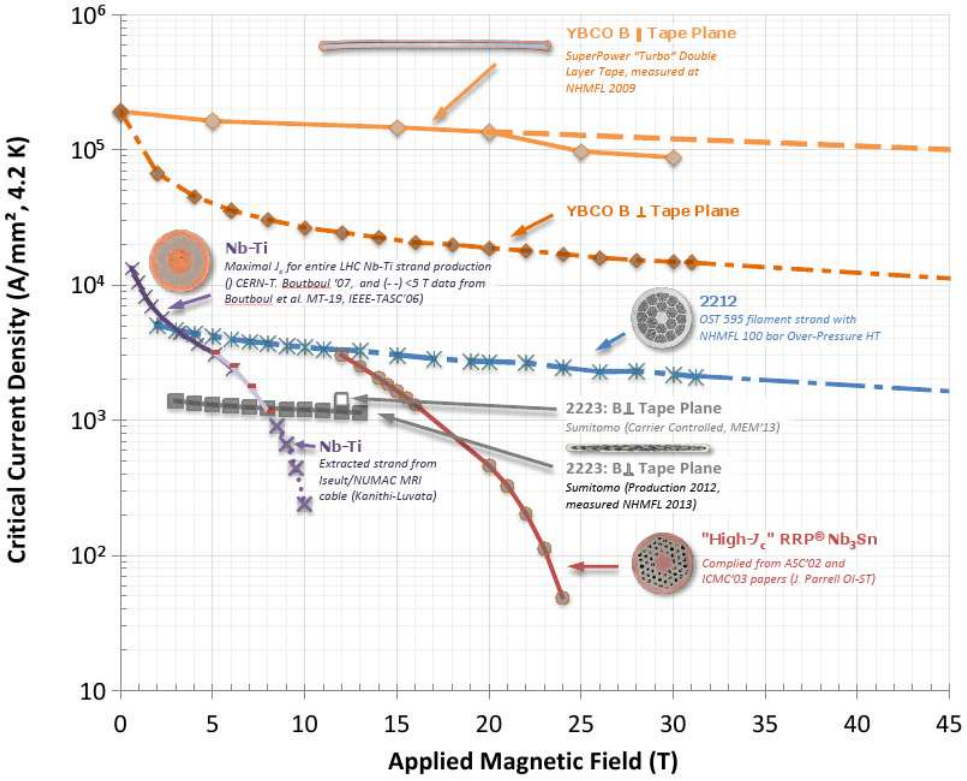

Figure 2.4: Critical current density as a function of applied magnetic field for materials to be utilized in HE-LHC [75].

be considered due to the large expenses in case of a damaged device due to the quench. In this section we present superconductor stability aspects and different classifications of quenches. In the end basics of numerical modelling of the quench event are presented, which are utilized throughout the thesis.

2.2.1 Stability aspects

Superconducting magnets may not achieve the design current based on the short sample measurements[4]. There exists two causes of instability, which force the magnet to be operated by a lower operation current than its short sample characterization would indicate: magnetic and mechanical instability [154].

[4]By short sample measurements we mean measurements done to short pieces of superconductors.

Magnetic instabilities and flux jumps are to be considered in all magnets manufactured from type II superconductors. Basically the instability arises from two properties of type II superconductors. First, the motion of flux dissipates heat within the conductor. Second, J_c decreases with increasing temperature, which in return generates flux motion. Figure 2.5 presents the chain of events which eventually leads to a quench. It is notable, that this chain of events may begin from any part of the figure, but the result is the same, a quench. [154, 156]

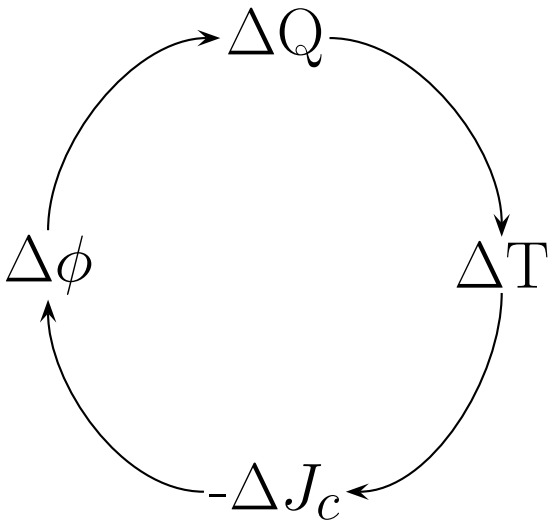

Figure 2.5: Chain of events eventually leading to a quench.

Degradation of coils, meaning premature quench considerably before the short sample critical current, is caused by mechanical disturbances [13]. Mechanical disturbances may occur, for example when the conductor moves due to the electromagnetic forces within the magnet and friction generates heat [53]. Thus, it is of common practice to eliminate the conductor motion by impregnating the winding with organic materials, most notably epoxy resins [28, 68, 134]. In these epoxy-impregnated magnets another source of mechanical disturbance emerges: epoxy fracture [53].

The first cure for instabilities and coil degradation was cryogenic stabilization presented by Stekly [135]. In this method a sufficient amount of normal conductor was placed in parallel with the superconductor to ensure it can carry

the excess current. Naturally, the electrical resistivity of the normal conductor was to be as low as possible, and thus, copper became a popular choice. This normal conductor is called matrix metal. According to Stekly's criterion if a normal region is formed it will always recover if $\alpha_s \leq 1$, when

$$\alpha_s = \frac{f^2 J_c^2 \rho_{Cu}}{(1-f)h(T_c - T_b)} \cdot \frac{A}{p}, \tag{2.2}$$

where ρ_{Cu} is the copper resistivity, f is the fraction of superconductor on a conductor cross-section, A cross-sectional area, p cooled perimeter, h heat transfer coefficient and T_b helium bath temperature. However, in reality cryogenic stabilization is not feasible for actual magnets due to the large necessary amount of matrix metal which increases the weight and cost of the magnet and decreases the overall current density. Thus, the advantages of using superconducting material in the magnet is partly negated.

Another form of stabilization is fine subdivision of superconductors to smaller filaments. Subdivision of superconductors does not contribute against mechanical disturbances, however, it reduces the amount of flux jumps considerably [154]. The improvement is twofold. Decreasing the superconductor filament size translates into smaller energy release in case of a flux jump. In addition, a better cooling in the conductor is possible if the superconducting filaments with low thermal conductivity are spread within the matrix metal.

As the cryogenic stabilization is not appropriate method to design superconducting magnets there is a need for method to approximate disturbance energies in different operation conditions. One of these methods is the minimum propagating zone (MPZ) introduced first by Martinelli and Wipf [89] and demonstrated later with computations and experiments by Wilson and Iwasa [155]. MPZ is the smallest normal conducting volume within the magnet that causes a propagating normal zone leading to a quench [156]. A conceptual drawing to illustrate the MPZ ellipsoid is presented in figure 2.6.

MPZ is created by the energy that equals to the minimum quench energy (MQE) [156]. The energy can be originally from any source, whether mechanical or magnetic in origin. When the MPZ is emerged in the superconductor, it propagates with a certain speed called the normal zone propagation velocity (v_{nzp}). Simulations and measurements of v_{nzp} are extremely important when studying quench dynamics because with a slower v_{nzp} the stored energy is dissipated in a smaller volume in the magnet, thus, causing higher hot spot temperature than with faster v_{nzp}. In addition, especially in HTS magnets due to the slow v_{nzp} the hot spot will remain localized [65, 104], increasing mechanical stresses due to the large temperature gradients which may lead to a damaged magnet [69, 141, 158].

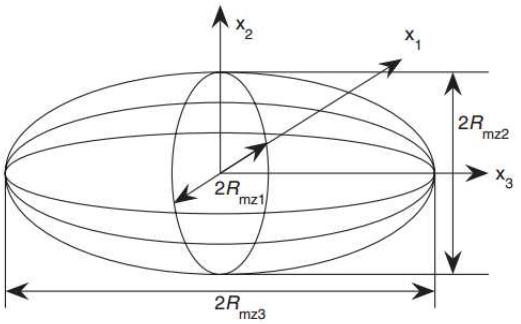

Figure 2.6: Normal zone ellipsoid.

Quench characteristics are different for LTS and HTS magnets as presented in Table 2.2. LTS magnets typically have low thermal margin and MQE, which makes them prone to quench. However, due to their extremely high v_{nzp} their protection is easier because larger volume of the magnet winding is dissipating the stored energy. In addition, the quench detection in LTS magnets is straightforward by measuring the voltage over the normal zone, which increases rapidly due to the fast v_{nzp}. HTS magnets on the other hand are extremely stable due to the high thermal margin and MQE but the quench detection and protection is difficult because of the slow v_{nzp}. In this thesis we model different quench scenarios and stability aspects for HTS accelerator magnets. In addition, we test techniques, that are widely used for LTS magnets, and evaluate their usability with HTS magnets.

Table 2.2: Comparison of quench characteristics of LTS and HTS magnets [52, 101, 107].

Quantity	**LTS**	**HTS**
Quench Process	Normal zone propagation	Temperature rise and "thermal runaway"
v_{nzp}	up to hundred m/s	several cm/s
Thermal margin	few K	several decades K
MQE	∼mJ	∼J
Typical n-value	>40	10-40

2.2.2 Classification of quenches

As described before, the quench is the event when the stability is lost. However, there are several possible reasons for losing stability, thus, it is important to detect and analyze the reason for quench to improve the performance of the device in the future. Classification of quenches was presented by Arnaud [27] and Wilson [156, p. 70]. Here we present these two classifications that estimate how the undesirable quench event originated in the magnet.

Devred's classification of quenches

Devred classified quenches according to the operation current of a magnet related to the conductor short sample measurements. Thus, measurements for a magnet are required to classify what type of quenches occurred. If a quench occurs at the operation current defined by the critical surface, a conductor-limited quench has occurred. If the quench happens at the same critical current I_c as predicted by the short sample measurements, a short sample quench occurred. However, if the quench happens at a lower I_c, the magnet has been degraded. Some degradation is common in superconducting magnets due to the mechanical load during the winding process, and thus, the short-sample quench is difficult to reach but good magnets reach more than 95% of the short-sample limit [137]. Figure 2.7 illustrates the conductor-limited, short sample quenches and how the degradation effects the magnet.

If, however, the quench occurs at considerably lower current than the critical surface predicts, it is typically due to an energy release in the coil. The energy release initiates the chain of events presented in figure 2.5, which eventually leads to a quench. In addition, in HTS magnets one type of premature quench may also occur due to the local degradation of the HTS tape. Thus, there exists an area with considerably lower J_c generating heat within the magnet leading to a quench [66, 151].

In figure 2.7 the inclined ellipse presents an area, where premature quenches occur but with increasing operation current. This behaviour illustrates training of the magnet. Training is an effect, where the magnet is quenched multiple times to release the energy, that is stored in the manufacturing phase to the magnet due to the mechanical stresses. When these energies are released, the magnet approaches the short sample quench limit.

Devred's classification mainly separates quenches that occurred due to the excessively high operation currents or without a clear explanation. It is used to determine if the magnet is manufactured properly or degraded during the

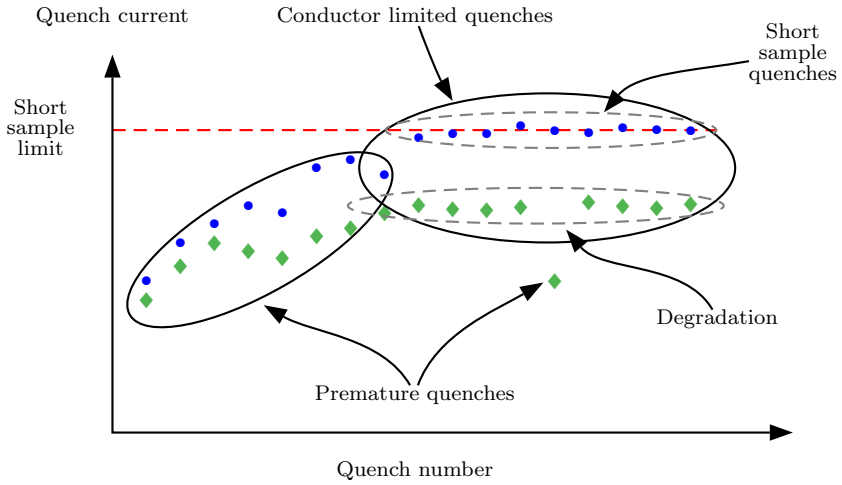

Figure 2.7: Quench history of two fictitious magnets. Quenches are classified according to the Devred's classification. [137]

manufacturing process. In addition, the training behaviour is illustrated clearly with the Devred's classification by creating a figure presented in figure 2.7 according to the characterization.

Wilson's classification of quenches

Wilson classified quenches based on the type of disturbance that caused a quench. Thus, all quenches are due to the energy release in the coil. Wilson divided quenches in space and time. Then, in space quenches were divided to point and distributed quenches and in time to transient and continuous quenches. Table 2.3 presents the disturbance spectrum and what kind of energies or powers are related to the disturbance category.

Table 2.3: Disturbance spectrum in Wilson's classification of quenches. [156]

		Space	
		Point	*Distributed*
Time	*Transient*	Joules	Joules/m^3
	Continuous	Watts	Watts/m^3

Continuous disturbances are caused by steady power input to the winding.

Slowly the temperature rises in the magnet causing a detectable quench. A continuous point disturbance can be clearly located and is caused possibly due to a bad joint or degradation of the wire. Distributed disturbances could be caused by excessive alternative current (AC) losses [49], heat leaks, mechanical hysteresis effects or by dissipative losses close to J_c, as power-law describes. These continuous disturbances cause a quench if the cooling cannot balance the heat generated by the disturbance.

Transient disturbance is an event that typically happens only once, and is difficult to predict. Flux jump is an example of a transient disturbance, but the spatial classification is difficult. Flux jump is located in a point, however, there are flux jumps, at different time instants, distributed in the coil volume. Another possible source for transient disturbances is mechanical in nature. A crack in the epoxy and release of the energy due to the training are located in a point causing a transient quench.

Usually quenches of transient nature are hard to prepare for. The quench detection and protection system has to be designed in a way, that a controllable and safe quench is possible in case of a transient quench. Continuous disturbances are typically avoided by designing a magnet in a way that AC losses or joints do not generate heat over the cooling systems capacity. Quench modelling is crucial to understand and predict the generated heat due to the continuous disturbances. In this thesis we study quench of HTS magnets by applying continuous disturbances and analyzing its effects on the magnet.

2.2.3 Numerical modelling of quench event

Quench simulation is a crucial task when designing a superconducting magnet. The most important outcome from the quench simulation is the temperature evolution and the normal zone resistance within the magnet during the quench. According to the quench simulation results, the detection and protection system of the magnet can be designed in a way that a safe operation of the magnet is ensured. Furthermore, the usability of the designed protection system may be demonstrated by including the protection system utilizing a circuit model in the quench simulation tool.

Quench modelling, in general, is divided into two popular approaches. First quench modelling method is related to model how the normal zone propagates within the magnet volume. This method was first introduced by Wilson [156], however, similar work has been continued also by others [117]. Second popular method is to solve the heat diffusion equation within the magnet volume using numerical methods, mainly finite element method (FEM), difference method

or a method based on solving thermal network model [31, 32, 35, 136, 130, 131, 157]. These approaches include both the commercial tools for solving general technical problems and home-made tools tailored for specific problems. But, this is not all. A quench simulation tool requires also at least magnetic fields and circuit analyses.

Heat diffusion equation

We have taken the approach to solve for the heat diffusion equation within the modelling domain (Ω) utilizing FEM. The heat diffusion equation, as presented in [111], can be written as

$$\nabla \cdot \lambda(T)\nabla T + Q(T, \mathbf{B}) = C(T)\frac{\partial T}{\partial t}, \tag{2.3}$$

where λ is the effective heat conductivity, T is the temperature, Q is the volumetric heat generation and C the volumetric heat capacity. Three different components can be seen in (2.3). The first term reflects the heat conduction, the second term the heat generation and the last term the local temperature time variation.

The volumetric heat generation in a superconducting magnet can be computed according to the current sharing model presented in [156, p.78]. In a superconductor above the critical current, the current is divided between the matrix metal and the superconductor. Due to the higher resistivity of the superconductor, the superconductor will continue to carry its critical current, while all the excess current transfers to the matrix metal. Thus, a longitudinal electrical field is set up, which is determined by the matrix metal resistivity and the operation current. Due to being parallel in the conductor, superconductor will always match this electrical field set up by the matrix, thus, heat is generated in both the matrix and the superconductor. Now Q is computed as

$$Q = fJE = \frac{f^2 J \rho_m [J - J_c(T)]}{1 - f}, \tag{2.4}$$

where ρ_m is the resistivity of the matrix metal. If one assumes that J_c varies linearly with temperature, i.e.

$$J_c(T) = J_{c0}\frac{T_c - T}{T_c - T_0}, \tag{2.5}$$

where T_0 is the initial temperature and J_{c0} the critical current density at T_0. Combining (2.4) and ((2.5)) one gets

$$Q(T) = \frac{\rho_m f^2 J}{(1 - f)}\left(J - J_{c0}\frac{T_c - T}{T_c - T_0}\right). \tag{2.6}$$

However, as described in [156, p.74], the ohmic heat generation starts when the temperature has risen to the current sharing temperature (T_{cs}), which is located between T_0 and T_c. Assuming linear slope of J_c with T, T_{cs} is computed as

$$T_{cs} = T_c - (T_c - T_0)J/J_{c0}. \tag{2.7}$$

When one combines equations (2.6) and (2.7) one gets for the heat generation

$$Q(T) = \frac{\rho_m f^2 J^2}{(1-f)} \frac{(T - T_{cs})}{(T_c - T_{cs})} = Q_c \frac{(T - T_{cs})}{(T_c - T_{cs})}, \tag{2.8}$$

where Q_c the is the maximum value of heat generation. Thus, the heat generation rises linearly from zero at T_{cs} to a maximum at T_c, when all the current is flowing in the matrix.

Another model to compute the volumetric heat generation is to compute Joule heat generation according to

$$Q = \rho_{eff} J^2, \tag{2.9}$$

where ρ_{eff} is the effective resistivity of the cable. Effective resistivity can be computed by assuming the materials of the cable being in parallel as shown in [136]

$$\frac{1}{\rho_{eff}(T)} = \sum_{i=1}^{m} \frac{f_i}{\rho_i(T)}, \tag{2.10}$$

where f_i volumetric fraction of the material i and $\rho_i(T)$ resistivity of the material i and m number of materials. In this approach the superconductor resistivity is computed utilizing the power law [16, 77]

$$\rho(\mathbf{B}, T, J) = E_c \frac{\|J\|^{n(\mathbf{B},T)-1}}{J_c(\mathbf{B}, T)^{n(\mathbf{B},T)}}. \tag{2.11}$$

Therefore, to solve ρ_{eff} locally at given T and J, one needs to solve a non-linear equation.

Magnetic flux density distribution

Solving $\mathbf{B}$ everywhere in the modelling domain is required for quench simulation for multiple reasons. First of all J_c is a function, among other variables, of B and α. Second, B is also required for input for some of the material parameters, such as the magnetoresistivity of copper [60].

For solving the magnetostatic problem we started from the Maxwell's equations: Gauss's law for magnetism, Ampére's law and constitutive law, which are, respectively, presented as

$$\nabla \cdot \mathbf{B} = 0, \tag{2.12}$$

$$\nabla \times \mathbf{H} = \mathbf{J}, \tag{2.13}$$

$$\mathbf{B} = \mu \mathbf{H}, \tag{2.14}$$

where $\mathbf{H}$ is the magnetic field intensity and μ is the permeability [19]. With the magnetic vector potential $\mathbf{A}$, which is defined, according to [19], as

$$\nabla \times \mathbf{A} = \mathbf{B}, \tag{2.15}$$

one can derive (2.12)-(2.15) into single partial differential equation (PDE)

$$\nabla \times \frac{1}{\mu} \nabla \times \mathbf{A} = \mathbf{J}, \tag{2.16}$$

from which $\mathbf{A}$ can be solved.

However, the solution of $\mathbf{A}$ is not unique unless a gauge condition defining its divergence is introduced [9]. To achieve uniqueness one can utilize the tree gauge, for which tree has to be selected in the graph defined by the finite element mesh and then set the degrees of freedom corresponding to those edges to zero [3, 9].

Circuit model

Circuit analysis is required to study the current decay. The expected outcome is the current decay curve, which gives the information how fast the magnet can be de-energized after the quench detection has been successfully accomplished. Figure 2.8 presents an electric circuit of a superconducting magnet where a quench protection branch with a dump resistor is located in the middle. Here we present one possible method to apply quench protection system for quench modelling which is based on [156].

During the normal operation of the magnet, switch s is closed and the normal zone resistance of the magnet R_{norm} is 0 Ω. When the quench initiates the normal zone starts to propagate and consequently R_{norm} increases. Typically quench detection system measures the voltage over the magnet, thus, when the R_{norm} increases over the quench detection threshold voltage the quench protection will be enabled. The quench protection system opens switch S and

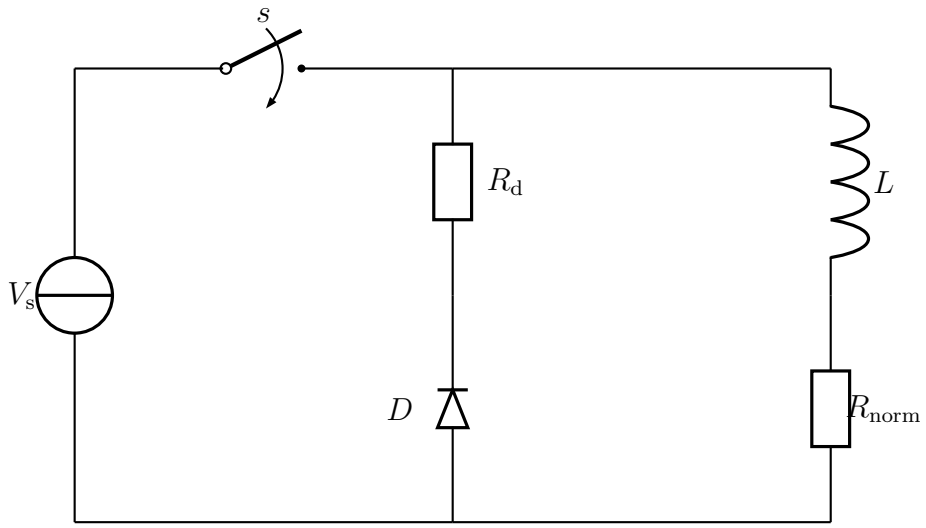

Figure 2.8: Electric circuit of a superconducting magnet including quench protection.

the current flows through the protection circuit consisting of diode D and the dump resistor (R_d).

According to Kirchhoff's voltage law, when the switch is closed

$$L\frac{dI}{dt} + IR_{norm}(t) = V_s, \tag{2.17}$$

where L and V_s are the inductance of the magnet and the voltage of the current source, respectively. When the magnet quenches and the switch opens, the Kirchhoff voltage law turns into

$$L\frac{dI}{dt} + I(R_{norm}(t) + R_d) + V_d = 0, \tag{2.18}$$

where V_d is the diode threshold voltage.

Chapter 3

The quench simulation tool

The base for the research of this thesis is the C++-language based quench simulation tool, QueST (Finite Element Method based **Que**nch **S**imulation **T**ool), that I developed during my doctoral studies. The simulation tool was used for the computations in all the publications included in this thesis. The motivation for the development of an in-house simulation tool was the result of an idea to have a dedicated tool for quench simulations which would allow to have a freedom within the code to modify all parts of the code, which is not possible with commercial softwares.

GMSH[1] [43] was a natural choice as the platform for QueST as my research group had experience in developing with it. The software that I have been developing consists of several modules such as heat diffusion and magnetostatic solvers. Homology and cohomology solvers, now available in open GMSH version, have been developed within my group [105]. However, for me the most important tool package and source of inspiration has been the in-house developed Riemannian manifold interface [106] and AC-loss simulation tools [70].

In this chapter we go through the constituents of a capable quench simulation tool. Then, the most important components of the QueST, and their connections, are presented in detail. In addition, the input and output of the quench simulation as well as their implementation in QueST is expressed. In the end, the spatial and temporal discretizations utilized in the software are shortly described. In addition, a small example is presented how to fasten the simulations by tweaking our software, which would not be possible with a commercial software. This chapter is not directly based on any publication

[1]GMSH is an open-source finite element mesh generator with pre- and post-processor facilities. Available online at `http://geuz.org/gmsh/`.

but the details given here come out throughout all the appended publications.

3.1 Motivation for the quench simulation software development

One problem with the home-made tools is that they are often programmed during doctoral studies and consequently when the developer leaves the institute senior, or permanent, staff members are not able to continue the development of the software. Then, there is certain time, perhaps 5-10 years, before the program becomes obsolete for the present day analysis. Also, rarely the internal structure of the program is designed with appropriate software engineering tools. This is not a good starting point for continuous development. General finite element environments present another extreme. The programs may be internally well structured to allow further development, but hardly any program is tailored to quench simulations and the source code is private.

Typically when we discuss about engineering problems, the focus is not on the solution method, but more on the problems and their solutions. The path from setting up the problem to solution is of primal importance when there are new problems that cannot be solved with existing tools whose feasibility is demonstrated. In our work, we focus on a variety of possible quench scenarios in particle accelerator magnets and development of tailored modelling tools for them.

To consider the solution method behind a quench problem and the solution; how does the magnet system behave during a quench, what kind of protection system needs to be designed in order to make a quench safe event; everything starts from the requirements for the quench software. These requirements are often laid by engineers who are seldom in the core of the modelling tool development but they have needs to address certain issues in their modelling.

The post-LHC accelerator at CERN, for example, will be very expensive and requires very detailed quench analysis. One needs to know what happens when a beam loss occurs in the beam tube, what happens when there is a short circuit between coils made of different superconductors, how coupling losses affect on temperature increase in coils, how quench protection heaters including heating stations [126] induce multiple quench origins to the coil and what happens if there is a failure in some part of the protection system [36]. To consider all these a modeller needs to have a possibility to simulate various electric circuit topologies, multiple connected thermal models, non-linear 3-D magnetic field, and possibly helium flow too.

These modelling problems would implicate that a general simulation environment, like Comsol Multiphysics [21], does not serve the needs of the quench modelling community. The community has needs to pose new models in the very flexible way in their quench modelling tasks. They do not necessarily want to depend on the interfaces provided by the commercial software vendors, but they need more expert-style approach, where, in principle, anything could be simulated. If this is not the case, some of the developers should be able to implement a feature taking into account also the new need. One possible solution for this is to start managing in the community an open-source software where experts in specific fields could provide modules that address the modelling needs.

Constructing this kind of a program requires good interfacing – i.e. abstracting out the details. Then a programmer who does not contribute to a specific module only needs to know about the public methods the interfaces offer. Natural way to achieve such is by using an object oriented approach, where the main modules arise from classes that offer well-defined services [42]. An expert user can construct a new kind of a simulation tool from the available modules by writing a main program and few classes connecting the required sub-modules to the main modules. At the same time, the expert user does not need to know how all the modules work. He just needs to know how to utilize them. Then, an expert in fluid dynamics could contribute to the software a module considering the cooling. Also, by this way new modules, and modules sharing the same interface but different implementations can be developed in order to constantly develop the software toward the needs that are not yet even known. However, a user should at the same time be able to change some parameters, like the operation current, very easily without compiling the program. For this a data transmission interface is needed for input data.

Next we present the basic constituents of the QueST. The most important modules, and submodules, and the connections between them are described. Then the most important inputs to the software, and the output an engineer desires from the computation are presented. Furthermore, the basic concept of including inputs and receiving the output from the QueST is presented. In the end, we express the spatial and temporal discretizations exploited in the QueST. I want to emphasise that QueST is not a comprehensive quench simulation tool as there are many optional modules missing, e.g. AC-loss computation module. However, the software development has a solid basic framework available for the community in addition to the continued development work at the Tampere University of Technology. [90]

3.2 Constituents of the software

The quench problem needs a multiphysical approach. The most important modules and their purposes are listed in Table 3.1. It should be noted, that not all of these constituents are relevant for all the cases and they may be interlinked. Further, by leaving something out, like the AC-losses during the current decay, a pessimistic estimate can be achieved. However, a modeller should not derive too pessimistic estimates because this can either prevent some technological advancements or lead to unnecessarily complicated protection system design.

Table 3.1: Important modules in quench modelling in alphabetical order.

Module	**Purpose**
Circuit / Protection analysis	Couple the magnet system to the external electric circuit
Magnetic field analysis	Input to local critical current, AC-losses during current decay, quench back (everything related to magneto(quasi)statics)
Material library	Includes the required, possibly temperature and B dependent, material properties and computes values for anisotropic materials
Thermal analysis	heat diffusion / quench propagation in the magnet

Thermal module is probably the most important single module when modelling a quench. Simulating how the heat diffuses from the hot spot in case of a quench is utilized to model maximum hot spot temperatures, normal zone propagation velocities and minimum quench energies. A thermal module is included in QueST, where (2.3), and consequently, the quench propagation can be solved. At the moment there is a possibility to include different boundary conditions such as Dirichlet boundary condition for constant temperature on the boundary or Neumann boundary condition for heat flux through the boundary. With this e.g. cooling can be modelled.

The computation of critical current depends on the magnetic field, which may result from a linear magnetostatic analysis, or in a multi-magnet system with an iron yoke a result of a considerably more complicated computation. On the other hand magnetic field depends on the current that is utilized in the circuit analysis module. The magnetic field computations may give also

required inductances for the circuit analysis. We have implemented a module for the QueST to solve for the linear magnetostatic problem. **A**-formulation has been utilized when solving the magnetostatic problem as presented in (2.12)-(2.16).

Circuit analysis is needed to analyze magnet's current decay. In QueST we have implemented a basic protection circuit module according to (2.17)-(2.18), where a dump resistor is utilized. Current decay can be computed utilizing the circuit analysis module, which affects considerably on the heat generation computed in the thermal module. Thus, the circuit analysis module is an important piece of the software to model the difference between protected and unprotected magnet designs.

Finally, many of these modules require material parameters, and consequently, a generic material property library is an essential tool for such a software. In QueST we have gathered a small material database for the materials that have been utilized in our work. From this database a user can define proper material parameters for each domain entity. The user can also introduce new materials to the database easily. Values for resistivity (ρ), heat capacity (C_p) and anisotropic thermal conductivity (λ) are available as a function of temperature (and as a function of ρ and B when applicable) from the database. Material properties are gathered from different sources [29, 30, 55, 60, 78, 80].

The presented modules need help from the other, say, sub-modules too. For example, the thermal analysis module, to solve (2.3), could be the same for many problems, but it may utilize different sub-modules to compute the local heat generation. In the most simplest case it may utilize current sharing model for the analysis of low temperature superconducting magnets, whereas YBCO magnets may require the consideration of power-law for the resistivity of the YBCO layer. In QueST both of these approaches have been implemented, and the user can choose whatever suits best for ones needs.

Platform to distribute and develop this kind of software, constructed of smaller toolboxes, is essential for successful software development. QueST is developed in the environment offered by GMSH [43], an open-source framework. It allows flexible utilization of finite elements with many essential parts already built-in, but does not prevent utilization of, for example, thermal network models. It is programmed in C++ and thus many packages available open-source for scientific computing can be easily utilized and retrieved, for example, from many Linux repositories. However, at least the dedicated parts specifically related to quench should be made within the community because these can be tailored to attain high-performance simulation tools. A simplified structure of the QueST is illustrated in figure 3.1.

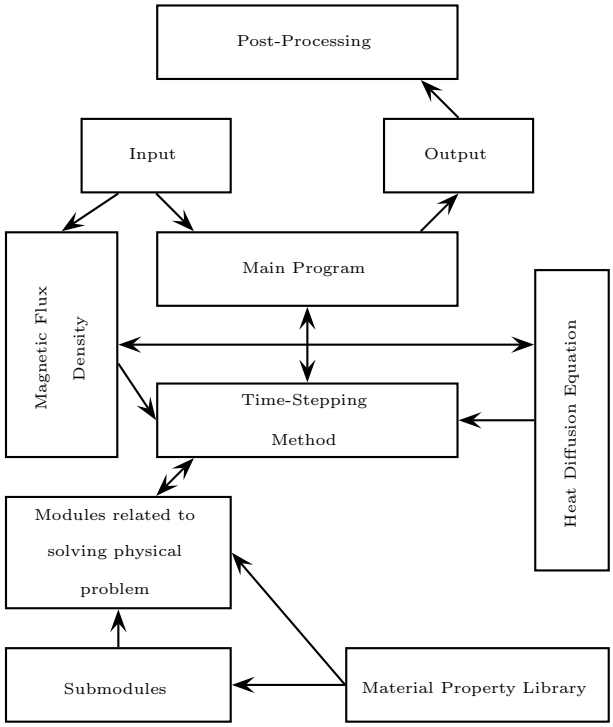

Figure 3.1: Structure of a flexible and extendable quench program, such as QueST, from an expert user perspective.

3.3 Input and output of a quench simulation

Input and output should be considered first when starting to describe the problem at hand to the computer. What we want as solution and what we need to solve for it are valid, but not trivial, questions. Magnetic flux density is probably the most important input for the quench simulation, however, many other smaller pieces of information are needed for successful quench simulation. Output on the other hand needs to be available in a format that is easily used in the post-processing phase. Here we first present the required inputs for the quench simulation, and how we utilize them with QueST. Then we present the most important outputs from the quench simulation and how they are exported from the QueST for further post-processing, e.g. data visualization.

3.3.1 Magnetic flux density distribution

Magnetic flux density ($\mathbf{B}$) distribution is required in the modelling domain due to the critical current (I_c) computation and also for the magnetoresistance of the copper that has influence on its ρ and λ [60]. In LTS magnets where I_c does not depend on the orientation of the $\mathbf{B}$, only B is required. However, in HTS magnets made of coated conductors one needs two components of $\mathbf{B}$: the one perpendicular to the tape's wide surface and the one parallel to it [133].

In QueST magnetostatic solver module we solve $\mathbf{B}$ with unit current and scale the solution by the actual current of the magnet design. This is possible when nonlinear materials, such as iron, are not present. However, further development is not prohibited. The solved $\mathbf{B}$ distribution is then used as an input to the heat diffusion equation solver and for computing superconductor I_c locally. However, if there exists nonlinear materials in the magnet design, $\mathbf{B}$ must be solved simultaneously with the heat diffusion equation if better accuracy is required which increases the computation time considerably.

Magnetic flux density distribution can also be imported from other software in GMSH post-processing file format. For HTS coated conductors parallel and perpendicular components for $\mathbf{B}$ are required for I_c, but they may be difficult to achieve from $\mathbf{B}$-distribution, especially with accelerator magnet designs where the ends of the magnet are bent. However, there are specialized software for this purpose [99], where the information is available and can be imported to QueST.

3.3.2 Operation conditions

Operation conditions are required to present the initial state of the simulation. In commercial software operation conditions are usually presented utilizing a graphical user interface (GUI). Because commercial software is typically aimed for a wide audience in different fields, GUI is rather simple and easy to use with tooltips to guide the user. On the other hand, in-house software is more often tailored specifically for a certain modelling situations, and thus, a GUI with tooltips is probably not necessary. Often in in-house programs inserting the operation conditions is handled by specific input files [125]. Furthermore, the user should be able to include own variables in the input file, by programming the specific addition to the code.

In QueST the user provides a specific JSON-formatted (JavaScript Object Notation) [56] file via the command line. This JSON-file is used to read the operation parameters for the simulation task, and to store them in a specific

object in the program. It is possible for the user to include additional variables in the JSON-file by modifying the object interface within the code. JSON-file as an input is convenient, as modifying the file does not require re-compiling of the C++-code and specific file type protocol is already there. Thus, if only operation parameters, such as the operation temperature or current is changed, one can start the simulation immediately afterwards.

3.3.3 Post-processing data

The solution is the main reason for the simulations to be done at the first place. But what is the solution of the quench simulation? The answer to that simple question is not that simple. There are multiple solutions or outputs from which engineer then draws the conclusions. It is also important to note, especially with in-house softwares, that some information should be displayed during the simulation. This is due to being able to predict what is happening, why is it happening and possibly restart the simulation if something seems to go completely wrong from the beginning.

The most important solutions from the quench simulation are hotspot temperature and voltage over the normal zone as a function of time. These should always be drawn in the post-processing phase. The hotspot temperature as a function of time illustrates the speed and shape of the temperature increase. From this information one can understand how severe problem quench is, and how fast it has to be dealt with to prevent magnet damage. Furthermore, it is interesting to compare the normal zone voltage to the hotspot temperature over the simulation period. This allows the engineer to observe if the quench detection threshold voltage can be detected before the hotspot temperature exceeds dangerous values.

The temperature profile in the whole magnet is also important result. The propagation of the normal zone can be understood more clearly from the temperature profile of the magnet, and it should be saved from multiple different time instants. However, usually it takes a lot of memory to store the whole temperature profile, and thus, it should not be saved from every time step, but for example after a certain hotspot temperature thresholds are exceeded.

The QueST displays during the simulation the operation current, maximum hot spot temperature, normal zone resistance and volumetric fraction of the normal zone. All of these are written to `.m`-files for post-processing purposes and Matlab can be used for visualization of the output. The temperature distributions are saved in GMSH formatted post-processing files at specific time steps. The time steps, when the temperature solution is saved,

can be determined in the JSON-formatted input file. GMSH can be used for post-processing the temperature distributions. In principle any tweaks and additions can be added to the code by programming and then compiling for specific purposes.

3.4 Spatial and temporal discretization

Before starting the simulation the modelling domain (Ω), i.e. the computer representation of the magnet under study, has to be discretized in space to use FEM. Furthermore, the adequate time-stepping method has to be decided and implemented, especially if commercial software is not used. In this section we briefly present the spatial and temporal discretizations for the quench simulation purposes.

3.4.1 Spatial discretization

To be able to utilize FEM, one needs to discretize Ω in space [139]. This means splitting Ω into connected polyhedra to create a finite element mesh for Ω. Usually for two dimensional domains triangles are used for discretization, and for three dimensional domains tetrahedra [139]. However, other possibilities are also present, such as hexahedra [64].

After meshing Ω, one attaches basis functions to, for example, the nodes or edges of the finite element mesh. Then, the unknown solution is approximated as a finite sum of basis functions with real number coefficients. These coefficients are called the degrees of freedom (DoF) of the problem. For example, in case of a heat diffusion equation, the temperature profile of the domain is approximated using

$$T(\mathbf{r}) = \sum_{i=1}^{\#Nodes} T_i N_i(\mathbf{r}), \tag{3.1}$$

where $T(\mathbf{r})$ is the temperature at point $\mathbf{r}$, T_i (DoF) is the temperature in node i and N_i is the the basis function related to node i. Now by combining all the unknown temperatures T_i to a vector

$$\mathbf{T} = [T_1\ T_2\ ...\ T_{\#Nodes}]^T, \tag{3.2}$$

and utilizing (3.1), the weak form[2] of (2.3) can be presented in the form

$$M\frac{\partial \mathbf{T}}{\partial t} = S\mathbf{T} + \mathbf{Q}, \tag{3.3}$$

where M is the mass matrix, S is the stiffnes matrix and $\mathbf{Q}$ is the load vector. Here M, S and $\mathbf{Q}$ depend on T, $\mathbf{B}$ and I_{op}. This type of matrix equation can be solved numerically using time-stepping method described in the following section.

3.4.2 Temporal discretization

Time-stepping is a crucial part of the quench simulation. When using commercial software time stepping is usually included in the software and there is no need for user to take any actions. Perhaps the time step size or solution tolerance needs to be adjusted but that might be all. However, when using (or coding) in-house software the time-stepping method needs to be implemented. There are multiple readily available packages, at least for C++-based codes, such as SUNDIALS [140].

Time stepping for quench simulation can be, however, rather easy to implement. Next we present one possible time-stepping method for an in-house software solving for quench based on the spatial discretization presented before. A generalized Euler algorithm [50] [Ch. II.7, p. 205] can be presented as

$$y_{k+1} = y_k + \Delta t F(t_k + \theta\Delta t, y_k + \Theta(y_{k+1} - y_k)), \tag{3.4}$$

where k refers to the time step, Δt to the time step size and F is the function to be integrated over time. θ and Θ are defined as $0 \geq \theta, \Theta \geq 1$. The extreme cases are $\theta = \Theta = 0$ (the explicit Euler method) and $\theta = \Theta = 1$ (the implicit Euler method). When (2.3) is discretized using FEM, the generalized Euler method can be written as

$$(M_k + \Delta t\theta S_k)y_{k+1} = (M_k + \Delta t(1-\theta)S_k)y_k - \mathbf{Q}_k\Delta t. \tag{3.5}$$

In QueST we have utilized implicit Euler method, and thus, we have selected that $\theta = 1$. This very simple time-stepping method is reasonable for quench simulation and remains stable with adequately selected time steps. Typically we use time step size of 0.1 ms.

[2]Detailed explanation of FEM and deriving the weak form are presented in [139].

3.5 Example: particular software engineering issues

When an in-house software is being developed and tailored for a very specific purpose, like for quench simulations, it is possible to consider how software implementation level details affect the performance of the program. Interesting details are, for example, whether one should use table or tree structures for presenting numeric data related to entities in the modelling domain, or whether one should use functions that are evaluated when the data is needed. This depends on the connection between the data and where it is used.

The modeller is interested in particular post-processing data, also during the simulations, in quench computations. For example, the normal zone resistance, or the heat dissipation is one of these. Then, while the differential equation system is being assembled, it makes sense to save this data so that it can be retrieved after the solution very rapidly. This data is needed constantly during the simulation by the circuit analysis module. Perhaps, in a general simulation environment this kind of preparation for the post-processing is not possible during the simulation. These issues are not critical when small problems are considered, but when one needs to solve time dependent non-linear problems with, perhaps, millions of degrees of freedoms altogether, it makes sense to optimize the software in every detail.

Here we demonstrate one specific detail with the software that we are developing. We consider how the computation time varies when we select three different ways to represent the material properties in the thermal analysis. The analysis is based on the magnet details in **Publication 1** and **Publication 2**. The emphasis here is on the variation of computation time. All the simulations recorded the same (time, hot spot temperature) curves with an accuracy of better than 0.01%. If one selects for the quench detection threshold voltage 50 mV, all the methods predicted the time instant for this within 1 ms.

The different implementations are as follows[3]. First, we evaluate a linear interpolation function for the data pairs in a table of (temperature, material property value), where volumetric specific heat, thermal conductivity and resistivities for the non-superconducting materials were considered. Then, we solved a non-linear problem which matches the electric fields in every layer of the cable. These steps were considered continuously while assembling the required matrices for the thermal problem. We call this approach the functional

[3]The particular modelling case is presented later in this thesis in Section 5.1. Here the focus is not on the case, but on the number of DoFs and how it affects the simulation time with different software implementations.

approach.

In the second and third approaches we saved to each element its temperature and material properties. Then, when the software was doing the assembly again, we retrieved the old values, if the new temperature differed from the old one less than 0.1 K. In the second approach we utilized a tree structure for solving the auxiliary element data. In the third approach we utilized a table where the index of given element in the table was the same as the element number. We gave to each element in the cell complex a unique number such that the maximum number was the amount of elements. In the tree approach, the search time from the random access memory of the computer is proportional to the logarithmic of the amount of elements, whereas in the table the search time does not depend on the number of elements. These approaches are called functional + store.

Tables 3.2 and 3.3 present the results of this comparison for two different cell complexes used to study the magnet system. In Table 3.2 we had 157 000 tetrahedral elements and 39 600 degrees of freedoms. For Table 3.3 the corresponding numbers were 940 000 and 209 000, respectively. For the sparser mesh, the functional approach resulted in the shortest computation time. However, when the amount of elements was increased, the situation was reversed and the functional + store in the table resulted in 14% shorter computation time. In that particular case, this corresponded to total time saving of 8 h.

Table 3.2: Computation times for a sparse mesh case. Normalization is done to 10 h 0 min - the computation time of the functional approach.

Method to compute material parameters	Normalized computation time
Functional	1
Functional + store in tree	1.08
Functional + store in table	1.05

3.6 Remarks

Structure for a finite element method based quench simulation tool QueST was presented in detail. Modules and submodules and their connection in QueST were explained. In addition, the required inputs for the quench simulation and

Table 3.3: Computation times for a dense mesh case. Normalization is done to 56 h - the computation time of the functional approach.

Method to compute material parameters	Normalized computation time
Functional	1
Functional + store in tree	1.04
Functional + store in table	0.86

the desired output were discussed and the implementation of the input and output interfaces were described. In the end a particular software engineering issue was addressed. We scrutinized a quench simulation in two cases with different number of DoFs utilizing different data storage implementations. With 940 000 DoFs we were able to decrease the computation time as much as 14%, which corresponded in a total of 8 h time saving, only by tweaking the data storage implementation within our in-house software.

Chapter 4

Stability and quench considerations of HTS magnets

Stability and quench of LTS materials and magnets have been extensively studied and documented [156]. HTS materials have also been widely studied after their discovery, however the quench methodology of HTS is still not completely understood [7, 18, 54, 77, 82, 136]. In this chapter we utilize numerical modelling to study the stability and quench of HTS, especially the normal zone propagation velocity (v_{nzp}) , hot spot temperatures and minimum quench energies. To these numerical models we compare widely used, usually analytical, models for quench studies utilized with LTS materials and analyze the usability of these models for HTS magnets. In addition, where applicable we offer guidelines for practical measurements based on the findings of our numerical models.

First, we study the v_{nzp} in a case where HTS cables and insulation layers are stacked next to each other. The results are based on **Publication 4**. The emphasis is on the values of v_{nzp} at different distances from the original hot spot as this topic is not extensively studied. In addition, T_{cs} dependent normal zone evolution is presented to illustrate the quench event for different stability margins.

Then, we present the hot spot temperature in an HTS magnet using finite element analysis and the zero-dimensional, so-called MIITs[1] concept [84], based on **Publication 5**. Hot spot temperatures and current decay curves are studied with different quench detection threshold voltages. Furthermore, the inductance of the magnet and its effect on the quench protection, when the

[1]MIITs is the unit of current square's time integral with multiplier mega (10^6).

magnet is protected using a dump resistor, is studied.

Finally, we study energies that quench an HTS magnet. First, we compute numerically the minimum energy required to quench an HTS magnet using a strip heater based on **Publication 6**. Results are compared to the MQE derived from an approximate solution of (2.3) in a simplified case. Then, the effect of the heater area and the heater pulse length on the energy that is required to quench the magnet are presented to demonstrate the considerably higher stability margin of HTS compared to LTS.

4.1 Variation of quench propagation velocities

It has been proposed that v_{nzp} is constant in HTS magnets as it is in LTS magnets [7]. This would allow one particular modelling method for the quench propagation of the HTS magnets: add isothermal shells on top of each other according to v_{nzp}. This method was originally proposed by Wilson [156], and later developed by, e.g. Rossi and Sorbi [117]. Naturally, when modelling quench evolution in the superconducting magnet using methods relying on v_{nzp}, knowing it with enough accuracy in the longitudinal and transverse direction is crucial.

Here we simulate a quench in a stack of cables with insulation layers in between. The normal zone propagation velocity, in longitudinal and transverse direction, is computed in the post-processing phase from the temperature evolution according to the quench simulation results. The emphasis is to observe how v_{nzp} behaves in a large area outside of the initial hot spot, and not only in its immediate vicinity, which has been done in the measurements [145, 150].

4.1.1 Modelling domain and operation conditions

The cable configuration utilized in the simulations is presented in figure 4.1 (a). It consists of two REBCO tapes soldered together with a copper shunt in the middle. This configuration was motivated by the HTS insert study in [112]. Relative material proportions of the cable are presented in Table 4.1. The thickness of the copper layer was 72 μm and the individual thicknesses of the two $CuBe_2$ and insulation layers were 100 μm and 30 μm, respectively. In addition, the thicknesses of the two REBCO tapes consisting of REBCO, buffer layers and the Hastelloy substrate, were 64 μm. The insulation layers were made of Kapton.

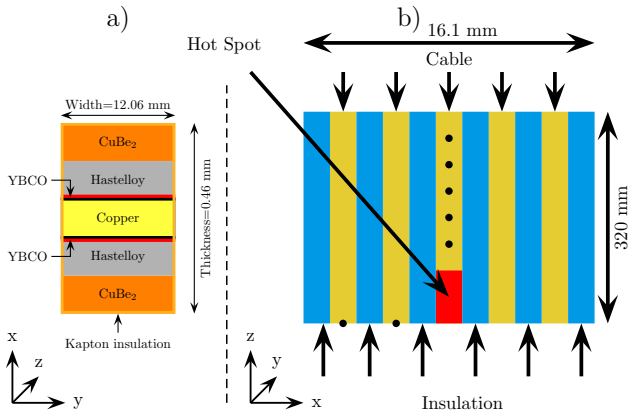

Figure 4.1: (a) Cable configuration with insulation layer used in the quench computations. (b) Schematic view of the part of the computational domain used in the simulation. Figures are not in scale. In (b) not all the modelled cables are shown.

Table 4.1: Relative material proportions of the non-insulated cable

Copper	18 %
$CuBe_2$	50 %
Hastelloy+REBCO	32 %

The modelling domain is presented in figure 4.1 (b). It consisted of 35 turns, each including the cable presented in figure 4.1 (a), with insulation layer between each turn. The quench origin, having the length of 5 mm, was located in the middle of the stack in the 18th cable. The stack length was 640 mm. Discrete symmetry [109] was utilized and only half of the stack, in the longitudinal direction, was modelled. We utilized homogenized material parameters for the cable sections [136]. Only the insulation of the cable was modelled as an insulation layer. In addition, adiabatic boundary conditions were applied to the boundary of the modelling domain.

Black dots in figure 4.1 (b) present the points in which the propagation of the quench frontier was monitored for post-processing purposes. Each point was considered as a quenched point when its temperature rose above T_{cs}. For the longitudinal quench propagation, we used points in the same cable with the hot spot. For the transverse propagation, we used one point in each cable. Points in figure 4.1 (b) do not indicate the real number of points used in the computation but are merely for visualization of the modelling setup. To be specific, we had points in the longitudinal direction every 10 mm. In the

transverse direction, the points were at the center of every cable, thus the distance between the points was 0.46 mm.

Magnetic field was set to a constant value in a way that a certain, uniform, T_{cs} was achieved over the whole modelling domain. However, due to the utilized power-law model for superconductor resistivity, there existed Joule heating even at sub-critical currents. By using constant T_{cs} in the modelling domain we could limit the study of v_{nzp} to the effect of temperature margin on the normal zone propagation velocity.

The current sharing temperature of 15 K is common in high field HTS magnet designs operating at LHe in a large fraction of the windings[2]. However, with LTS magnets the margin from operation temperature to T_{cs} is typically around 1 K [96]. The current sharing temperature selection of 5 K corresponds to the typical temperature margin of an LTS magnet and T_{cs} of 10 K and 15 K are closer to T_{cs} values of HTS magnets. The parallel and perpendicular field values and corresponding values of T_{cs} used in the computations are presented in Table 4.2. The field values were selected to achieve the corresponding T_{cs} values and are not taken from any existing magnet design.

Table 4.2: Magnetic field values used in the computation

Parallel [T]	Perpendicular [T]	T_{cs} [K]
15.0	2.0	15.2
17.0	2.5	10.0
15.5	3.0	5.0

The operation temperature and operation current in the simulations were 4.2 K and 2800 A, respectively. The operation current corresponds to the engineering current density of 250 A/mm^2. A constant value of 20 was used for n.

4.1.2 Computation of normal zone propagation velocities

The quench simulation was followed by v_{nzp} computation. Here we present the computation of v_{nzp} utilizing the quench simulation results..

During the simulation, we saved temperature of every point P (those shown in figure 4.1 (b)) at every time step k. Then, we collected those time instants

[2]Based on the findings in **Publication 2**.

t_q^P at which each point shifted above T_{cs} by finding t_q^P such that

$$\forall k < q \qquad T(t_k^P) < T_{cs} \tag{4.1}$$
$$\text{and} \qquad T(t_q^P) \geq T_{cs} \tag{4.2}$$

hold. In other words t_q^P is the time where the temperature of the point P rose above current sharing temperature.

The normal zone propagation velocity between points P and $P+1$ was computed with

$$v_{nzp} = \frac{\Delta}{t_q^{P+1} - t_q^P}, \tag{4.3}$$

where Δ is the distance between the points i.e. Δz and Δx for the longitudinal and transverse propagation according to figure 4.1 (b), respectively.

4.1.3 Results

Shown and discussed here, are the longitudinal and transverse propagation velocities. In addition, the evolution of the normal zone in time within the modelling domain is presented. Furthermore, guidelines for performing v_{nzp} measurements at low temperatures for HTS with relatively large temperature margins are presented.

Longitudinal propagation

The simulated longitudinal normal zone propagation velocities are presented in figure 4.2. The normal zone propagation velocity is not constant near the hot spot but increases or decreases considerably depending on T_{cs}. However, the early behaviour may depend on the way the quench was initiated. With T_{cs} of 15 K, v_{nzp} levelled off to a 30% higher value than the one recorded 25 mm away from the hot spot. Lower v_{nzp} near the hot spot is the result of a higher T_{cs} when the heat from the hot spot diffused further into the magnet without extending the quenching volume immediately.

The change in v_{nzp} levelled off at about 100 mm distance from the hot spot when T_{cs} was 15 K. Further modelling is required to study if there is some correlation between T_{cs}, temperature increase and the distance where v_{nzp} levels off. However, we can derive a conclusion, that when measuring v_{nzp} in a longitudinal direction, there is a minimum distance from the hot spot where the voltage taps should be attached to get reliable measurement data of

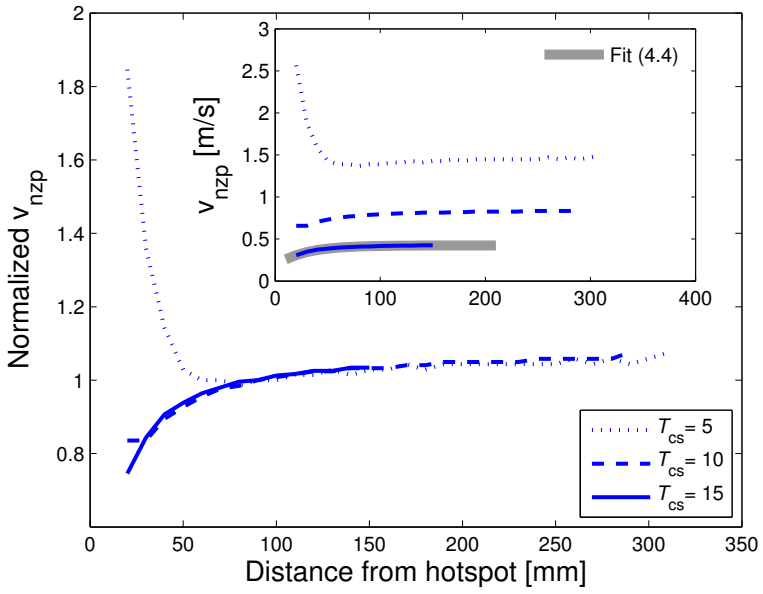

Figure 4.2: Longitudinal v_{nzp} as a function of distance from the hot spot with different values of T_{cs}. Plot is normalized to a v_{nzp} value achieved from the distance of 100 mm from the hot spot. The inset presents absolute values.

v_{nzp}. For example using simulation data with T_{cs}=15 K, we fitted a curve

$$v_{nzp}(x) = 0.4237 - 0.2399 \cdot \exp(-0.037 \cdot x), \tag{4.4}$$

where x is the distance from the hot spot. According to the fit (4.4) v_{nzp} is 98.6 % of its asymptotic value of 0.4237 m/s at the distance of 100 mm from the hot spot. The fit for v_{nzp} is presented in the inset of figure 4.2 to illustrate the correspondence with the computation.

With T_{cs} of 5 K, v_{nzp} decreased very rapidly at first. The quench was ignited by setting I_c to 0 A in the hot spot. Consequently, the area in the immeadiate vicinity of the hot spot quenched rapidly due to the high Joule heat generation in the hot spot. However, when the quench propagated further from the hot spot, the effect of the quench ignition diminished, and v_{nzp} levelled off.

Transverse propagation

The transverse v_{nzp} results are presented in figure 4.3. The normal zone propagated a substantially shorter distance in the transverse direction than in the

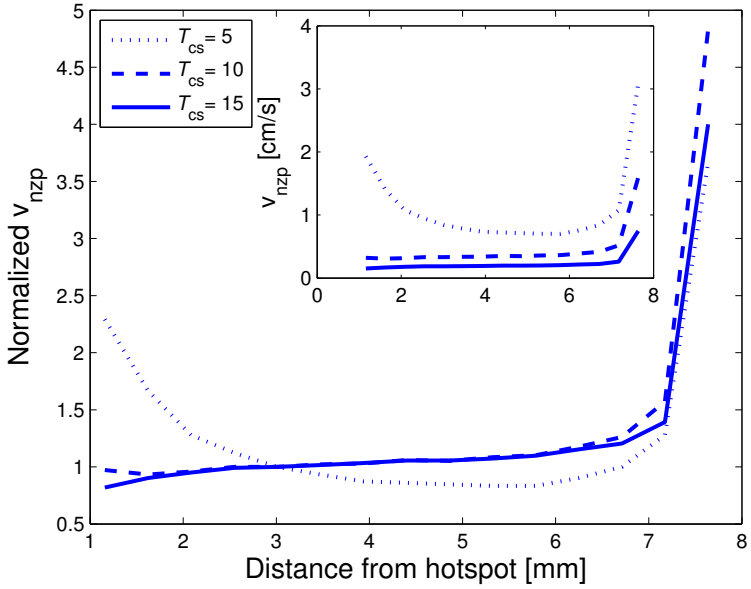

Figure 4.3: Transverse v_{nzp} as a function of distance from the hot spot with different values of T_{cs}. Plot is normalized to a v_{nzp} value achieved from the distance of 3 mm from the hot spot. Inset shows absolute values.

longitudinal one. This was due to the considerably lower thermal conductivity of the insulation compared to that of the HTS cable. When the simulation was terminated, the normal zone had propagated to the edge of our modelling domain in the transverse direction in every simulation case, which was about 8 mm from the hot spot.

According to figure 4.3 the quench evolved in a similar way in both the transverse and longitudinal directions. Rapid v_{nzp} increase at 8 mm distance from the hot spot in figure 4.3 seems to result from the closely-pitched adiabatic boundary of the modelling domain. Thus, further modelling and measurements are required to analyze the longitudinal and transverse normal zone propagation at various values of T_{cs} as a function of the distance from the hot spot.

Normal zone evolution in time

Normal zone evolution is different depending on the value of T_{cs}. In LTS magnets heat diffusion always increases the normal zone volume. However, when the magnet T_{cs} is high, that is typical for HTS magnets, the heat diffuses

to a longer distance from hot spot, when comparing to LTS magnets, before the area in the vicinity of the hot spot begins the transition. Here we present how the normal zone evolves with three different values of T_{cs}, 5 K, 10 K and 15 K.

We used 4.3 K as a value to define where the heat had diffused from the hot spot, as the temperature had increased at least 0.1 K from the initial temperature of 4.2 K. As the quench evolved, the heat diffused from the hot spot increasing the volume in the modelling domain, that was between 4.3 K and T_{cs}. This behaviour is illustrated in figure 4.4. Small plateaus on the curves are due to the temperature rise above 4.3 K in the whole magnet. When T_{cs} of 5 K was considered, the whole modelling domain transitioned into normal state in about 0.25 s. With a larger T_{cs} of 10 K, it took 0.1 s longer to reach 4.3 K temperature in the whole domain, when compared to the case where T_{cs} was 5 K. Furthermore, when T_{cs} was 5 K, the whole modelling domain was in normal state when the simulation was terminated due to the hot spot reaching the temperature of 400 K. However, when T_{cs} was 10 K or 15 K only 80% or 40% had transitioned to normal state, respectively, when 400 K was reached. Thus, large temperature gradients are present when the HTS materials are used.

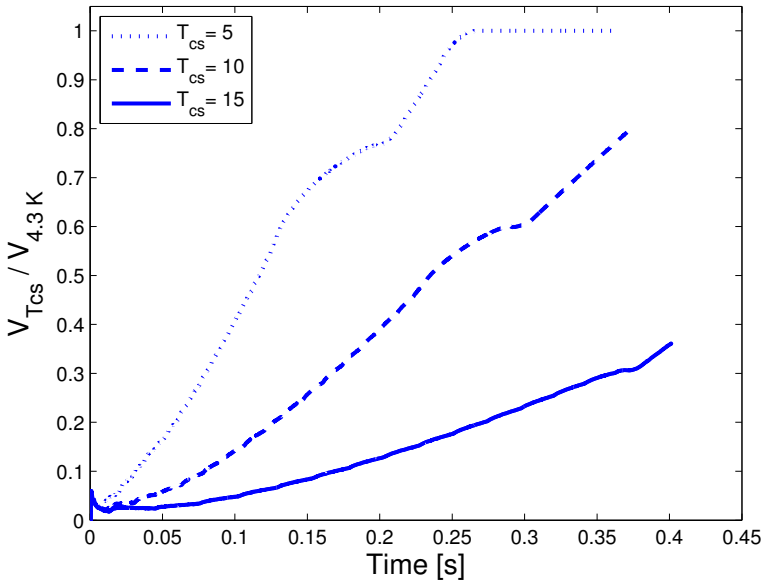

Figure 4.4: Volumetric fraction of the volume that has reached T_{cs} compared to the volume where the temperature has increased at least 0.1 K, thus $T \geq 4.3$ K.

Due to the large temperature margin between the operation and the current sharing temperatures, the normal zone does not propagate with the temperature front, which is illustrated in figure 4.4. This means that the temperature will rise in a considerably larger volume when compared to the quenched volume. Thus, the evolution of the temperature distribution below the current sharing temperature T_{cs}, after the quench onset, affects v_{nzp} in HTS more than in LTS magnets. This shows, that the quench evolution is completely different in HTS magnets compared to their LTS counterparts, and is worth noting when studying quench detection and protection in HTS magnets.

4.2 Hot spot temperature studies: finite element analysis vs. a zero-dimensional concept

A zero-dimensional concept to study the hot spot temperature was first introduced in [84], and later presented by others [40, 138, 156]. In this concept, known as MIITs, it is assumed, that during a quench the heat generated in the matrix metal of the superconductor is fully absorbed by the specific heat of the conductor and insulation. Thus, at the dissipative conditions, the operation current characteristic can be directly utilized to compute the hot spot temperature at the time instant of the de-energization.

Quench simulations using FEM are time consuming for detailed magnet analyses. However, the actual shape and the structure are not taken into account when using MIITs. For this reason MIITs has been widely used for conceptual protection studies for LTS accelerator magnets [39, 88, 143]. The heat diffusion is completely neglected, when MIITs are utilized. Thus, due to the slow v_{nzp} [7, 145, 150] and different normal zone evolution of HTS magnets, compared to the LTS magnets, the usability of MIITs concept for HTS magnets is studied in this section.

The MIITs concept has also been used to study the magnet protection utilizing a dump resistor [144]. When protecting a magnet using a dump resistor, the resistance has to be selected in a way that the terminal voltage does not exceed safety limit. However, large magnets are characterized with high inductances, and the time it takes to de-energize the magnet is long. The magnet discharge time depends on the values of the dump resistor and the magnet inductance [143]. Thus, there exists a limit for the magnet inductance, after which the energy of the magnet can not be discharged without high hot spot temperature or exceeding the safe terminal voltage limit. For these situations other protection methods are innovated [34, 110]

In this section we consider hot spot temperatures via MIITs and finite element analysis (FEA). Hot spot temperatures given by MIITs and FEA are computed in a scenario where the magnet is protected only with a dump resistor. Hot spot temperature results from MIITs and FEA are presented and compared. Also, the feasibility of the MIITs concept with HTS magnets is discussed. In addition, the maximum allowed inductance of the magnet is studied.

4.2.1 Simulation setup

The investigated modelling domain for FEA is presented in figure 4.5. The magnet is named Feather-M0 (FM0), designed for R&D purposes before manufacturing the 5 T HTS insert magnet, namely Feather-M2 (FM2) [62], in EuCARD-2 project. The FM0 magnet is designed to have five turns of Roebel cable made from 15 REBCO tapes each having width of 12 mm before the punching operation. The inner radius of the magnet is 20 mm, outer radius is 25 mm and the height is 12.2 mm. The operation current of the magnet is 6000 A, which results in the engineering current density J_e of 491 A/mm^2. It is notable, that in the bending dipoles the particle beam direction is the same as the arrow in figure 4.5.

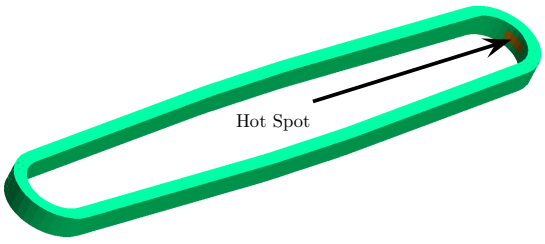

Figure 4.5: Modelling domain used for FEM simulations.

Manufacturing long length REBCO Roebel cables is still a demanding task [44]. However, Roebel cable length required for FM0 is 5 m [100], which is manageable [45]. Figure 4.6 presents the dummy cable that is similar to

the REBCO based cable which will be manufactured in the future to assemble the FM0 magnet. Table 4.3 presents the relative material proportions of the magnet unit cell. In the manufacturing process of Roebel cable void areas emerge in the cable, which has to be taken into account in material parameters. Fiber-glass epoxy insulation was used in this study, however, other insulation materials are still considered for the actual realization of the FM0 magnet.

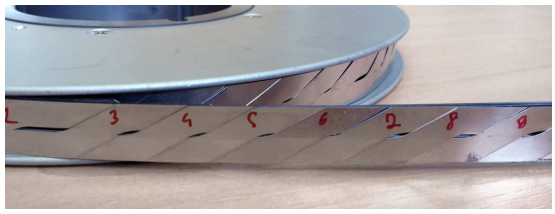

Figure 4.6: Dummy cable produced from stainless steel imitating the cable that will be used to manufacture the FM0 magnet in the future.

Table 4.3: Relative material proportions of magnet unit cell

Copper	31.5 %
Hastelloy + REBCO	38.5 %
Glass Epoxy Insulation	10 %
Void	20 %

Operation conditions used in this work are presented in Table 4.4. FEM simulation was terminated when the hot spot temperature rose over 400 K or the operation current decayed under 20 A, due to the protection, after which the heat generation is negligible in the magnet. We utilized 400 K as a safety limit, though in practice this may not be the case. The safety limit for the hot spot temperature has been a continuous topic within the community, however, there exists no test results to support any actual temperature value. To unify the conditions for FEA and MIITs, we applied a constant B of 2.5 T, in the direction parallel to the tape's wide surface, in the modelling domain.

Protection resistance of 0.15 Ω was selected to achieve a terminal voltage of 900 V, which is less than the usual safety limit of 1 kV [144], with nominal operation current. We also used different values for quench detection voltages (10 mV, 30 mV and 50 mV). Higher detection voltage leads to a longer detection time delay. Thus, we studied how the hot spot temperature is affected by the slower quench detection. Validation time was set to zero.

Table 4.4: Operation Conditions

Parameter	Value
Initial Current	6 kA
Initial Temperature	4.2 K
Cable Area (insulated)	12.2 mm^2
Magnetic Flux Density	2.5 T
Inductance (varied)	8.16 μH - 81.6 mH
Protection Resistance	0.15 Ω
Quench Detection Voltage (varied)	10, 30, 50 mV
Copper RRR-value	100
Superconductor n-value	20

To determine the maximum inductance of the magnet, that could be protected only with a dump resistor, the inductance of the studied magnet was varied during the simulations. The inductance for FM0 is 8.16 μH [100], but we increased the inductance from 8.16 μH up to 81.6 mH in the simulations. For reference, the inductance of the LHC dipoles is 98.7 mH [14]. Also, the nominal operation current of LHC dipoles is 11 850 A, making them even more difficult to protect. It is important to acknowledge the maximum inductance of the magnet, that can be protected with only a dump resistor, which is one of the aspects studied in this section.

4.2.2 Computation of MIITs

The computation of MIITs is based on the formula presented by Wilson [156, p. 201]

$$\int_0^\infty I^2(t)dt = A^2 \int_{T_0}^{T_{max}} \frac{C(T)}{\rho(T)} dT, \tag{4.5}$$

where T_0 is the initial temperature and T_{max} is the maximum temperature of the hot spot, t is the time, A is the area of the cable. According to [144] the right hand side integral of (4.5) is the "quench capital", i.e. what we have available to spend in terms of specific heat and resistivity to absorb the energy of the magnet:

$$\Gamma(T_{max}) = A^2 \int_{T_0}^{T_{max}} \frac{C(T)}{\rho(T)} dT, \tag{4.6}$$

where $\Gamma(T_{max})$ is the MIITs. The left hand side integral of (4.5) is the "quench tax", i.e. what is consumed by the magnet

$$\Gamma_q = \int_0^\infty I^2(t)dt. \tag{4.7}$$

To approximate the maximum hot spot temperature we compute the Γ_q, and then we search the appropriate value for T_{max} to achieve equal values for $\Gamma(T_{max})$ and Γ_q.

In case of dump resistor protected magnet the quench tax can also be computed, according to [144], as

$$\Gamma_q = \frac{L}{R_d}\frac{I_0^2}{2}, \tag{4.8}$$

where I_0 is the initial current. In (4.8) the normal zone resistance is neglected, and the current decays according to the magnet inductance and dump resistor values. However, we utilized identical current decay profile for both FEA and MIITs to minimize the variation between FEA and MIITs. First we performed FEA, where the normal zone resistance is taken into account, including a circuit analysis with a dump resistor. Then we computed the quench tax Γ_q using (4.7) with the current profile from FEA, which means utilizing the current value of every time step and linear interpolation in between. Often, similar approach is taken when the maximum hot spot temperature is approximated from the measured current decay curve [88, 92].

4.2.3 Results

First we present the hot spot temperature behaviour as a function of time. In this first study a constant value for quench detection threshold voltage was used and the emphasis was on the difference of results given by FEA and MIITs. Then we studied the effect of quench detection voltage on the hot spot temperature. From these results we predicted the maximum inductance of the magnet with different quench detection voltages.

Hot spot temperatures with FEA and MIITs

Hot spot temperatures as a function of time from FEA and MIITs computation are presented in figure 4.7. A constant quench detection threshold voltage of 10 mV was used. Using MIITs, the hot spot temperature rose almost linearly from the start, however, in FEA the hot spot temperature rose slowly at the

beginning because the heat diffused from the original hot spot. When the temperature at the hot spot had increased to a certain value, the hot spot temperature started to rise again with almost the same time derivative as with MIITs computation at the beginning. Thus, here the same behaviour, typical for HTS magnets, is also seen in the FEA as when computing v_{nzp}, where the heat diffused out from the original hot spot without quenching the area around the hot spot immediately.

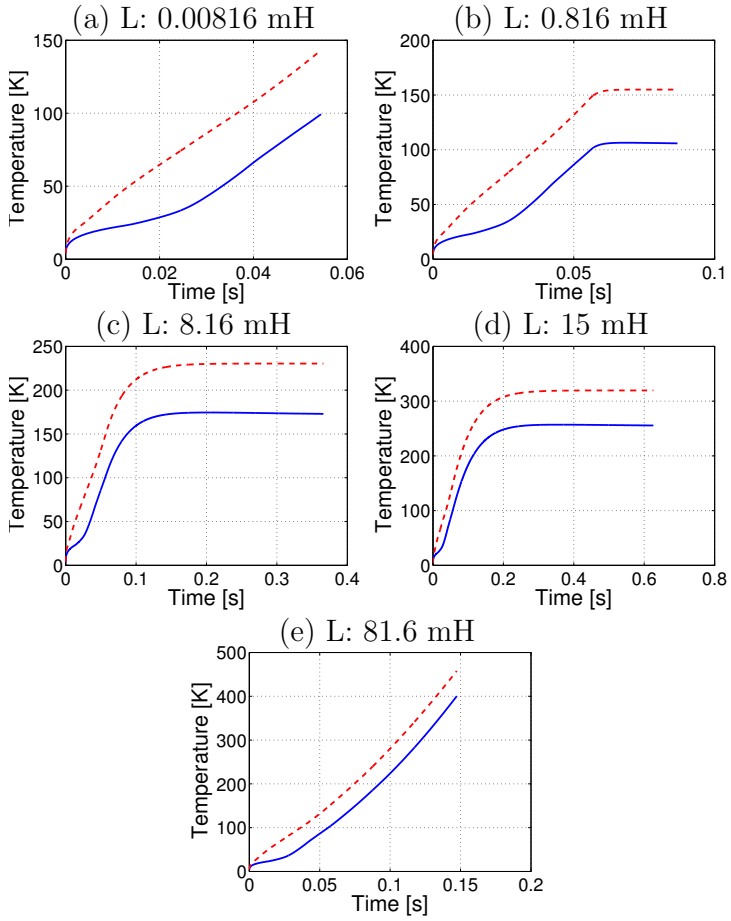

Figure 4.7: Hot spot temperature as a function of time with the quench detection voltage of 10 mV. Dashed line presents MIITs computation and solid line FEA results.

Temperature rise in figure 4.7 (a) and (e) stopped suddenly, but for different reasons. In the case of figure 4.7 (a), after reaching the quench detection

threshold voltage, the current decayed from 6 kA to the simulation termination condition of 20 A in around 0.1 ms ($\frac{L}{R_d} = 0.05$ ms). However, in the case of figure 4.7 (e), the considerably higher inductance of 81.6 mH resulted in such a slow current decay, that the hot spot temperature reached the other simulation termination condition of 400 K. The plateaus in figure 4.7 (b)-(d) were due to the prolonged current decay and simulations were carried on with operation current of less than 33% of the initial current, which resulted in almost negligible heat generation.

The hot spot temperatures with the inductances used in the computation are presented in Table 4.5. Hot spot temperature differences between MIITs and FEA, while MIITs always results in a higher value, were from 60 K to 150 K with inductances being between 8.16 μH and 81.6 mH. The temperature difference of 60 K is rather large when estimating the maximum hot spot temperature in case of a quench for a magnet. Therefore, when estimating a hot spot temperature for an HTS magnet protected with a dump resistor, the utilization of MIITs has a lot of uncertainty. The uncertainty of MIITs is due to the neglected heat diffusion from the hot spot at the start of the quench, as presented in figure 4.7. However, when the hot spot temperature begins to rise rapidly, the derivative of the temperature rise slope given by FEA and MIITs, as presented in figure 4.7 (c), is 2.14 K/ms, when the hot spot temperature is 100 K. Thus, after the initial heat diffusion in FEA, the simulation results given by FEA and MIITs are alike. As a conclusion, the MIITs concept is convenient when comparing two magnet designs, and when the absolute values are not desired as primary results from the computation.

Table 4.5: Hot spot temperatures

Inductance	FEA [K]	MIITs [K]
8.16 μH	100	160
0.816 mH	106	174
8.16 mH	175	264
15 mH	257	377
81.6 mH	400	554

Effect of the quench detection voltage on the hot spot temperatures

We studied the effect of different quench detection threshold voltages to the hot spot temperature. The results of FEA and MIITs with the quench detection voltages of 30 mV and 50 mV are presented in Table 4.6. The temperature

differences were from 65 K to 150 K with both quench detection voltages. The interesting breaking point is the magnet inductance of 15 mH. In that case, with the quench detection voltage of 30 mV the hot spot temperature rose to 282 K. However, with 50 mV, the hot spot temperature rose to the simulation termination temperature of 400 K. Therefore, the quench detection is equally crucial part in the magnet protection scheme as is the protection method itself.

Table 4.6: Hot spot temperatures

Inductance	FEA [K]		MIITs [K]	
	30 mV	50 mV	30 mV	50 mV
8.16 μH	114	123	179	190
0.816 mH	121	130	193	200
8.16 mH	194	206	290	306
15 mH	282	400	410	554
81.6 mH	400	400	554	554

Current decay curves with different values of inductance and quench detection threshold voltages are presented in figure 4.8. The current decay profiles are almost identical in the case of all three different quench detection voltages. This is due to the normal zone resistance being negligible compared to the dump resistor value. Only the duration of the constant current before the detection was different due to the different quench detection times.

Figure 4.8 (a) shows that the current decayed to 20 A within 1 ms, when the magnet inductance was 8.16 μH. Thus, in this case the magnet protection was determined by the quench detection due to the extremely fast current decay. However, in figure 4.8 (e) it is evident, that the magnet can not be protected using only a dump resistor due to the slow current decay when the magnet's inductance was 81.6 mH. Other protection methods have to be utilized, or the terminal voltage limitation must be increased to allow a larger dump resistor. In figure 4.8 (b)-(d) the current decayed to 20 A in 0.1 s, 0.4 s and 0.6 s with inductances 0.816 mH, 8.16 mH and 15 mH, respectively. However, in figure 4.8 (d) it can be seen, that the dump resistor of 0.15 Ω was not sufficient with the quench detection voltage of 50 mV as the hot spot temperature reached 400 K.

Hot spot temperatures as a function of the magnet inductance is presented in figure 4.9. By interpolating from the data, one can estimate the maximum tolerable inductance, for a magnet protected only with a dump resistor, for

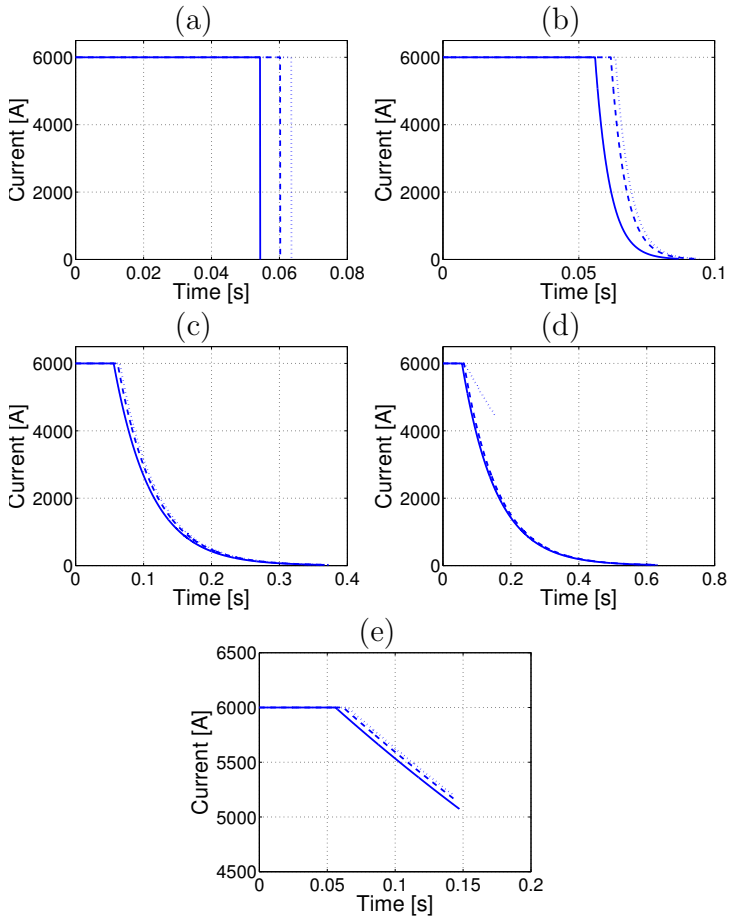

Figure 4.8: Current decay as a function of time. Varying inductance was used, i.e. a) 8.16 μH, b) 0.816 mH, c) 8.16 mH, d) 15 mH and e) 81.6 mH. Solid line, dashed line and dotted line present the quench detection voltages of 10 mV, 30 mV and 50 mV, respectively.

a given hot spot temperature limit. Figure 4.9 shows, that the maximum inductance with this type of Roebel cable is close to 50 mH with the quench detection threshold voltage of 50 mV.[3] With inductances below 50 mH the hot spot was limited to under 400 K, however, the maximum allowed hot spot temperature should be measured to verify this assumption. If the magnet inductance was above 50 mH, higher protection resistance value has to be used

[3]Here we did not take into account any validation or activation time for the protection circuit equipment.

or other protection scheme has to be utilized. In addition, better quench detection methods might be invented, thus allowing larger maximum inductance of the magnet.

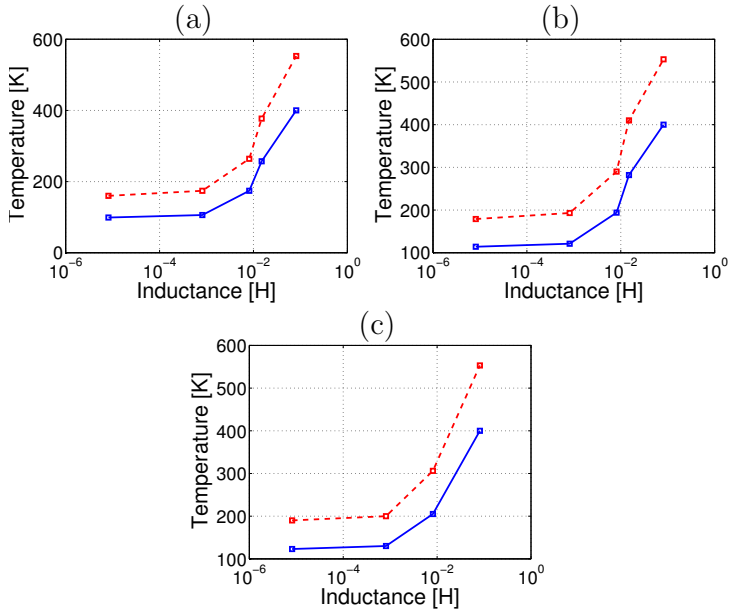

Figure 4.9: Hot spot temperature as a function of inductance of the magnet with different values of quench detection voltage: a) 10 mV, b) 30 mV and c) 50 mV. Dashed line presents MIITs computation and solid line FEA results.

4.3 Minimum energy required to quench an HTS magnet

Wilson presented the MQE concept to estimate the energy that is required to quench an LTS magnet. By using the MQE concept, an engineer is able to estimate the energy that quenches the magnet, or in a similar way the required heater energy to quench the magnet for measurement purposes. This concept is useful when the heat conduction during the disturbance is small when compared to MQE.

Considerably larger temperature margin between T_{op} and T_{cs} is typical in

large parts of HTS magnets, operated at liquid helium, than in LTS magnets. Due to the high T_{cs} the normal zone does not start propagating as rapidly as in LTS magnets, but due to the conduction large fraction of the disturbance energy, may diffuse away from the disturbance volume before T_{cs} is reached. Finally a quench occurs, but the energy required to create MPZ can be considerably higher than the MQE estimated similarly as for LTS magnets. Here we show that the MQE computed using the analytical formula is not feasible when studying HTS magnets.

In this section we present that the MQE could only be investigated numerically for HTS magnets. To avoid confusion, we use the term minimum energy required to quench (MERQ) to express the MQE obtained using numerical computation. When quenching a magnet using a strip heater for measurement purposes, estimating MERQ is crucial. With too large heater energies the magnet could be damaged and with too small energies the quench does not ignite due to the very high temperature margin.

4.3.1 Modelling domain and operation conditions

The modelling domain for MERQ study is presented in figure 4.10. The domain is identical to that of figure 4.5, however, the quench was initiated using a strip heater in the middle of the straight section in the inner radius of the magnet. Homogenized material parameters were used in the whole modelling domain,

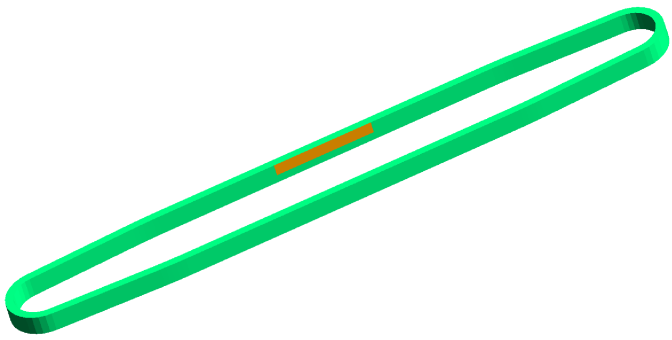

Figure 4.10: Modelling domain for our simulations. Heater is located on the magnet inner radius in the middle of the straight part.

and the relative material proportions of the magnet unit cell are presented in Table 4.7.

The location of the heater was selected in a way that only the innermost turn of the magnet would heat up. We varied the heater area during the

Table 4.7: Relative material proportions of the magnet unit cell.

Copper	31.5 %
Hastelloy + REBCO	38.5 %
G-10	30 %

simulations, thus, the heater should have been extremely long to achieve large area on top of the magnet due to the magnet having only 5 turns. Otherwise, by using a wider heater, the heater would have covered most of the turns, which would quench the magnet too rapidly due to the much faster longitudinal v_{nzp} compared to transverse v_{nzp}. The current sharing temperature varies in the heater area between 36-58 K.

As a particular modelling decision, the strip heater was modelled as a Neumann boundary condition. This means that the heater had no volume but an area on the magnet surface and there was a heat flux through the boundary to the magnet. Thus, in this study we did not take into account the temperature rise inside the heater or the heat conduction to the coolant. Our aim was to only study the internal behaviour of the magnet. This also allowed us to compare the simulation results to the MQE. The heater energy, that was transferred to the magnet, was computed using

$$Q_h = P_h t_h, \tag{4.9}$$

where P_h is the (uniform) heater power and t_h is the time that the heater was active. Rest of the boundary of the modelling domain, i.e. excluding the heater connection, was constrained by the adiabatic boundary condition.

The operation conditions used in this study are presented in Table 4.8. The magnetic flux density within the magnet area was computed using external program called Field [99] and then imported to QueST. The Roebel cable critical current as a function of T, B and α was computed according to [38].

4.3.2 Computation of minimum quench energy

Here we present how the volume of the normal zone ellipsoid, and consequently the MQE, of the MPZ concept is computed. The major radius R_{mz3} of figure 2.6 is computed, according to [136], as

$$R_{mz3} = \sqrt{\frac{3\lambda_l \left(T_{cs}\left(\mathbf{B}, J_{op},\right) - T_{op}\right)}{\rho_m J_m^2}}, \tag{4.10}$$

Table 4.8: Operation conditions

Parameter	Value
Initial Current	6 kA
Initial Temperature	4.2 K
Cable Area (insulated)	12.2 mm^2
Copper RRR-value	100
Superconductor n-value	20

where λ_l, ρ_m and J_m are the thermal conductivity along the cable, the resistivity of the matrix metal and the current density in the matrix metal after the transition the the normal state, respectively.

Due to the anisotropic thermal conductivity within the cable the radii R_{mz1} and R_{mz2} in the MPZ ellipsoid are not identical to the R_{mz3}. According to [156] we can estimate the radii with

$$R_{mzi} = \sqrt{\frac{\lambda_i}{\lambda_l}} R_{mz3}, \tag{4.11}$$

where λ_i is the thermal conductivity at the direction of the x_i-axis.

When the volume of the MPZ ellipsoid, V_{MPZ}, is known, we can compute the MQE with

$$MQE = V_{MPZ} \int_{T_{op}}^{T_{cs}(\mathbf{B},J_{op})} C_p(T) dT. \tag{4.12}$$

4.3.3 Results

The presentation of results is divided into two parts. First we compute MERQ for a reference case, with predefined heater area and heater pulse length. For the reference case the heater area was selected to be 130 mm^2 (18 mm long and 7.2 mm wide) and the pulse length 25 ms. The obtained MERQ is then compared to the MQE computed with (4.12). Then, we consider parameteric analyses to observe the effect of heater area and pulse length to the MERQ. When one variable was varied, the other was kept constant.

MERQ vs. MQE: reference case

Figure 4.11 presents the hot spot temperature as a function of heater energy at different time instants after the heater ignition. After 25 ms, i.e. the time

instant when the heater was turned off, the hot spot temperature varied from 65 K to 198 K, when the heater energy increased from 1 J to 4 J, respectively. The MERQ in this case was 1.55 J, because below that value the hot spot temperature kept decreasing when the time elapsed and the magnet did not quench. However, above 1.55 J the hot spot temperature increased after the heater was switched off and the magnet quenched. It is notable, that increasing the hot spot temperature to even 65 K from the operation temperature of 4.2 K with heater energy of 1 J was not sufficient to quench the magnet. The hot spot temperature of 95 K had to be reached to quench the magnet with the MERQ of 1.55 J.

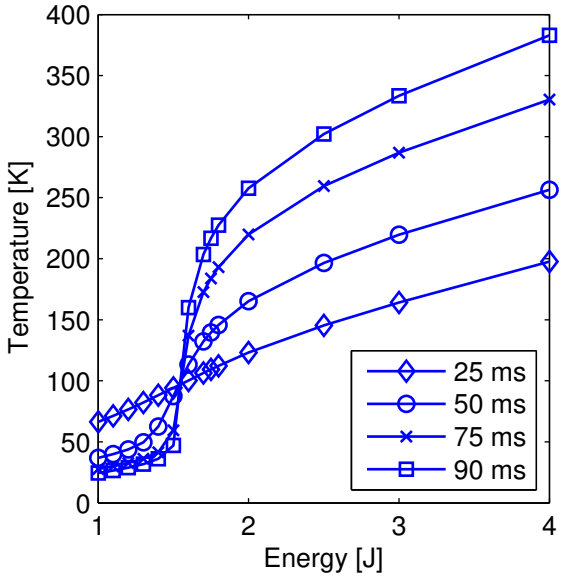

Figure 4.11: Hot spot temperature at different time instances after the heater ignition. Heater is switched off after 25 ms.

Computing the MQE for this magnet using the analytical formula resulted in the MQE of 50 mJ and 150 mJ with T_{cs} of 36 K and 58 K, respectively. With the minimum T_{cs} of the magnet, 36 K, the MQE was 30 times smaller than the MERQ of 1.55 J and using the maximum T_{cs}, 58 K, the MQE was 10 times smaller than the MERQ. As the MQE values are considerably smaller than the MERQ values, (4.12) should not be used to estimate the energy required to quench the HTS magnet. According to this study the energy computed using the MQE concept is not sufficient to quench the corresponding HTS magnet when utilizing a strip heater.

Parametric analyses

In the first parametric analysis we studied the effect of heater pulse length on the MERQ. Figure 4.12 presents the MERQ as a function of pulse length. MERQ varied between 0.8 J and 7 J with pulse lengths varying from 5 ms to 500 ms. With short pulse lengths, less than 100 ms, the MERQ increased rapidly, but with longer pulse lengths MERQ increased almost linearly. Figure 4.12 shows that with short pulse lengths much less energy is required to quench the magnet. However, short pulses translate into high power densities within the heater, and may burn the heater. This was not studied here, however, when designing a strip heater for measurements this analysis has to be done. Furthermore, if long pulse lengths have to be used, the long simulation time may prove to be difficult for numerical simulations. The linear behaviour with long pulse lengths can be utilized in these cases.

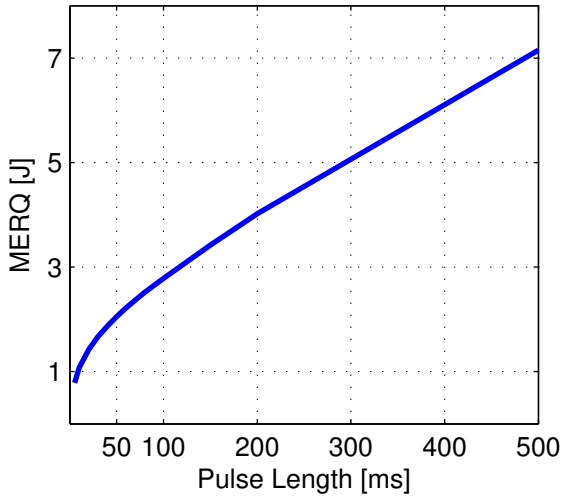

Figure 4.12: MERQ as a function of heater pulse length.

In the second parametric study the heater's cross-section area was varied. Figure 4.13 presents the MERQ and MERQ relative to the heater's cross-sectional area as a function of heater area. The MERQ increased from 1.2 J to 2.2 J with heater area varying from 22 mm^2 to 300 mm^2 (by lengthening the heater from 3 mm to 31 mm). The MERQ increased almost linearly as a function of heater area. However, the MERQ divided by heater area saturated towards a certain value, 8 mJ/mm^2. Surprisingly, this value corresponded to the enthalpy margin, from 4.2 K to the average T_{cs} of 47 K within the heater area.

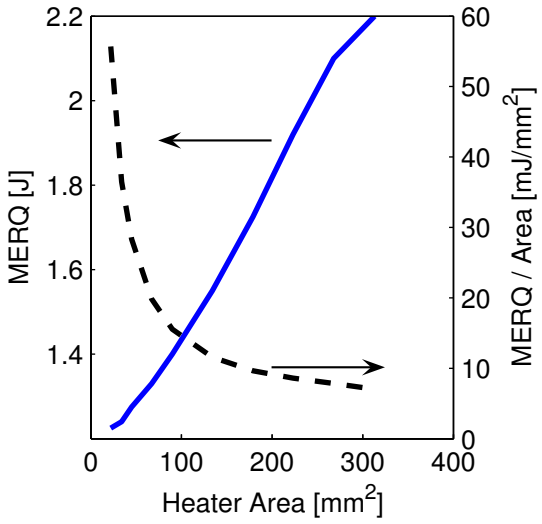

Figure 4.13: Solid line and dashed line present MERQ and MERQ divided by heater area as a function of heater area, respectively.

Figure 4.13 shows that the smaller heater area means smaller MERQ. However, the hot spot became more localized, where the hot spot temperature rose more rapidly. This means that damaging the magnet due to overheating is a larger threat due to the difficult quench detection in HTS magnets. Furthermore, small heater area corresponds to a large power density within the heater in the same way as with a short heater pulse length. Large power density may burn the heater [127], thus, avoiding spot heaters when quenching an HTS magnet is advisable.

4.4 Summary

First the normal zone propagation velocity for HTS magnets was studied. The normal zone propagation velocity in longitudinal direction varied as much as 30% until it levelled off while absolute values were in the range of 0.5 m/s with the T_{cs} of 15 K. The simulated transverse propagation velocity was slow, around 0.1 cm/s slightly depending on the T_{cs}, when insulation layers between the cables were present in the model. We showed that v_{nzp} was not constant during the quench but it depended on the evolution of the temperature distribution. After a certain threshold v_{nzp} levelled off. Thus, studying the placement of the

voltage taps is crucial for reliable v_{nzp} measurements for HTS magnets. The normal zone propagation velocity should be measured at sufficient distance, even at the range of 100 mm from the hot spot, to get reliable measurement results.

Next, we studied the hot spot temperature in an HTS magnet using finite element analysis and the MIITs concept. In particular, the difference between FEA and MIITs with varying quench detection threshold voltages and magnet inductances were under investigation. The hot spot temperature differences between FEA and MIITs, while always being higher with MIITs, varied from 60 K to 150 K with inductances varying from 8.16 μH to 81.6 mH, respectively. Similar results were obtained with the quench detection threshold voltages of 10 mV, 30 mV and 50 mV. Temperature differences of 100 K are rather large for quench studies, thus, MIITs concept seems unreliable when considering hot spot temperatures in HTS magnets. However, MIITs concept is usable when quickly comparing different magnet designs.

At the end of this chapter a numerical approach was taken to estimate the minimum energy required to quench an HTS magnet for measurement purposes. First we estimated MERQ in a reference case, where the heater area was 130 mm^2 and the heater pulse length was 25 ms. At the operation temperature of 4.2 K and with the operation current of 6 kA the MERQ was 1.55 J, which was 10-30 times larger than the result given by an approximative analytical solution of MQE, when T_{cs} was between 36 K and 58 K in the magnet at the heater area. In the parametric analyses the MERQ increased almost linearly from 0.8 J to 7 J with heater pulse lengths varying from 5 ms to 500 ms. In addition, the MERQ increased linearly as a function of heater area from 1.2 J to 2.2 J with heater areas varying from 22 mm^2 to 300 mm^2. In conclusion, when one prepares for quench detection and protection measurements for HTS magnets, numerical approach to design a strip heater for quench ignition is preferred over the analytical one.

Chapter 5

Quench simulation of an HTS racetrack magnet

For the preparation of the post-LHC accelerator complex, the European wide EuCARD (see Section 2.1.4) project was launched in 2009. During the project, a 6 T HTS insert magnet was designed. The plan was to manufacture and finally test the magnet inside an LTS outsert producing 13 T. Due to the limited information about stability and quench of HTS accelerator magnets characterized with high current densities and high magnetic fields, part of the WP 7 in EuCARD project was to study the quench characteristics of the insert. This particular design was never completed during the EuCARD project, however, the work continues within the EuCARD2 (see Section 2.1.4) project with a different HTS magnet design. In this chapter we present the results of the quench analysis for the HTS insert designed in the EuCARD project.

Utilizing QuEST the quench was analyzed for an YBCO insert coil based on **Publication 1** and **Publication 2**. First we present the overview of the analyzed cases including the modelling domain and the operation conditions. In addition, due to the extremely high stability margin, i.e. high T_{cs}, the method to quench the magnet for simulation purposes was studied. It has been shown that using a spot heater the hot spot temperatures at the beginning of the quench will rise to questionably high values [33] with HTS magnets. A method based on reducing the I_c locally to initiate the quench is presented. Eventually the quench simulation results for the HTS insert are presented.

The slow normal zone propagation velocity (v_{nzp}) in HTS magnets can, and should, be taken into account when simulating a quench. We show that exploiting this possibility, large savings in computation time is possible without

sacrificing the accuracy of the results. A study on reducing the modelling domain to decrease the computation time of the quench simulation is presented at the end of the chapter. This is based on **Publication 3**.

5.1 Quench simulation for the EuCARD 6 T HTS insert magnet

5.1.1 Modelling domain and operation conditions

The modelling domain utilized in the simulation is presented in figure 5.1. The HTS insert consists of 3 double pancakes, totaling in 6 coils. The lengths of the insert pancakes and number of turns in coils are presented in Table 5.1, where it is notable that not all the coils have the same length. Also, it is worth mentioning, that usually the accelerator magnets have flared ends, so that the beam pipe can be inserted to go through the magnet. Here this is not the case, as due to the completely new design as an HTS insert, the main goal was to learn manufacturing of such a magnet, as well as to perform quench experiments among other things.

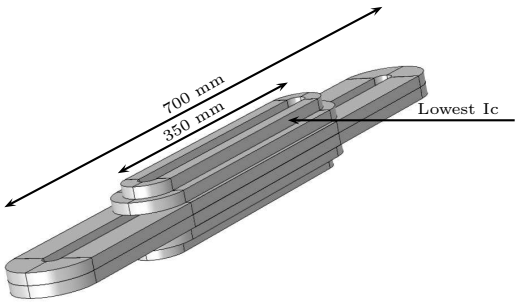

Figure 5.1: Investigated magnet.

The cable configuration is presented in figure 5.2. The cable consists of two YBCO tapes that are soldered together with a copper shunt between the tapes to achieve a good thermal and electrical connection between the tapes. The added copper is for stabilization during the quench. A portion of

Table 5.1: Magnet characteristics [26]

Pancake	Number of turns	Length (mm)
mid plane	73	700
medium	61	350
top	35	326.1

$CuBe_2$ was also considered to be included in the cable to strengthen the cable mechanically. A 30 μm thick kapton insulation was used. Table 5.2 presents the material constituents of the magnet unit cell.

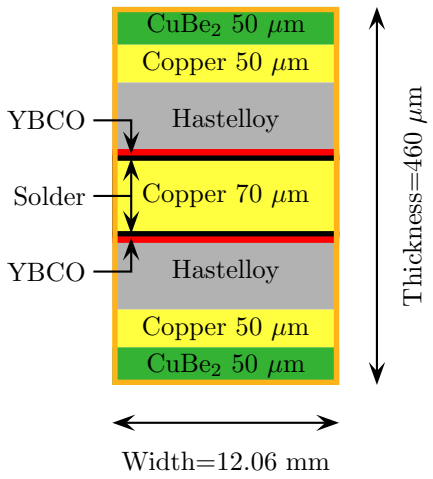

Figure 5.2: Schematic view of the cable for the YBCO racetrack insert. Orange outer boundary represents the kapton insulation. Figure is not in scale.

Table 5.2: Relative material proportions of magnet unit cell.

Copper	31 %
$CuBe_2$	19 %
Hastelloy+YBCO	35 %
Kapton	15 %

The critical current of the cable when magnetic field is parallel to the

cable's wide surface was computed from

$$I_c(T,B) = I_0(T)\frac{1}{\left(1+\frac{B}{B_{peak}(T)}\right)^{\beta}}, \tag{5.1}$$

where I_0(T) is I_c value at 0 T, B_{peak}(T) is the magnetic flux density corresponding to the maximal macroscopic pinning force and the constant parameter β is 1.43 [73]. Angular dependency of I_c was taken into account by formula

$$I_c(B,\alpha) = I_c(T,B)\exp\left(\frac{-|90-\alpha|}{\beta_0 B^{-d}}\right), \tag{5.2}$$

where β_0 and d are 62.864 and -0.727, respectively. I_c computed with (5.1) and (5.2) is presented in figure 5.3.

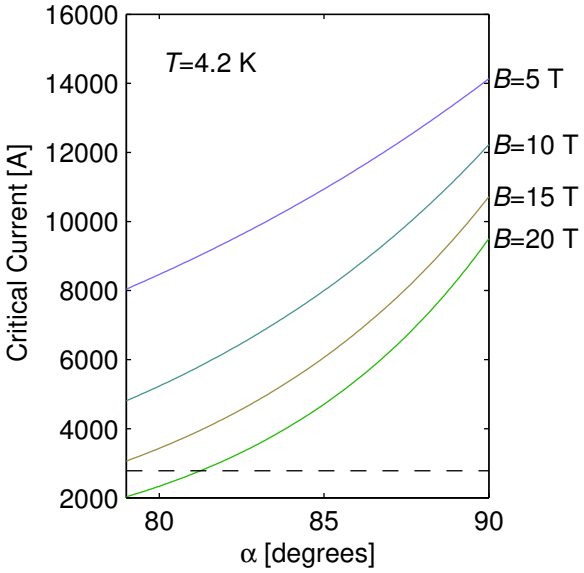

Figure 5.3: YBCO cable critical current as a function of α. Dashed line represents the nominal operating current of 2800 A.

HTS magnets are extremely stable in case of a disturbance. To demonstrate the high T_{cs} of HTS magnets, figure 5.4(a) and figure 5.4(b) present T_{cs} for this particular case for the cross-section of the magnet in the middle of the straight section as well as for the end of the magnet, respectively. From these figures one can see, that even with a rather high operating current density (250 A/mm^2), which corresponds to an operating current of 2800 A, T_{cs} is from 10 K to even

25 K. Also, T_{cs} of 25 K is reached in the high field region of the magnet in the inner radius, which is usually the place, where the LTS magnets quench more easily. However, for HTS magnets manufactured using an anisotropic cable, magnet's short sample limit is reached where B is high and the direction of the field is perpendicular to the tape. In this case it can be seen that the area of low T_{cs} is at the top of the magnet, where $\mathbf{B}$ is almost completely perpendicular to the tape's surface. The magnet boundary was considered to be adiabatic in the simulations.

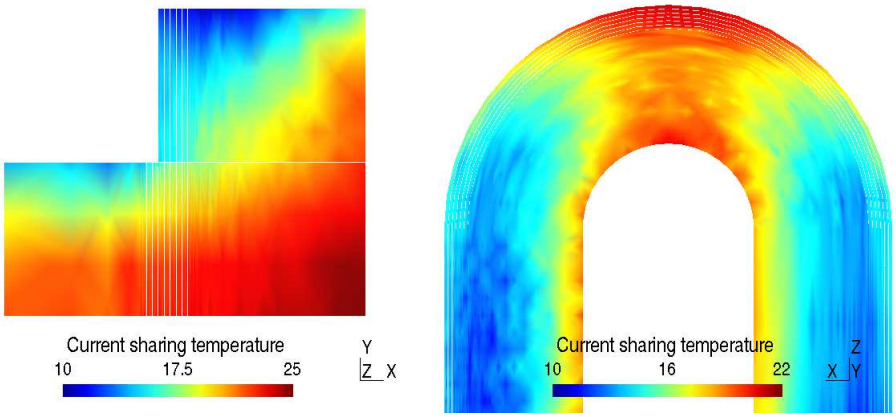

(a) (b)

Figure 5.4: Current sharing temperature in the cross-section of the coil in the middle of the hot spot region (a) and on top of the coil (b).

5.1.2 Utilizing reduced critical current to ignite the quench

Due to the very high stability margin of HTS magnets, quenching the magnet on purpose during the measurement is not a trivial task. In the simulations similar dilemma is faced. There are at least two possible options to quench the magnet in a simulation. First, it is possible to increase the temperature in small volume within the magnet. However, using an external heater, the small volume could require peak temperature in the range of 100 K to achieve a propagating normal zone as shown in section 4.3.3. Another option is to set a decreased I_c to a small volume within the magnet and let the quench develop. In principle this means that there exists a small volume in the magnet where heat is the constantly generated from the beginning of the simulation. By doing this, we can create a much smoother quench compared to triggering the quench with a short heat pulse [33]. In addition, this method can also be used

to model a magnet with a lower quality area, in terms of J_c. It is common that HTS wires suffer from inhomogenous critical currents [151] in long lengths, which leads to a lower critical current.

Figure 5.5(a) presents the hotspot temperature as a function of time with three different values of I_c set to a location described in figure 5.1. From here it can be seen, that the value for the reduced I_c does not modify the behaviour of the quench in the hot spot. Furthermore, figure 5.5(b) shows that the voltage within the normal zone increases in a similar way with the different values of reduced I_c. However, the value of reduced I_c affects greatly on the time it takes to quench the magnet, which has a significant effect on the simulation time. Therefore, when quench is ignited with the reduced I_c, one should use I_c of 0 A in the hot spot.

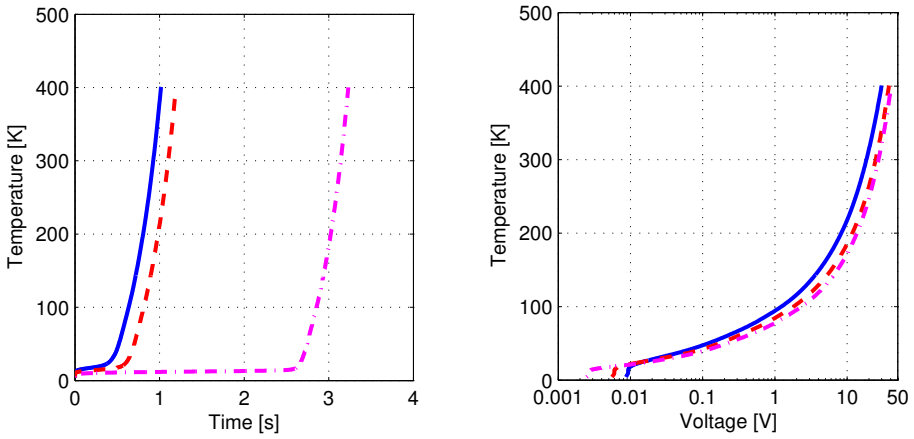

(a) (b)

Figure 5.5: Quench simulation results of YBCO insert. The solid (–) line corresponds to a reduced critical current of 0 A, dashed (– –) line 1000 A and dash-dotted (–.–) line 2000 A.

5.1.3 Quench simulation results

Here we present the quench simulation results for the HTS insert. Due to the low inductance (4 mH) and overall current density of the insert, we did not include quench protection to the simulations but kept the operation current constant during the simulation. With such a low inductance the operation current decayed to 10% of the initial operation current in 50 ms, so we decided to simulate the quench until the hotspot temperature reaches 400 K. Then,

in the post-processing phase we were able to study the hotspot temperature related to different quench detection voltages (delay in the protection needs to be taken into account nevertheless).

Figure 5.6 shows the temperature distribution in the magnet where the temperature was between 8 K and 400 K at the end of the simulation. As can be seen, due to the very low v_{nzp}, the heat distributes only to a small volume outside of the original hotspot, which is typical for HTS magnets. The quench detection is diffcult due to the small volume of the hot spot, which consequently means low R_{norm}.

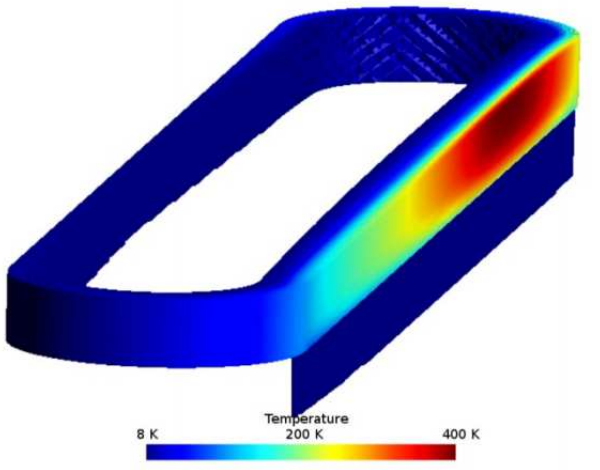

Figure 5.6: Temperature distribution within the coil at the end of the quench simulation.

The hotspot temperature and voltage over the normal zone are presented in figure 5.7(a) and figure 5.7(b), respectively. The quench detection threshold voltage was expected to be 100 mV. Quench detection threshold voltages in today's state-of-the-art devices are in the range of 10-50 mV [20]. However, according to figure 5.7(b) (b), with a detection threshold voltage of 100 mV the corresponding hotspot temperature would still be closer to 50 K than to that of 100 K, which is more than safe from the magnet operation point of view [149]. This hotspot temperature allows rapid discharge of the magnet before the coil is damaged due to overheating and insulation or YBCO layer melting. However, due to the very localized hotspot there may arise unexpected problems for example related to the thermal stresses [69], but that is not in the scope of this thesis.

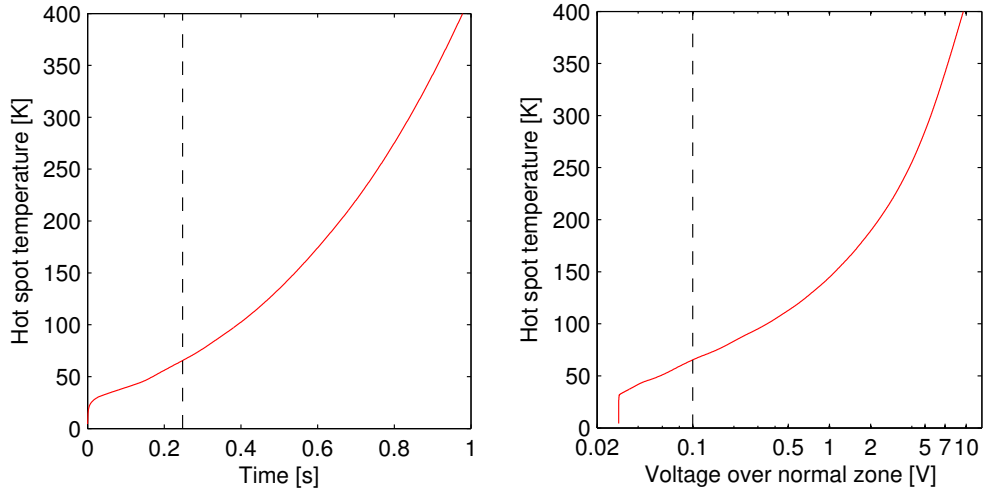

(a) (b)

Figure 5.7: Hot spot temperature as a function of (a) time and (b) terminal voltage. Dashed lines present detection threshold voltage.

5.2 Reducing modelling domain to speed-up quench simulations for HTS coils

Due to the very slow v_{nzp} of HTS magnets, large volume from Ω can be discarded without affecting notably to the quench simulation results if heat diffuses in the magnet only due to the Joule heating. In this section we will demonstrate how the quench simulation results vary when different fractions of Ω are considered in the computation. First we present the simulation setup for the reduction of Ω and then the results of the study.

5.2.1 Simulation Setup

Studies in this section are based on the HTS insert magnet presented in figure 5.1. The starting point was to include all the 6 coils of the magnet in the Ω. The superconducting material for the magnet was YBCO as before, however, the material constituents in the cable differed. The renewed cable is presented in figure 5.8. The portion of $CuBe_2$ was increased and the portion of copper was decreased to achieve mechanically stronger cable. Other modelling decisions such as heat generation computation and boundary conditions were similar as in the previous section. Heat generation was computed according to the current sharing model and adiabatic boundary conditions were used.

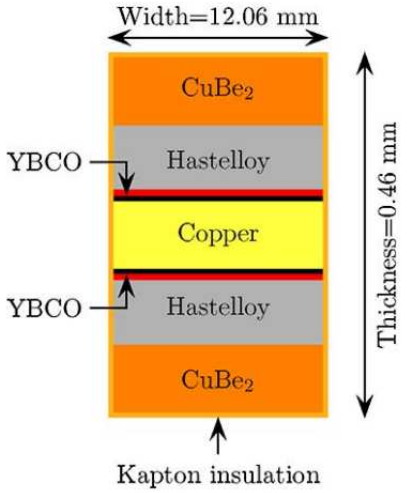

Figure 5.8: Cable configuration with insulation layer used in quench computations. Figure is not in scale.

As opposed to the common approach to use homogenized material parameters in Ω, we modelled part of the magnet using actual cable and insulation layers. However, inside the cable the actual YBCO layers were not modelled, but the materials in the cable were homogenized [18]. By using insulation layers between the cable layers we were able to observe the effect of the insulation layers to the heat conduction. Figure 5.9 presents the different regions in our Ω. Only the two topmost coils are presented in the figure, but the same structure was utilized in all the coils, only the number of accurate cable layers varied. The topmost coil had 17 accurate cables modelled from the total of 35 cables. The remained 18 cables, and the insulation layers between them, were modelled as a homogenous material. Table 5.3 presents the material constituents for the homogenous region and for the cable. Insulation layers were Kapton.

Table 5.3: Relative material proportions of unit cells.

	Coil	Cable	Insulator
Copper	15 %	17.7 %	0 %
$CuBe_2$	42 %	49.4 %	0 %
Hastelloy+YBCO	28 %	32.9 %	0 %
Kapton	15 %	0 %	100 %

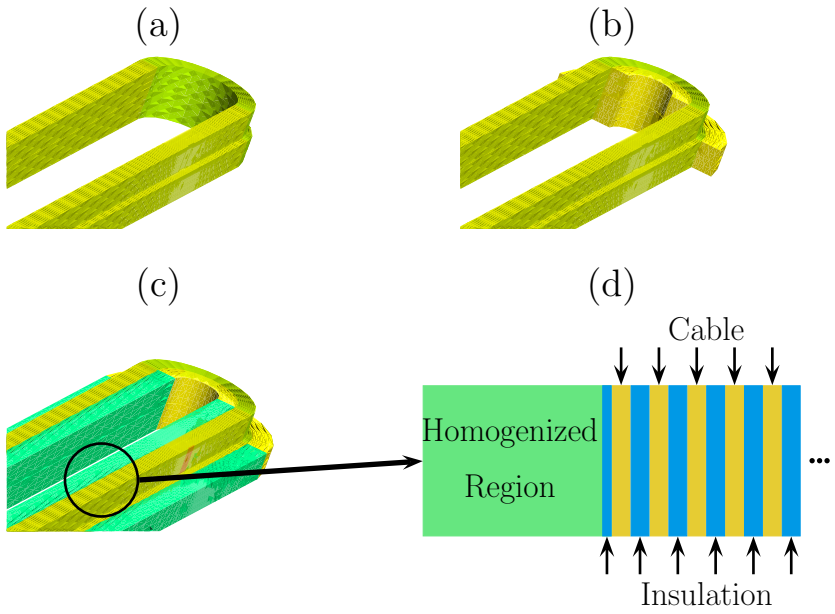

Figure 5.9: Different regions of the insert. However, only two top coils are shown. a) only accurate cable layers b) included homogenized part in the magnet end c) included homogenized part in the straight section and degraded cable length on the outermost layer of the topmost coil (orange part on the coil outer layer) d) cross-section from the top coil in the middle of the straight part showing homogenized part and accurate cable layers

5.2.2 Number of coils in the modelling domain

First we considered the effect of the number of coils included in Ω. Figure 5.10 shows that the quench simulation results vary only slightly, when including only the topmost coil to Ω, when compared to the simulation using the whole magnet. There is only 3 ms difference in the quench detection time, which was 71 ms for 6 coils, when only the top coil was included in Ω. The quench detection threshold voltage was 100 mV in this study. Hotspot temperatures at the time of detection were 67 K and 68.5 K for the 1 coil and 6 coils, respectively. This is a clear indication that one can decrease the size of Ω considerably without effecting on the simulation results meaningfully. It is notable, that even though the plots are not similar in figure 5.10 (d) the result is similar. The difference is due to the calculated percentage of normal zone in Ω, where the total volume used was always the volume of the magnet with 6 coils. However, the normal zone was not able to propagate to the other coils in the simulation with 1 coil, thus, resulting in a lower percentage of the normal

zone volume. Still, this affected the most important characteristics (t,T) and (V,T) only a little.

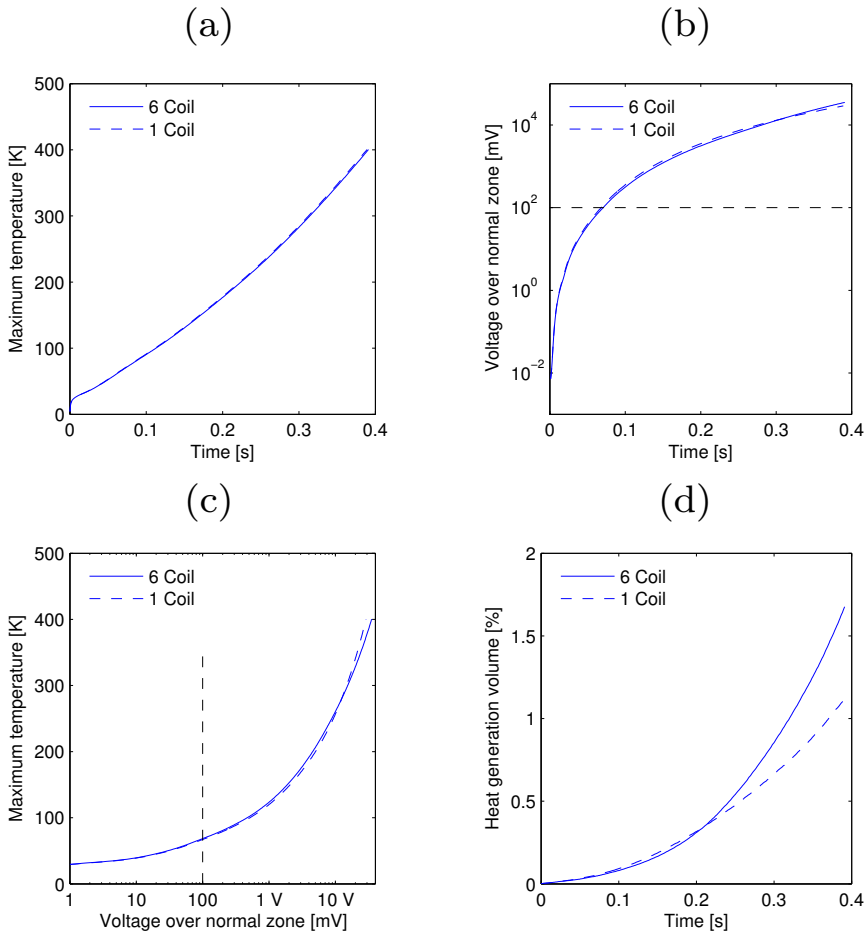

Figure 5.10: Quench simulation results for variation of the amount of coils in Ω. Figure a) presents hot spot temperature as a function of time, b) voltage over the normal zone as a function of time c) hot spot temperature as a function of normal zone voltage d) heat generation volume. Dotted line in figures b) and c) presents the considered quench detection threshold voltage, 100 mV.

What is the benefit of reducing the modelling domain in computations? Quench modelling can take a lot of time, especially when Ω is large and detailed structures are modelled. Table 5.4 presents the achieved reductions in the computation time when parts of the magnet were removed. As can be seen, the computation time reduced very rapidly when we reduced the number of elements and, consequently, the degrees of freedom from Ω. In every case the

mesh was kept the same. As figure 5.10 shows, we could reduce Ω from 6 coils to 1 coil without losing the reliability of the results, which meant in this case the total time saving of 46 h per simulation.

Table 5.4: Number of elements and computation time with different geometries

No. Coils	No. of Elements	No. of DoFs	Computation time
1	157 058	39 622	0 d 10 h
2	386 189	90 127	1 d 2 h
3	631 355	142 418	1 d 11 h
4	820 000	182 935	2 d 0 h
6	940 000	209 009	2 d 8 h

5.2.3 Number of cables in the modelling domain

When the reduction from the whole magnet to only the topmost coil did not change the simulation results, we decreased the size of Ω even more until we observed the change in the results. In this study we removed the homogenized region completely (green region and solid yellow in the end of the upper coil in figure 5.9) and took into account only accurate cable layers and insulation layers between them. Only the top coil was studied here, as the previous study showed that the other coils did not contribute to the results.

In figure 5.11 varying number of cables are compared to the results of 1 coil, which was investigated earlier. Here we can distinguish a difference when less than 10 cables were present in Ω. With 10 cables the results were practically the same than achieved with 1 coil. Quench detection times were 67.8 ms and 68 ms and hot spot temperatures at the time when voltage reached 100 mV are 67 K and 67.1 K with 10 cable modelling domain and 1 coil, respectively. When less than 10 cables were included in Ω, the heat diffusion was limited too much, which resulted in higher hot spot temperature with lower voltage.

Table 5.5 presents the computation times and number of elements in this study. When compared to the Table 5.4, it can be seen that the computation time for 10 cables, which corresponds to the same result as with 1 coil, is less than half of the computation time for 1 coil. Reducing the modelling domain may lead to new possibilities in situations, where the computation seems too time consuming due to the need for a large number of degrees of freedom and should be kept in mind when doing quench simulations for HTS magnets.

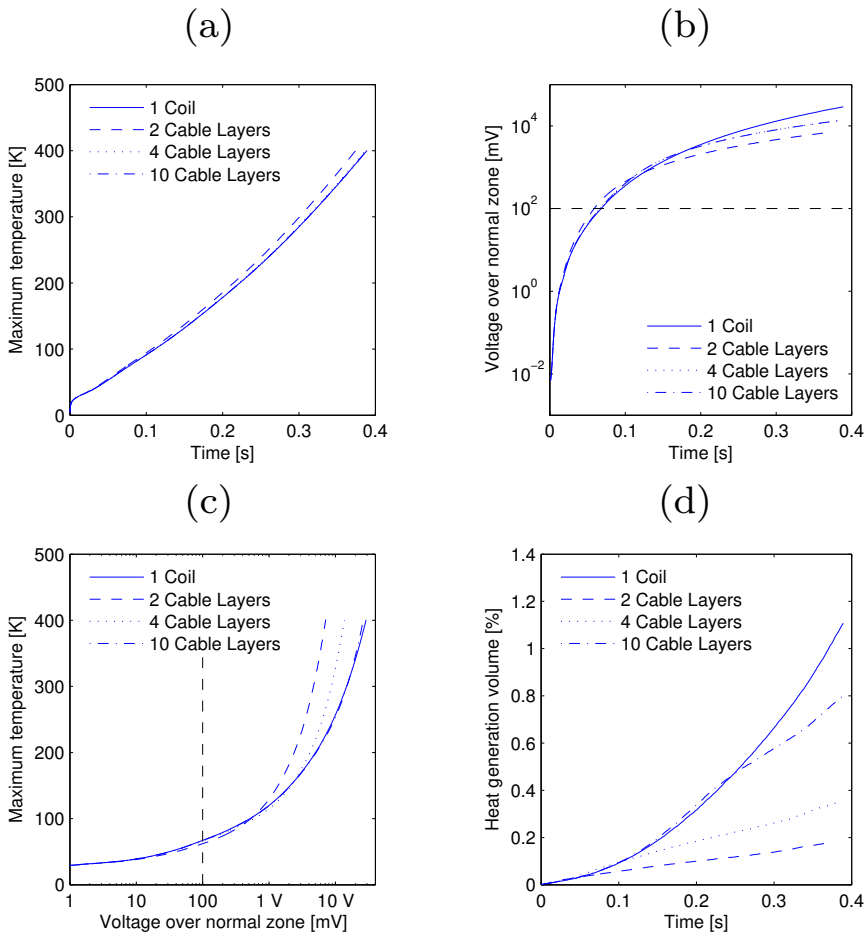

Figure 5.11: Quench simulation results for the variation of the amount of cables in Ω. Subfigures correspond to those in figure 5.10.

Table 5.5: Number of elements and computation time with amount of cables

No. Cables	No. of Elements	No. of DoFs	Computation time
1	2476	1218	8 min
2	14856	4283	50 min
4	29712	7961	1 h 53 min
10	74280	18995	4 h 25 min

5.3 Concluding remarks

An HTS insert magnet designed in the EuCARD project was presented and the quench simulation was considered. The focus was on the modelling decisions,

due to the completely different nature of HTS magnets compared to their LTS counterparts. The quench mechanism for the magnet was discussed as different quench scenarios are possible in HTS magnets. To acquire a smooth quench, we decided to utilize a reduced I_c in a small volume in the magnet to quench the coil slowly. By doing this, large, and possibly artificial, temperature spikes do not exist in the simulation.

The quench was scrutinized for the investigated magnet. The temperature in the coil just below the quenched one reached barely 10 K when the hot spot temperature reached 400 K. This lead to the question that should one even simulate the quench using the whole magnet as a modelling domain? The hot spot temperature was considerably below 100 K, when the quench detection threshold voltage of 100 mV was reached. This indicates, that with the low stored energy, a safe operation of such a magnet is possible using only dump resistor for the protection. However, due to the very localized hot spot, the concern on large thermal stresses was expressed.

We showed that it is not necessary to simulate the whole modelling domain when simulating a quench for HTS magnets. Simulation results were similar even when using only a small portion of the original modelling domain of 6 coils. The computation time could be reduced to below 8 percent of the original. Of course this modelling domain reduction is case dependent, and we did not give any universal methodology how to reduce Ω in a given case. However, this possible reduction should be kept in mind, especially when simulating quench for very large magnets with hundreds of thousands of degrees of freedom.

Chapter 6

Conclusions

The usability of high temperature superconducting (HTS) magnets in high energy physics is under thorough investigation. However, due to the high engineering current density, the quench detection and protection system has to be flawless in order to prevent permanent damage in the magnet in case of a quench. In this thesis we concentrated on numerical simulations to study the quench event of HTS magnets, which is required for quench detection and protection system development. Unfortunately, due to the delays in the magnet manufacturing process within the EuCARD-2 project, there was no possibility to benchmark the simulation results with the measurements.

This thesis is based on six publications while being an independently readable entity. Chapter 2 and Chapter 3 establish the foundation for all the publications. Superconducting phenomenon is discussed in detail in Chapter 2 followed by the numerical background for quench modelling. Chapter 3 presents the in-house software development for quench modelling, which was used for modelling in all publications. Our in-house software, QueST (finite element method based Quench Simulation Tool), is described in detail starting from the main constituents of the software. Furthermore, we show a particular case, where the source code is polished to decrease the computation time, which would not have been possible with a commercial software.

In Chapter 4, which is based on **Publications 4, 5** and **6**, we study the differences of quenches in LTS and HTS magnets. First, we show that the normal zone propagation velocity (v_{nzp}) is not constant in HTS magnets, but increases until levelling off at a certain distance from the hot spot, as described in **Publication 4**. Due to the large temperature margin, the quench frontier does not propagate with the temperature frontier, which means different quench evolution in LTS and HTS magnets. Then, we study the usability

of a zero-dimensional, so-called MIITs concept, for studying the hot spot temperature of HTS magnet in case of a quench, based on **Publication 5**. We show that the hot spot temperature computed using MIITs is considerably higher than based on numerical analysis, and thus, the MIITs concept should not be used to estimate hot spot temperatures in HTS magnets at least before the quench protection is activated. However, MIITs concept can be utilized to compare different magnet designs, when absolute values are not desired, to achieve faster computation time. Finally, as presented in **Publication 6**, we show that Wilson's analytical formula to compute the minimum quench energy (MQE) is not feasible for HTS magnets. Analytical result is considerably lower than the MQE computed utilizing numerical approach, and thus, MQE estimation for measurement purposes should be done numerically. In addition, a strip heater, in place of a traditional spot heater, should be used to ignite the quench for HTS magnet measurements due to the large temperature margin.

The quench simulation is scrutizined for an HTS research magnet in Chapter 5, based on **Publications 1, 2** and **3**. First, we present the magnet design used for simulations. Then, we describe an alternative method to ignite the quench for numerical computations. By reducing the critical current in small part of the magnet, the quench can be ignited without a large temperature peak, that occurs when a small heat pulse is used for quench triggering. Finally, we present the quench simulation results, which indicate that the quench is rapid in HTS magnets and the quench protection system needs to be designed carefully to prevent irreversible damage to the magnet, as described in **Publication 1** and **Publication 2**. Especially the quench detection system is crucial, when magnets with low inductance, and thus, fast current decay, are considered. In addition, we study the possibility to decrease the computation time considerably by reducing the modelling domain volume, as presented in **Publication 3**. As the quench propagates slowly in HTS magnets, it is not necessary to include the whole magnet in the simulation. Still, the same accuracy can be maintained in the results while achieving considerable reduction in computation times.

In conclusion, multiple completely new ideas and approaches for simulating quench event in HTS magnets are presented in this thesis. Especially, the proposed modelling domain reduction and quenching the magnet using reduced I_c are remarkable for upcoming quench simulation tasks. In addition, the thorough explanation of diverse quench evolution in LTS and HTS magnets, due to the much higher stability margin of HTS, is crucial to understand when analyzing the quench event of superconducting magnets. Furthermore, due to the diverse quench evolution, many previously used quench modelling approaches for LTS magnets are not usable with HTS magnets.

Bibliography

[1] A. B. Abrahamsen *et al* , "Superconducting Wind Turbine Generators", *Supercond. Sci. Technol.*, vol. 23, id: 034019, 2010, doi: 10.1088/0953-2048/23/3/034019

[2] Accelerators for Society, sponsored by the TIARA project http://www.accelerators-for-society.org/.

[3] R. Albanese and G. Rubinacci, "Solution of Three Dimensional Eddy Current Problems by Integral and Differential Methods", *IEEE Trans. Magn.*, vol. 24, pp. 98-101, 1988, doi: 10.1109/20.43865

[4] D. Baldomir, "Differential Forms and Electromagnetism in 3-Dimensional Euclidean Space R^3", *IEEE Proceedings*, vol. 133, pp. 139-143, 1986, doi: 10.1049/ip-a-1.1986.0025

[5] A. Ballarino, "HTS Current Leads for the LHC Magnet Powering System", *Physica C*, vol. 372 - 376, pp. 1413 - 1418, 2002, doi: 10.1016/S0921-4534(02)01042-0

[6] J. Bardeen, L. N. Cooper, and J. R. Schrieffer, "Theory of Superconductivity", *Phys. Rev.*, vol. 108, pp. 1175 - 1204, 1957, doi: http://dx.doi.org/10.1103/PhysRev.108.1175

[7] R. H. Bellis and Y. Iwasa, "Quench Propagation in High T_c Superconductors" *Cryogenics* vol. 34, pp. 129 - 144, 1994, doi: 10.1016/0011-2275(94)90036-1

[8] J. K. Bednorz and K. A. Müller, "Possible High T_c Superconductivity in the Ba-La-Cu-O System" *Z. Phys. B* vol. 64, pp. 189 - 193, 1986, doi: 10.1007/BF01303701

[9] O. Bíró, K. Preis, and K. Richter, "On the Use of the Magnetic Vector Potential in the Nodal and Edge Finite Element Analysis of 3D Magne-

tostatic Problems", *IEEE Trans. Magn.*, vol. 32, pp. 651-654, 1996, doi: 10.1109/20.497322

[10] M. Bonura and C. Senatore, "High-Field Thermal Transport Properties of REBCO Coated Conductors", *Supercond. Sci. Technol.*, vol. 28, id: 025001, 2015, doi: 10.1088/0953-2048/28/2/025001

[11] A. Bossavit, "Whitney Forms: a Class of Finite Elements for Three-Dimensional Computations in Electromagnetism", *IEEE Proceedings*, vol. 135, pp. 493-500, 1988, doi: 10.1049/ip-a-1.1988.0077

[12] L. Bottura, G. de Rijk, L. Rossi, and E. Todesco, "Advanced Accelerating Magnets for Upgrading the LHC", *IEEE Trans. Appl. Supercond.*, vol. 22, id: 4002008, 2012, doi: 10.1109/TASC.2012.2186109

[13] H. Brechna and P. Turowski, "Training and Degradation Phenomena in Superconducting Magnets", *Proc. 6th Intl. Conf. Magnet Tech.(MT6)(ALFA, Bratislava, Czechoslovakia)*, vol. 597, 1978.

[14] O. Brüning *et al* , "LHC Design Report, Vol.1 The LHC Main Ring", CERN 2004-003, 2004.

[15] O. Brüning and P. Collier, "Building a Behemoth", *Nature*, vol. 19, pp. 285 - 289, 2007, doi: 10.1038/nature06077

[16] P. Bruzzone, "The Index n of the Voltage-Current Curve, in the Characterization and Specification of Technical Superconductors", *Physica C*, vol. 401, pp. 7 - 14, 2004, doi: 10.1016/j.physc.2003.09.005

[17] W. Buckles and W. V. Hassenzahl, "Superconducting Magnetic Energy Storage", *IEEE Power Eng. Review*, vol. 20, pp. 16 - 20, 2000, doi: 10.1109/39.841345

[18] W. K. Chan and J. Schwartz, "A Hierarchical Three-Dimensional Multiscale Electro-Magneto-Thermal Model of Quenching in $REBa_2Cu_3O_{7-\delta}$ Coated-Conductor-Based Coils", *IEEE Trans. Appl. Supercond.*, vol. 22, id: 4706010, 2012, doi: 10.1109/TASC.2012.2198647

[19] D. K. Cheng, "Fundamentals of Engineering Electromagnetics", Prentice Hall, 1993.

[20] Y. Chu *et al* , "Quench Detection Based on Voltage Measurement for the KSTAR Superconducting Coils", *IEEE Trans. Appl. Supercond.*, vol. 19, pp. 1565 - 1568, 2009, doi: 10.1109/TASC.2009.2018238

[21] Comsol Multiphysics is a commercial FEM program. http://www.comsol.com

[22] Conectus, Consortium of European Companies Determined to Use Superconductivity, http://www.conectus.org.

[23] T. C. Cosmus and M. Parizh, "Advances in Whole Body MRI Magnets", *IEEE Trans. Appl. Supercond.*, vol. 21, pp. 2104 - 2109, 2011, doi: 10.1109/TASC.2010.2084981

[24] M. Cyrot and D. Pavuna, "Introduction to Superconductivity and High-Tc Materials", *Singapore: World Scientific*, 1992.

[25] D. W. Deis, "Multifilament Nb_3Sn Conductors: Progress and Prospects", *IEEE Trans. Magn.*, vol. 13, pp. 447 - 453, 1977, doi: 10.1109/TMAG.1977.1059289

[26] M. Devaux *et al* , "HTS Insert Magnet Design Study", *IEEE Trans. Appl. Supercond.*, vol. 22, id: 4203605, 2011, doi: 10.1109/TASC.2011.2174600

[27] A. Devred, "Quench Origins", *AIP Conf. Proc.*, vol. 249, pp. 1262 - 1308, 1992, doi: 10.1063/1.41993

[28] C. H. Dustmann and H. Köfler, "An Attempt to Reduce Training", *Cryogenics*, vol. 17, pp. 667 - 670, 1977, doi: 10.1016/0011-2275(77)90222-3

[29] Phil Eckels, "CryoComp Rapid Cryogenic Design: 88 Materials in Properties Database. Thermal Analysis Software.", http://www.eckelsengineering.com/

[30] J. W. Ekin, "Experimental Techniques for Low-Temperature Measurements", Oxford: Oxford University Press, 2006.

[31] Y. Eyssa and W. D. Markiewicz, "Quench simulation and thermal diffusion in epoxy-impregnated magnet system", *IEEE Trans. Appl. Supercond.*, vol. 5, pp. 487 - 490, 1995, doi: 10.1109/77.402572

[32] Y. Eyssa, W. D. Markiewicz, and J. Miller, "Quench, thermal, and magnetic analysis computer code for superconducting solenoids", *IEEE Trans. Appl. Supercond.*, vol. 7, pp. 159 - 162, 1997, doi: 10.1109/77.614453

[33] P. Fazilleau, M. Devaux, M. Durante, T. Lecrevisse, and J.-M. Rey, "Protection of the 13 T Nb_3Sn Fresca II Dipole", *CERN Yellow Report CERN-2013-006* pp. 65-69, 2014, doi: 10.5170/CERN-2013-006.65

[34] H. Felice *et al* , "Instrumentation and Quench Protection for LARP Nb_3Sn Magnets", *IEEE Trans. Appl. Supercond.* vol. 19, pp. 2458 - 2462, 2009, doi: 10.1109/TASC.2009.2019062

[35] H. Felice, "Quench Protection Analysis in Accelerator Magnets, A Review of the Tools", *CERN Yellow Report CERN-2013-006* pp. 17-20, 2014, doi: 10.5170/CERN-2013-006.17

[36] A. V. Fernandez and F. Rodríguez-Mateos, "Reliability of the Quench Protection System for the LHC Superconducting Elements", *Nucl. Instrum. Meth. A*, vol. 525, pp. 439 - 446, 2004, doi: 10.1016/j.nima.2004.01.081

[37] A. Fevrier, J. P. Tavergnier, Y. Laumond, and M. Bekhaled, "Preliminary Tests on a Superconducting Power Transformer", *IEEE Trans. Magn.*, vol. 24, pp. 1477 - 1480, 1988, doi: 10.1109/20.11523

[38] J. Fleiter, Private Discussion, 2014. To be published.

[39] E. Floch *et al* , "Quench Measurement on SIS 100 Dipole Model", *IEEE Trans. Appl. Supercond.*, vol. 19, pp. 2450 - 2453, 2009, doi: 10.1109/TASC.2009.2019061

[40] R. H. Flora, M. Kuchnir, and A. V. Tollestrup, "Quench Development in Magnets with Multifilamentary NbTi Cable", *IEEE Trans. Magn.*, vol. 13, pp. 28 - 30, 1977, doi: 10.1109/TMAG.1977.1059379

[41] A. M. Forrest, A translation of the original article by Meissner W and Ochsenfeld R 1933 "Ein Neuer Effekt Bei Eintritt der Supraleitfähigkeit", *Eur. J. Phys* vol. 4, p. 117, 1983, doi: 10.1088/0143-0807/4/2/011

[42] E. Gamma, R. Johnson, J. Vlissides, and R. Helm, "Design Patterns: Elements of Reusable Object-oriented Software", Pearson Education, 2004.

[43] C. Geuzaine and J.-F. Remacle, "Gmsh: a Three-Dimensional Finite Element Mesh Generator with Built-in Pre- and Post-processing Facilities", *Int. J. Numer. Meth. Engng*, vol. 79, pp. 1309-1331, 2009, doi: 10.1002/nme.2579

[44] W. Goldacker *et al* , "Status of high transport current ROEBEL assembled coated conductor cables", *Supercond. Sci. Technol.*, vol. 22, id: 034003, 2009, doi: 10.1088/0953-2048/22/3/034003

[45] W. Goldacker, F. Grilli, E. Pardo, A. Kario, S. Schlachter, and M. Vojenčiak, "Roebel Cables from REBCO Coated Conductors: A One-Century-Old Concept for the Superconductivity of the Future", *Supercond. Sci. Technol.*, vol. 27, id: 093001, 2014, doi: 10.1088/0953-2048/27/9/093001

[46] L. F. Goodrich, L. T. Medina, and T. C. Stauffer, "High Critica-Current Measurements in Liquid and Gaseous Helium", *Adv. Cryog. Eng. Mat.*, vol. 44, pp. 873 - 880, 1982, doi: 10.1007/978-1-4757-9056-6_115

[47] K. C. Goretta *et al* , "Fabrication of High-T_c Superconductors", *Mat. Manufac. Processes*, vol. 4, pp. 163 - 175, 1989, doi: 10.1080/10426918908956282

[48] P. M. Grant and T. P. Sheahen, "Cost Projections for High Temperature Superconductors", *arXiv*, arXiv:cond-mat/0202386v1.

[49] F. Grilli, E. Pardo, A. Stenvall, D. N. Nguyen, W. Yuan, and F. Gömöry, "Computation of Losses in HTS Under the Action of Varying magnetic Fields and Currents", *IEEE Trans. Appl. Supercond.*, vol. 24, id: 8200433, 2014, doi: 10.1109/TASC.2013.2259827

[50] E. Hairer, S. P. Nørsett, and G. Wanner, "Solving Ordinary Differential Equations: Nonstiff Problems", Springer-Verlag, 1993.

[51] W. V. Hassenzahl, "Superconducting Magnetic Energy Storage", *Proc. of the IEEE*, vol. 71, pp. 1089 - 1098, 1983, doi: 10.1109/PROC.1983.12727

[52] A. Ishiyama and H. Asai, "A Stability Criterion for Cryocooler-Cooled HTS Coils", *IEEE Trans. Appl. Supercond.*, vol. 11, pp. 1832 - 1835, 2001, doi: 10.1109/77.920204

[53] Y. Iwasa, "Mechanical Disturbances in Superconducting Magnets - A Review", *IEEE Trans. Magn.*, vol. 28, pp. 113 - 120, 1992, doi: 10.1109/20.119824

[54] Y. Iwasa, "Case Studies in Superconducting Magnets: Design and Operational Issues, 2nd edition", Springer, 2009.

[55] J. Jensen, W. Tuttle, R. Stewart, H. Brechna, and A. Prodell, "Selected Cryogenic Data Notebook", *Brookhaven National Laboratory* , 1981

[56] JSON (JavaScript Object Notation). http://json.org/

[57] Y. Kamihara *et al* , "Iron-Based Layered Superconductor: LaOFeP", *J. Am. Chem. Soc.*, vol. 128(31), pp. 10012 - 10013, 2006, doi: 10.1021/ja063355c

[58] H. ten Kate, "The Superconducting Magnet System for the ATLAS Detector in CERN", *IEEE Trans. Appl. Supercond.*, vol. 10, pp. 347 - 352, 2000, doi: 10.1109/77.828245

[59] H. ten Kate, "The ATLAS Superconducting Magnet System: Status of Construction & Installation", *IEEE Trans. Appl. Supercond.*, vol. 16, pp. 499 - 503, 2006, doi: 10.1109/TASC.2006.871348

[60] S. W. Kim, "Material Properties for Quench Simulation (Cu, NbTi and Nb_3Sn)", Fermilab TD Note 00-041, 2000.

[61] Y. B. Kim, C. F. Hempstead, and A. R. Strnad, "Flux-Flow Resistance in Type-II Superconductors", *Phys. Rev.*, vol. 139, id: A1163, 1965, doi: 10.1103/PhysRev.139.A1163

[62] G. Kirby *et al* , "Accelerator Quality HTS Dipole Magnet Demonstrator Designs for the EuCARD-2, 5 Tesla 40 mm Clear Aperture Magnet", *IEEE Trans. Appl. Supercond.*, vol. 25, id: 4000805, 2015, doi: 10.1109/TASC.2014.2361933

[63] T. Kiss *et al* , "Angular Dependence of Critical Current Properties in YBCO Coated Tape Under High Magnetic Field up to 18 T", *Physica C*, vol. 378 - 381, pp. 1113 - 1117, 2002, doi: 10.1016/S0921-4534(02)01720-3

[64] C. Kokkinos, J. C. Perez, M. Karppinen, P. Manil, F. Regis, M. Guinchard, and M. Bajko, "The SMC (Short Model Coil) Nb_3Sn Program: FE Analysis with 3D Modelling", *IEEE Trans. Appl. Supercond.*, vol. 22, id: 4900705, 2012, doi: 10.1109/TASC.2011.2177949

[65] A. Korpela, T. Kalliohaka, J. Lehtonen, R. Mikkonen, J. Pitel, and P. Kováč, "Relation Between Different Critical Current Criteria and Quench Current in HTS Magnets", *Physica C*, vol. 372 - 376, pp. 1360 - 1363, 2002, doi: 10.1016/S0921-4534(02)01029-8

[66] A. Korpela, J. Lehtonen, R. Mikkonen, R. Perälä, "Temperature Dependent CurrentŰVoltage Characteristics of an HTS Coil Having a Poor Resistive Joint", *Physica C*, vol. 386, pp. 457 - 461, 2003, doi: 10.1016/S0921-4534(02)02211-6

[67] H. Kumakura, K. Togano, H. Maeda, J. Kase, and T. Morimoto, "Anisotropy of Critical Current Density in Textured $Bi_2Sr_2Ca_2Cu_3O_x$ Tapes", *Appl. Phys. Lett.*, vol. 58, p. 2830, 1991, doi: 10.1063/1.104749

[68] K. Kuroda, "Superconducting Coils Impregnated with Wood's Metal", *Cryogenics*, vol. 15, pp. 675 - 677, 1975, doi: 10.1016/0011-2275(75)90101-0

[69] D. C. van der Laan, J. W. Ekin, C. C. Clickner, and T. C. Stauffer, "Delamination strength of YBCO coated conductors under transverse tensile stress", *Supercond. Sci. Technol.*, vol. 20, pp. 765 - 770, 2007, doi: 10.1088/0953-2048/20/8/007

[70] V. Lahtinen, "Searching for Frontiers in Contemporary Eddy Current Model Based Hysteresis Loss Modelling of Superconductors", *Ph. D. thesis*, Tampere University of Technology, Finland, 2014 http://URN.fi/URN:ISBN:978-952-15-3352-5

[71] D. C. Larbalestier, V. W. Edwards, J. A. Lee, C. A. Scott, and M. N. Wilson, "Multifilamentary Niobium Tin Solenoids", *IEEE Trans. Magn.*, vol. 11, pp. 555 - 558, 1975, doi: 10.1109/TMAG.1975.1058665

[72] D. C. Larbalestier*et al* , "Isotropic Round-Wire Multifilament Cuprate Superconductor for Generation of Magnetic Fields Above 30 T", *Nature Materials*, vol. 13, pp. 375 - 381, 2014, doi: 10.1038/nmat3887

[73] T. Lecrevisse *et al* , "Quench Propagation in YBCO Pancake: Experimental and Computational Results", *IEEE Trans. Appl. Supercond.*, vol. 23, id: 4601805, 2013, doi: 10.1109/TASC.2013.2246753

[74] H. J. Lee, G. Cha, J.-K. Lee, K. D. Choi, K. W. Ryu, and S. Y. Hahn, "Test and Characteristic Analysis of an HTS Power Transformer", *IEEE Trans. Appl. Supercond.*, vol. 11, pp. 1486 - 1489, 2001, doi: 10.1109/77.920055

[75] P. J. Lee, ASC maintained pages for The Applied Superconductivity Center, available online: http://fs.magnet.fsu.edu/~lee/plot/plot.htm "Master Jc Plots and Nb_3Sn Scaling Spreadsheet".

[76] M. Leghissa *et al* , "Development and Application of Superconductign Transformers", *Physica C*, vol. 372 - 376, pp. 1688 - 1693, 2002, doi: 10.1016/S0921-4534(02)01102-4

[77] J. Lehtonen, R. Mikkonen, and J. Paasi, "A Numerical Model for Stability Considerations in HTS Magnets", *Supercond. Sci. Technol.*, vol. 13, pp. 251-258, 2000.

[78] J. Lehtonen, R. Mikkonen, and J. Paasi, "Effective Thermal Conductivity in HTS Coils", *Cryogenics*, vol. 40, pp. 245-249, 2000, doi: 10.1016/S0011-2275(00)00030-8

[79] E. M. Leung, "Superconducting Fault Current Limiters", *IEEE Power Eng.Review*, vol. 20, pp. 15 - 18, 2000, doi: 10.1109/39.857449

[80] J. Lu, E. Choi, and H. Zhou, "Physical Properties of Hastelloy C-276 at Cryogenic Temperatures", *Journal of Appl. Physics* , vol. 103, id: 064908, 2008, doi: 10.1063/1.2899058

[81] Luvata, Products Superconducting Wires, 2015, www.luvata.com

[82] Y. Lvovsky, "Conduction Crisis and Quench Dynamics in Cryocooler-cooled HTS Magnets", *IEEE Trans. Appl. Supercond.*, vol. 12, pp. 1565 - 1569, 2002, doi: 10.1109/TASC.2002.1018702

[83] Y. Lvovsky and P. Jarvis, "Superconducting Systems for MRI-Present Solutions and New Trends", *IEEE Trans. Appl. Supercond.*, vol. 15, pp. 1317 - 1325, 2005, doi: 10.1109/TASC.2005.849580

[84] B. J. Maddock and G. B. James, "Protection and Stabilisation of Large Superconducting Coils", *Proc. of the Inst. of Elec. Eng.*, vol. 115, pp. 543 - 547, 1968. doi: 10.1049/piee.1968.0101

[85] B. J. Maddock, "Superconducting Power Cables", *Phys. in Tech.*, vol. 7, pp. 266 - 272, 1975.

[86] J. F. Maguire, *et al* , "Development and Demonstration of a HTS Power Cable to Operate in the Long Island Power Authority Transmission Grid", *IEEE Trans. Appl. Supercond.*, vol. 17, pp. 2034 - 2037, 2007, doi: 10.1109/TASC.2007.898359

[87] A. P. Malozemoff *et al* , "HTS Wire at Commercial Performance Levels", *IEEE Trans. Appl. Supercond.*, vol. 9, pp. 2469 - 2473, 1999, doi: 10.1109/77.784978

[88] G. Manfreda, G. Ambrosio, V. Marinozzi, T. Salmi, M. Sorbi, and G. Volpini, "Quench Protection Study of the Nb_3Sn Low-β Quadrupole for the LHC Luminosity Upgrade", *IEEE Trans. Appl. Supercond.*, vol. 24, id: 4700405, 2014, doi: 10.1109/TASC.2013.2285099

[89] A. P. Martinelli and S. L. Wipf, "Investigation of Cryogenic Stability and Reliability of Operation of Nb_3Sn Coils in Helium Gas Environment", *IEEE Proc. Appl. Supercond. Conf. Annapolis, 1972*, pp. 331, 1973.

[90] MassiPara project: Advanced Numerical Computation Methods for Massive Parabolic Problems, Funded by Academy of Finland for the period of 01.09.2015-31.08.2019.

[91] B. T. Matthias, "The Search for High-Temperature Superconductors", *Physics Today*, vol. 24, pp. 23 - 28, 2008, doi: 10.1063/1.3022880

[92] A. D. McInturff *et al* , "Test results for a high field (13 T) Nb_3Sn dipole", *IEEE Trans. Appl. Supercond.*, vol. 3, pp. 3212 - 3214, 1997, doi: 10.1109/PAC.1997.753158

[93] K.-H. Mess, P. Schmüser, and S. Wolff, "Superconducting Accelerator Magnets", World Scientific Publishing, 1996.

[94] A. Milanese *et al* , "Design of the EuCARD High Field Model Dipole Magnets FRESCA 2", *IEEE Trans. Appl. Supercond.*, vol. 22, id: 4002604, 2012, doi: 10.1109/TASC.2011.2178980

[95] N. Mitchell *et al* , "The ITER Magnet System", *IEEE Trans. Appl. Supercond.*, vol. 18, pp. 435 - 440, 2008. doi: 10.1109/TASC.2008.921232

[96] T. Mito *et al* , "Development of UPS-SMES as a Protection From Momentary Voltage Drop", *IEEE Trans. Appl. Supercond.* vol. 14, pp. 721 - 726, 2004, doi: 10.1109/TASC.2004.830084

[97] K. A. Müller and J. K. Bednorz, "High-Temperature Superconductivity" *Proc. Natl. Acad. Sci.* vol. 84, pp. 4678 - 4680, 1987.

[98] M. Noe and M. Steurer, "High-Temperature Superconductor Fault Current Limiters: Concepts, Applications, and Development Status", *Supercond. Sci. Technol.*, vol. 20, pp. R15 - R29, 2007, doi: 10.1088/0953-2048/20/3/R01

[99] J. van Nugteren, "Internship Report: CERN, Software development for the Science and Design behind Su- perconducting Magnet Systems," tech. rep., University of Twente: Energy Materials and Systems and CERN: ATLAS magnet team, 2011.

[100] J. van Nugteren, G. Kirby, G. de Rijk, L. Rossi, H.H.J ten Kate, and M.M.J. Dhallé, "A Study of a 5 T Research Dipole Insert-Magnet Using

an Anisotropic ReBCO Roebel Cable", *IEEE Trans. Appl. Supercond.*, vol. 25, id: 4000705, 2015, doi: 10.1109/TASC.2014.2361797

[101] J. Ogawa, Y. Sawai, H. Nakayama, O. Tsukamoto, and D. Miyagi, "n value and J_c Distribution Dependence of AC Transport Current Losses in HTS Conductors", *Physica C*, vol. 401, pp. 171 - 175, 2004, doi: 10.1016/j.physc.2003.09.031

[102] H. K. Onnes, "The Superconductivity of Mercury", *Comm. Phys. Lab.* vol. 122, pp. 124, 1911.

[103] A. den Ouden, S. Wessel, E. Krooshoop, and H. ten Kate, "Application of Nb_3Sn Superconductors in High-Field Accelerator Magnets", *IEEE Trans. Appl. Supercond.*, vol. 7, pp. 733 - 738, 1997, doi: 10.1109/77.614608

[104] J. Paasi, J. Lehtonen, T. Kalliohaka, and R. Mikkonen, "Stability and Quench of a HTS Magnet with a Hot Spot", *Supercond. Sci. Technol.*, vol. 13, pp. 949 - 954, 2000, doi: 10.1088/0953-2048/13/7/307

[105] M. Pellikka, S. Suuriniemi, L. Kettunen, and C. Geuzaine, "Homology and Cohomology Computation in Finite Element Modeling", *SIAM J. Sci. Comput.*, vol. 35, pp. B1195 - B1214, 2013, doi: 10.1137/130906556

[106] M. Pellikka, "Finite Element Method for Electromagnetics on Riemannian Manifolds: Topology and Differential Geometry Toolkit", *Ph. D. thesis*, Tampere University of Technology, Finland, 2014 http://URN.fi/URN:ISBN:978-952-15-3285-6

[107] I. Pong *et al* , "Worldwide Benchmarking of ITER Internal Tin Nb_3Sn and NbTi Strands Test Facilities", *IEEE Trans. Appl. Supercond.*, vol. 22, id: 4802606, 2012, doi: 10.1109/TASC.2012.2182972

[108] R. Qu, Y. Liu, and J. Wang, "Review of Superconductor Generator Topologies for Direct-Drive Wind Turbines", *IEEE Trans. Appl. Supercond.*, vol. 23, id: 5201108, 2013, doi: 10.1109/TASC.2013.2241387

[109] P. Raumonen, S. Suuriniemi, T. Tarhasaari, and L. Kettunen, "Dimensional Reduction of Electromagnetic Boundary Value Problems", *Boundary Value Problems*, id: 9, January 2011, doi: 10.1186/1687-2770-2011-9

[110] E. Ravaioli, V. I. Datskov, C. Giloux, G. Kirby, H. H. J. ten Kate, and A. P. Verweij, "New, Coupling Loss Induced, Quench Protection System for

Superconducting Accelerator Magnets", *IEEE Trans. Appl. Supercond.*, vol. 24, id: 0500905, 2014, doi: 10.1109/TASC.2013.2281223

[111] J. N. Reddy and D. K. Gartling, "The Finite Element Method in Heat Transfer and Fluid Dynamics", CRC Press LLC, 2001.

[112] J.-M. Rey *et al* , "HTS Dipole Insert Developments", *IEEE Trans. Appl. Supercond.*, vol. 23, id: 4601004, 2013, doi: 10.1109/TASC.2013.2237931

[113] P. F. Ribeiro, B. K. Johnson, M. L. Crow, A. Arsoy, and Y. Liu, "Energy Storage Systems for Advanced Power Applications", *Proc. of the IEEE*, vol. 89, pp. 1744 - 1756, 2001, doi: 10.1109/5.975900

[114] G. de Rijk, "The EuCARD High Field Magnet Project", *IEEE Trans. Appl. Supercond.*, vol. 22, id: 4301204, 2012, doi: 10.1109/TASC.2011.2178220

[115] A. C. Rose-Innes and E. H. Roderick, "Introduction to Superconductivity", *Glasgow: Pergamon Press*, 1969.

[116] L. Rossi, "State-of-the Art Superconducting Accelerator Magnets", *IEEE Trans. Appl. Supercond.*, vol. 12, pp. 219 - 227, 2002, doi: 10.1109/TASC.2002.1018387

[117] L. Rossi and M. Sorbi, "QLASA: A Computer Code For Quench Simulation in Adiabatic Multicoil Superconducting Windings", INFN/TC-04/13, July 2004.

[118] L. Rossi, "The Large Hadron Collider and the Role of Superconductivity in One of the Largest Scientific Enterprises", *IEEE Trans. Appl. Supercond.*, vol. 17, pp. 1005 - 1014, 2007, doi: 10.1109/TASC.2007.899260

[119] L. Rossi, "Superconductivity: its role, its success and its setbacks in the Large Hadron Collider of CERN", *Supercond. Sci. Technol.*, vol. 23, id: 034001, 2010, doi: 10.1088/0953-2048/23/3/034001

[120] L. Rossi and E. Todesco, "Conceptual Design of 20 T Dipoles for High-energy LHC", *EuCARD-AccNet-EuroLumi Workshop The High-Energy Large Hadron Collider, Malta 14-16 October 2010, Proceedings* (CERN-2011-003, EuCARD-Conf-2011-001) pp. 13-19. 2010.

[121] L. Rossi, "LHC Upgrade Plans: Options and Strategy", *Proc. 2nd International Particle Accelerator Conference, San Sebastian, Spain, 4-9 Sep 2011* (CERN-ATS-2011-257) pp. TUYA02. 2011.

[122] L. Rossi *et al* , "The EuCARD-2 Future Magnets European Collaboration for Accelerator-Quality HTS Magnets", *IEEE Trans. Appl. Supercond.*, vol. 25, id: 4001007, 2015. doi: 10.1109/TASC.2014.2364215

[123] F. Ruggiero, "LHC Accelerator R&D and Upgrade Scenarios", *Eur. Phys. J. C.*, vol. 34, pp. 433 - 442, 2004. doi: 10.1140/epjcd/s2004-04-047-1

[124] M. Runde and N. Magnusson, "Design, Building and Testing of a 10 kW Superconducting Induction Heater", *IEEE Trans. Appl. Supercond.*, vol. 13, pp. 1612 - 1615, 2003, doi: 10.1109/TASC.2003.812806

[125] S. Russenschuck, "ROXIE: A Computer Code for the Integrated Design of Accelerator Magnets", *CERN, LHC-Project-Report-868*, 1999.

[126] T. Salmi *et al* , "A Novel Computer Code for Modeling Quench Protection Heaters in High-Field Nb_3Sn Accelerator Magnets", *IEEE Trans. Appl. Supercond.* vol. 24, id: 4701810, 2014, doi: 10.1109/TASC.2014.2311402

[127] T. Salmi *et al* , "Protection heater Delay Time Optimization for High-Field Nb_3Sn Accelerator Magnets", *IEEE Trans. Appl. Supercond.*, vol. 24, id: 4701305, 2014, doi: 10.1109/TASC.2013.2287634

[128] T. Salmi, "Optimization of Quench Protection Heater Performance in High-Field Accelerator Magnets through Computational and Experimental Analysis", *Ph. D. thesis*, Tampere University of Technology, Finland, 2015 http://URN.fi/URN:ISBN:978-952-15-3570-3

[129] K. H. Sandhage, G. N. Riley, and W. L. Carter, "Critical Issues in the OPIT Processing of High-J_c BSCCO Superconductors", *JOM*, vol. 43, pp. 21 - 25, 1991, doi: 10.1007/BF03220158

[130] N. Schwerg, B. Auchmann and S. Russenschuck, "Quench Simulation in an Integrated Design Environment for Superconducting Magnets", *IEEE Trans. Appl. Supercond.* vol. 19, pp. 934-937, 2009, doi: 10.1109/TMAG.2007.916304

[131] N. Schwerg, B. Auchmann and S. Russenschuck, "Challenges in the Thermal Modeling of Quenches With ROXIE", *IEEE Trans. Appl. Supercond.* vol. 19, pp. 1271-1273, 2009, doi: 10.1109/TASC.2009.2018747

[132] Multiple authors, edited by B. Seeber, "Handbook of Applied Superconductivity", IOP Publishing LTD, 1998.

[133] V. Selvamanickam *et al* , "The Low-Temperature High-Magnetic-Field Critical Current Characteristics of Zr-Added (Gd,Y)$Ba_2Cu_3O_x$ Superconducting Tapes", *Supercond. Sci. Technol.*, vol. 25, id: 125013, 2012, doi: 10.1088/0953-2048/25/12/125013

[134] P. F. Smith and B. Colyer, "A Solution to the 'Training' Problem in Superconducting Magnets", *Cryogenics*, vol. 15, pp. 201 - 207, 1975, doi: 10.1016/0011-2275(75)90034-X

[135] Z. J. J.Stekly and J. L. Zar, "Stable Superconducting Coils", *IEEE Trans. NS-12*, p. 367, 1965.

[136] A. Stenvall, A. Korpela, R. Mikkonen, and G. Grasso, "Quench analysis of MgB_2 Coils With a Ferromagnetic Matrix", *Supercond. Sci. Technol.*, vol. 19, 581 - 588, 2006, doi: 10.1088/0953-2048/19/6/028

[137] A. Stenvall, T. Salmi, and E. Härö, "Basics of Stability Analysis of Superconductors - What is it There Behind the Numerical Approaches and How They Can Be Utilized to Aid the Complete Superconducting Systems Engineering?" in "Numerical Modeling for Applied Superconductivity", edited by F. Grilli, B. Dutoit, and F. Sirois, World Scientific, In Press.

[138] R. Stiening, R. Flora, R. Lauckner, and G. Tool, "A Superconducting Synchrotron Power Supply and Quench Protection Scheme", *IEEE Trans. Magn.*, vol. 15, pp. 670 - 672, 1979, doi: 10.1109/TMAG.1979.1060065

[139] G. Strang and G. Fix, "An Analysis of the Finite Element Method", Wellesley-Cambridge Press, 2008.

[140] SUite for Nonlinear and DIfferential/ALgebraic Equation Solvers (SUNDIALS), available online at: https://computation.llnl.gov/casc/sundials/

[141] T. Takematsu *et al* , "Degradation of the Performance of a YBCO-Coated Conductor Double Pancake Coil Due to Epoxy Impregnation", *Physica C*, vol. 470, pp. 674 - 677, 2010, doi: 10.1016/j.physc.2010.06.009

[142] P. Tixador, "Development of Superconducting Power Devices in Europe", *Physica C*, vol. 470, pp. 971 - 979, 2010, doi: 10.1016/j.physc.2010.05.014

[143] E. Todesco, L. Bottura, G. De Rijk, and L. Rossi, "Dipoles for High-Energy LHC", *IEEE Trans. Appl. Supercond.*, vol. 24, id: 4004306, 2014, doi: 10.1109/TASC.2013.2286002

[144] E. Todesco, "Quench Limits in the Next Generation of Magnets", *CERN Yellow Report CERN-2013-006* pp.10-16, 2014, doi: 10.5170/CERN-2013-006.10

[145] F. Trillaud, H. Palanki, U. P. Trociewitz, S. H. Thompson, H. W. Weijers, and J. Schwartz, "Normal Zone Propagation Experiments on HTS Composite Conductors", *Cryogenics*, vol. 43, pp. 271 - 279, 2003, doi: 10.1016/S0011-2275(03)00044-4

[146] P. Vase, R. Flükiger, M. Leghissa, and B. Glowacki, "Current Status of High-Tc Wire", *Supercond. Sci. Technol.*, vol. 13, p. R71, 2000, doi: 10.1088/0953-2048/13/7/201

[147] A.P. Verwei *et al* , "1.9 K Test Facility for the Reception of the Superconducting Cables for the LHC", *IEEE Trans. Appl. Supercond.*, vol. 9, pp. 153 - 156, 1999, doi: 10.1109/77.783259

[148] K. Vinod, R. G. Abhilash, and U. Syamaprasad, "Prospects of MgB_2 Superconductors for Magnet Application", *Supercond. Sci. Technol.*, vol. 20, p. R1, 2007, doi: 10.1088/0953-2048/20/1/R01

[149] Q. Wang, L. Yan, B. Zhao, S. Song, and Y. Lei, "Development of Wide-Bore COnduction-Cooled Superconducting Magnet System for Material Processing Applications" *IEEE Trans. Appl. Supercond.*, vol. 14, pp. 372 - 375, 2004, doi: 10.1109/TASC.2004.829673

[150] X. Wang *et al* , "Normal Zone Initiation and Propagation in Y-Ba-Cu-O Coated Conductors with Cu Stabilizer" *IEEE Trans. Appl. Supercond.*, vol. 15, pp. 2586 - 2589, 2005, doi: 10.1109/TASC.2005.847661

[151] Y. Wang *et al* , "Detecting and Describing the Inhomogeneity of Critical Current in Practical Long HTS Tapes Using Contact-free Method", *Cryogenics*, vol. 47, pp. 225 - 231, 2007, doi: 10.1016/j.cryogenics.2007.01.006

[152] H. Wiedemann, "Particle accelerator physics", Springer, 2007.

[153] E. J. N. Wilson, "An Introduction to Particle Accelerators", Oxford University Press, 2001.

[154] M. N. Wilson, "Stabilization of Superconductors for Use in Magnets", *IEEE Trans. Magn.*, vol. 13, pp. 440 - 446, 1977, doi: 10.1109/TMAG.1977.1059290

[155] M. N. Wilson and Y. Iwasa, "Stability of Superconductors Against Localized Disturbances of Limited Magnitude", *Cryogenics*, vol. 18, pp. 17 - 25, 1978, doi: 10.1016/0011-2275(78)90132-7

[156] M. N. Wilson, "Superconducting Magnets", Clarendon Press Oxford, 1983.

[157] R. Yamada, E. Marscin, A. Lee, M. Wake, and J.-M. Rey, "2-D/3-D quench simulation using ANSYS for epoxy impregnated Nb_3Sn high field magnets", *IEEE Trans. Appl. Supercond.*, vol. 13, pp. 1696 - 1699, 2003, doi: 10.1109/TASC.2003.812870

[158] Y. Yanagisawa *et al* , "Remarkable Weakness Against Cleavage Stress for YBCO-Coated Conductors and Its Effect on the YBCO Coil Performance", *Physica C*, vol. 471, pp. 480 - 485, 2011, doi: 10.1016/j.physc.2011.05.003

[159] L. Ye, L. Lin, and K.-P. Juengst, "Application Studies of Superconducting Fault Current Limiters in Electric Power Systems", *IEEE Trans. Appl. Supercond.*, vol. 12, pp. 900 - 903, 2002, doi: 10.1109/TASC.2002.1018545

[160] A. V. Zlobin *et al* , "R&D of Nb_3Sn Accelerator Magnets at Fermilab", *IEEE Trans. Appl. Supercond.*, vol. 15, pp. 1113 - 1118, 2005, doi: 10.1109/TASC.2005.849507

Quench Considerations and Protection Scheme of a High Field HTS Dipole Insert Coil

E. Härö, A. Stenvall, T. Lecrevisse, J. Fleiter, J.-M. Rey, M. Sorbi, M. Devaux, C. Trophime, P. Fazilleau, G. Volpini, P. Tixador, F. Hornung, and C. Pes

2013 *IEEE Trans. Appl. Supercond.* **23** 4600104

Publication 1

Protection of the 6 T YBCO Insert in the 13 T Nb_3Sn Fresca II Dipole

A. Stenvall, E. Härö, P. Fazilleau, M. Devaux, M. Durante, T. Lecrevisse, J.-M. Rey, J. Fleiter, M. Sorbi, G. Volpini, and P. Tixador

2013 *CERN Yellow Report 2013-006, Proc. Workshop on Accelerator Magnet, Superconductor, Design and Optimization*

Publication 2

Reducing Modelling Domain to Speed-Up Simulations of HTS Coils

E. Härö and A. Stenvall

2014 *IEEE Trans. Appl. Supercond.* **24** 4900705

Publication 3

Variation of Quench Propagation Velocities in YBCO Cables

E. Härö, J. Järvelä, and A. Stenvall

2015 *J. Supercond. Nov. Magn.* **28** 1705

Publication 4

Hot Spot Temperature in an HTS Coil: Simulations with MIITs and Finite Element Method

E. Härö, A. Stenvall, J. van Nugteren, and G. Kirby

2015 *IEEE Trans. Appl. Supercond.* **25** 4901107

Publication 5

Modelling of Minimum Energy Required to Quench an HTS magnet with a Strip Heater

E. Härö, A. Stenvall, J. van Nugteren, and G. Kirby

2015 *IEEE Trans. Appl. Supercond.* **25** 4701505

Publication 6

Tampereen teknillinen yliopisto
PL 527
33101 Tampere

Tampere University of Technology
P.O.B. 527
FI-33101 Tampere, Finland

ISBN 978-952-15-3768-4
ISSN 1459-2045